POLITECNICO DI TORINO

Corso di Laurea Magistrale in Ingegneria Civile

in collaborazione con
UNIVERSITY OF LEEDS
School of Civil Engineer

Tesi di Laurea Magistrale

Sensitivity analysis on the geothermal potential of energy walls

Relatore:

Prof. Marco Barla
Politecnico di Torino

Candidato:

Miriam Piemontese

Relatori esterni:

Dr. Fleur Loveridge
University of Leeds

Dr. Alice Di Donna
Université Grenoble Alpes

Luglio, 2018

INDEX

LIST OF FIGURES

LIST OF TABLES

APPENDIX

INTRODUCTION

The development of sustainable energy sources has been experiencing a great growth in the past decades. It is well known that the continued emission of fossil carbon (in the form of CO_2, produced mainly by traditional production of energy exploiting coal, petroleum and gas) to our atmosphere is altering our planet's climate and ecology. Furthermore, from political and economical points of view, it is not prudent to wholly depend on fossil fuel resources located in unstable parts of the world or within nations whose interests may not coincide with ours. This is a good reason to give a great impulse in promoting local energy sources. In this particular scenario, geothermal energy can be considered a suitable solution, combining sustainability and widespread availability.

Geothermal energy exploits the heat coming from the ground. Geothermal resource can be considered in distinct ways, based on the different ranges of temperatures involved, referring to "high enthalpy" or "low enthalpy" geothermics. In the first case the energy is derived from the heat flux from the earth's interior, that is typically at high temperature; this is mainly produced by the decay of radionuclides in the core of the Earth that propagates towards the shallow substrates. It is used for the direct production of electrical power through deep boreholes and steam turbines. The second one concerns indirect exploitation of ground heat, that is at low temperature (usually temperatures of less than 30°C are considered) in the relatively shallow geosphere (depths of down 200 m), for air heating/cooling in surrounding buildings, with the help of heat pumps.

In this case heat comes principally from solar energy that is absorbed and stored in the ground. It is evident that low enthalpy systems do not depend on geological anomalies and this is the reason why they are more widespread all over the world than high enthalpy technology, that also requires big and expensive plants to reach great depths and high temperatures.

Compared to other forms of renewable and sustainable energy, low enthalpy geothermal energy can be considered always available, since it is mostly independent from the alternation of day and night and from the local climatic and weather conditions. Indeed, below a few meters depth, the temperature of the subsurface is approximately stable. As the temperature of the ground is constant throughout the year, it is warmer than the external air in winter and cooler in summer. This allows heat exchange for heating during winter and conditioning during summer. Moreover, if the alternation of heating and cooling is well balanced during the year, the ground just stores the heat temporarily and it can be considered independent from the solar resupply. To exploit low enthalpy geothermal resources heat exchange between the ground and a fluid circuit connected to a heat pump it is required. Pipework is usually embedded underground where the fluid is circulated absorbing heat that is later properly converted in the heat pump: the latter is directly linked to the building heating/cooling distribution system.

Besides traditional systems and installations, so called energy geostructures in geotechnical engineering have a relatively new and important role in the applications. Structures that by their nature have direct contact with the ground (such as foundation piles, tunnels and diaphragm walls) can be equipped with pipes systems to use them as heat exchangers, combining structural and energy functions. This allows reduction in both operational costs and pollution due to traditional fossil carbon energy sources. Thus, foundation piles and retaining walls have been used for this purpose respectively since the mid-1980s and since the mid-1990s and more recently also tunnels lining. Such energy geo-structures are now common in Austria, Germany, the UK and Switzerland.

However, from the design point of view, for this type of structure it is necessary to take into account the effects that heat exchange have on the stress/strain field of the reinforced concrete. It is well known that temperature variation causes thermal strains or induced stresses in the material, that need to be added to the operational state of stress in a design stage, but lack of evidence regarding the impact of the thermal cycles on the serviceability and safety performance of the geostructures is still an actual problem. Moreover, to justify higher initial costs of the installation, it is necessary to make a preliminary assessment of the effective energy advantages in the operational phase, in terms of energy efficiency of the structure.

A lot of studies have already been made. Starting from Brandl (1998 and 2006), experimental and numerical assessment have been carried out – Gao et al. (2008), to disclose for example the influences on the thermal efficiency of energy piles – Cecinato and Loveridge (2015), and the geotechnical behaviour of energy piles for different design solutions – Knellwolf et al. (2011), Batini et al. (2015). In the tunnelling field, application of energy equipment in the lining have been tested – Markiewicz and Adam (2006), Franzius and Pralle (2011), Barla et al. (2016), Zhang et al. (2013), as well as the influence of underground conditions on the heat exchange capacity of energy tunnels by Di Donna and Barla (2015). Little work has been carried out for energy walls. Concerning retaining walls, thermal and mechanical aspects of their response as shallow geothermal heat exchanger has been investigated – Bourne-Webb et al. (2015 and 2016), as well as the energy performance of diaphragm walls and their influences – Di Donna et al. (2016), Barla et al. (2017). Even though operative applications of energy walls have been presented and analysed – Markiewicz and Adam (2009), Suckling and Smith (2002), Amis et al. (2010), there has been no study of the impact of ground conditions on energy efficiency of thermo-activated diaphragm walls.

Aim and objectives

The aim of this work is to provide guidelines for the preliminary design procedure for energy walls, based on the assessment of energy efficiency of the structure. Through numerical modelling, a parametric analysis is performed to produce design charts useful for a preliminary quantification of exploitable heat for any possible user or designer. For the development of this study, the following objectives are addressed:

- To review previous case studies and relevant works. Scientific and technical progresses, as well as knowledge gaps, concerning energy walls will be highlighted.
- To set up the numerical model. The general equations that govern the convection-diffusion problem will be defined.
- To validate the model. A validation analysis will be run from collected real data.
- To run a parametric numerical analysis. Assuming fixed geometry and pipe configuration, the efficiency of an energy wall working under different ground conditions and properties will be investigated through numerical analyses.
- To interpret the results. Design charts for the assessment of energy efficiency will be drawn from the analysis.

Structure of the dissertation

In Chapter 1 background information is presented to focus the general argument of this dissertation: geothermal energy is defined and its main aspects are described.

In Chapter 2 energy geostructures, mainly energy walls, are introduced. It is important to re-examine scientific disclosures in this area. From these significant works, it is also possible to get important indications about the geometry and the boundary conditions to be used in following numerical simulations.

In Chapter 3 the numerical software is introduced and its thermo-hydro formulation is defined. Some guidelines for its use are provided and a validation is carried out to confirm the appropriateness of the results.

In Chapter 4 the geometry and the properties of this case study are presented. Important issues concerning boundary conditions, that will be varying in the simulations, and groundwater presence are set out. Ranges of variation of the factors chosen for the parametric analysis are reported and justified.

In Chapter 5 the results are collected and interpreted, in terms of temperature and then heat power. Preliminary charts for the energy assessment of the energy geostructure are presented. Comparisons between the results, as well as with previous studies, are made and discussed.

In the conclusive chapter, the outlines of the study are presented and recapped and further developments are suggested.

1. GEOTHERMAL ENERGY

1.1 The geothermal energy resource

The Earth has an inner energy responsible of the dynamics of our planet: volcanic activity is its most evident display, but it can also reach the shallow layers through heat transmission. This is uninterruptedly happening in every location of the Earth: deeper in the ground, higher temperatures become. This geothermal gradient varies considerably between different locations, although typical values are in the range 2 – 3.5°C per 100 m.

There are some anomalous areas of the earth's surface where high temperatures can be encountered at relatively shallow depths; usually they are located in current or historic volcanic zones and this is the case of the geothermal power plant of Larderello, Italy. These geothermal fields allow the exploitation of the deep energy of the Earth for the electrical power production. This is what is called "high enthalpy" geothermal source: enthalpy is the thermal content in energy terms and it can be considered proportional to the fluid temperature responsible for the heat transport.

The heat of the ground can also be used when temperatures are not very high and it is referred to as "low enthalpy" resource or shallow geothermal energy. Rocks and sediments have high values of volumetric heat capacity but modest values of thermal conductivity: the ratio of these two parameters is known as thermal diffusivity and represents the rate and the extent to which a heat signal or heat pulse is propagated throughout a medium.

Therefore, the ground has rather low values of thermal diffusivity: heat pulses do not propagate very fast or far throughout the subsurface of the Earth. Whilst most shallow substrates are subjected to temperature variation during the day and the year, according to the local climatic changes, below a few meters depth the temperature of the subsurface is remarkably stable, at a value approximating to the long-term annual average surface temperature. Usually the range is 8-20°C: for example it has been evaluated that in the UK values are in the range 9-12°C (Banks, 2008) and in Italy around 11-15°C as it is shown in Figure 1.1 and Figure 1.2.

Through heat exchangers connected to heat pump, it is possible to extract heat from the ground during winter and inject heat into the ground during summer for heating and cooling the external air, respectively. This allows the extraction and the economical use of ground heat at lower temperature and a larger spread of this indirect use of geothermal energy is possible even in locations without particular geological conditions such as geothermal fields.

With the use of heat pumps it has been possible to exploit shallow geothermal energy mainly for heating (winter season) and cooling (summer season) residential buildings and public utilities, but also to produce domestic hot water or other industrial uses. More recent applications are dealing with the possibility to use ground source heating for deicing airport runways and bridge decks.

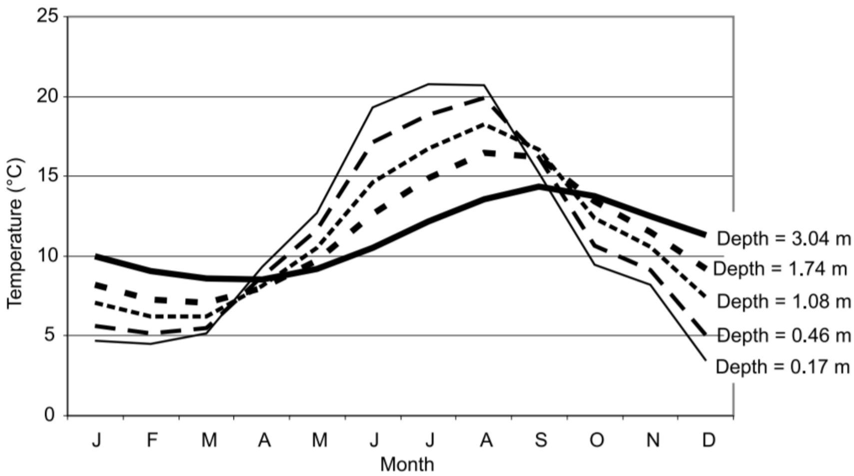

Figure 1.1. The seasonal temperature fluctuation in the subsurface at various depths, Oxford (Banks, 2008)

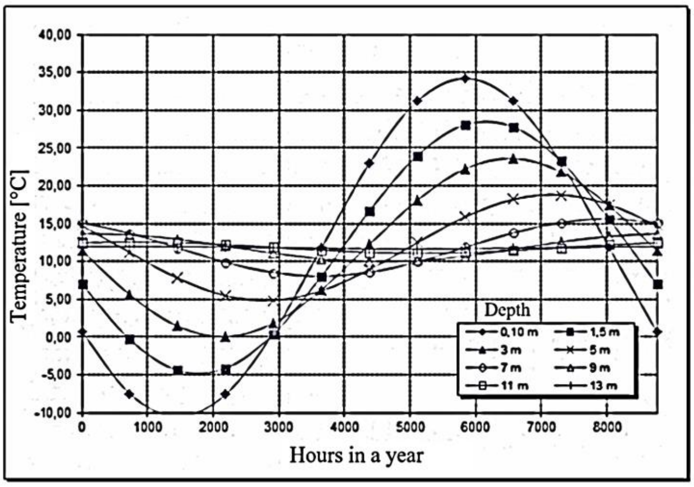

Figure 1.2 The seasonal temperature fluctuation in the subsurface at various depths, North Italy (source not available)

1.2 Ground source heat pump system (or GSHP system)

A traditional shallow geothermal plant is relatively simple, composed by three main elements:

- Ground heat exchanger: it is a pipes system embedded in the ground with the purpose of absorbing heat, through the circulation of a thermo-carrier fluid, that has high thermal conductivity.
- Heat pump: it is the heart of the system, a generator that uses the extracted heat form ground heat exchangers to make it exploitable in the distribution system.
- An internal system for the distribution of the heat, such as a domestic radiator system.

The same plant can be used for air conditioning during warm periods by use of a reversible heat pump.

A heat pump is a device that allows heat exchange between an energy source (for example ground, air or phreatic water) and an environment with different temperature: a GSHP is a heat pump where source of energy is the ground. Its functioning is similar to the one of a refrigerator, and it can be used both for winter heating or summer cooling. From the laws of physics, heat tends to move from a high-temperature environment to a low-temperature one: heat pumps are engines that force the heat to move in the opposite direction, expending energy and mechanical work.

The heat pump absorbs heat from the carrier fluid in the pipe system, making it evaporates in an evaporator, then in a compressor it raises temperature and yields heat to the environment through a condenser, connected to the distribution plant (Figure 1.3).

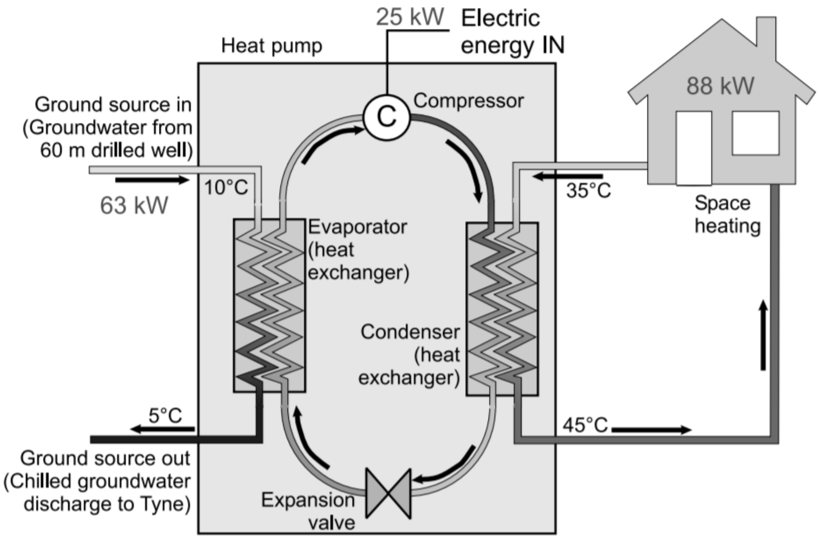

Figure 1.3 A schematic application and diagram of a GSHP (Banks, 2008)

This process requires an energy input, typically electrical power. However, modern devices are efficient and high performance system, able to produce much more energy than that expended on the pump + compressor engine.

The efficiency of a heat pump is usually expressed in terms of its coefficient of performance COP, that is the ratio between the total heating effect and the electrical energy required to power the heat pump. These machines have usually a COP of 4-5, it means that 1 kW of expended electrical power allows to produce 4-5 kW of thermal energy.

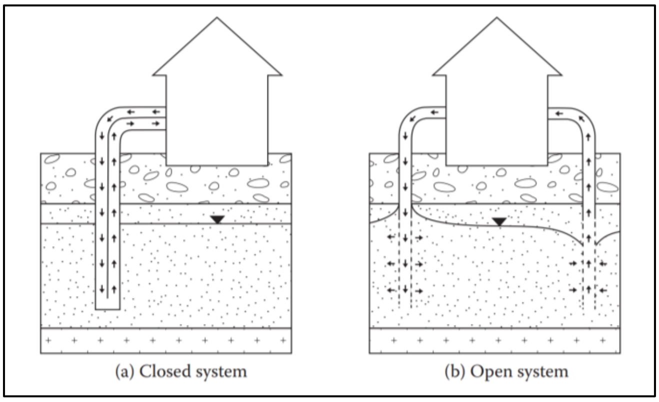

Figure 1.4 (a) Scheme of closed-loop and (b) open-loop shallow geothermal systems (Stauffer et al., 2013)

To capture heat, there are two fundamental ground source options: the open-loop and the closed-loop systems (Figure 1.4). In a closed-loop system, a closed loop of a pipe is installed underground horizontally (in trenches at a depth of 1 to 2 m) or vertically (in boreholes down to a depth of a few tens to about 400 m), acting as a heat exchanger. An environmentally safe heat carrier fluid, usually, a water-antifreeze solution, is circulated through the pipes to collect heat from the ground in winter and/or to inject heat to the ground in summer. It is then connected to a heat pump, where refrigerant fluid circulates. A special variant of collectors is the direct exchange system (Figure 1.5(a)): the heat pump's refrigerant fluid circulates into the subsurface in a closed loop of tube. Open circuit exchangers physically abstract water from the groundwater. Heat is extracted from this flux of pumped water in the circuit or, in cooling mode, dumped into it, and then it is put back into the ground (Figure 1.4 (b)). A direct variant can be possible also in open-loop (Figure 1.5 (b)). However, indirect circulation is most common, for both the two systems.

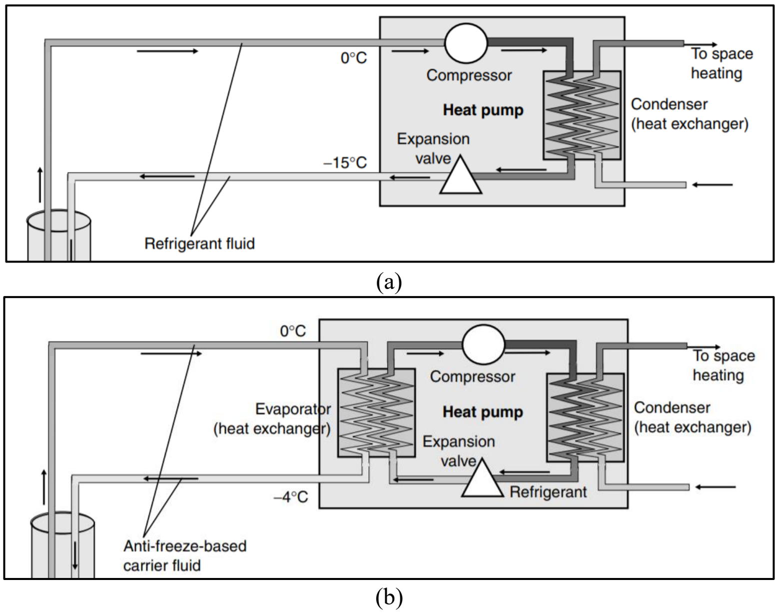

Figure 1.5 A schematic diagram of (a) direct circulation and (b) indirect closed-loop scheme, installed in a borehole
(Banks, 2008)

1.3 Sustainable energy source

It is wise to be clear about the definition of the word "sustainable" when it is used referring to energy concept. Also referred as "green energy", it is the production and use of energy that allows a sustainable development: "it meets the needs of the present without compromising the ability of future generations to meet their own needs" (Gro Harlem Brundtland's commission, Banks, 2008). This can be achieved through three fundamental components: one is linked to the production (thus, renewable energies), another one linked to its utilization (thus, efficiency and energy conservation) and the last one linked to the environmental impact in terms of pollution.

Concerning deep geothermal energy, the discovery of radioactivity (Becquerel, 1896) and radioactive elements (Curie, 1902) had a significant role in understanding the heat phenomenon of the Earth: now it is well known that its interior is kept hot by the continuous decay of radioactive isotopes of uranium, potassium and thorium, and only in part by the residual primordial heat.

However, in the nineteenth Century already there were men of science that stated that the Earth is loosing heat and cooling down: afterwards, it was possible to demonstrate it, showing how there is no balance between the heat produced by the radionuclides and the one dissipated from the surface into the space. Nevertheless, the cooling is a very slow process and the thermal energy of our planet is huge: this is the reason why deep geothermal resource can be considered a renewable energy form.

In the Directive 2009/28/EC, the European Union recognized shallow geothermal as a renewable energy form and its applications are expected to rise more and more in years. Shallow geothermal energy is subject to resupply by solar gain: therefore continuous extraction of heat cannot be made indefinitely (Sterpi et al., 2014). However, if the use of heating and cooling is balanced then the ground is just storing the temporarily and its exploitation can be considered practically unlimited.

Besides being almost inexhaustible, ground heat energy is also very clean: GSHP systems have very low emission of carbon dioxide and of other noxious gases. This is strictly linked to the electrical power requested for the functioning of the heat pump. However, as it has been stated before, modern devices have good efficiency and it is possible to get 4 times more energy than it is expended. In high enthalpy geothermal, deep fluids are carried towards the surface: they are usually very mineralized and therefore there could be the danger of polluting shallow aquifer ground. For the low enthalpy systems this problem is obviously insignificant, because there is no taking of deep fluids; thermal carrier fluids that circulate in close-loop system do not make contact with groundwater and it has to be guaranteed anyhow the use of no toxic substances for the environment. Closed circuits allow also a great saving of water that, once it is in the plant, it is continuously reused.

In terms of energy conservation it is not easy to make general evaluations, because it strongly depends on different conditions, such as type of circuit, intended use and size of the system itself, as well as on the plant technology. To make an example, for a domestic geothermal plant with heating through radiant panels, savings for heating costs are estimated to be around 60% comparing to the traditional methane based heating systems.

However, the initial investment of a GSHP system is stated to be around 20% - 45% higher than that in traditional heating and air-conditioning systems due to the high cost of installation. The extra investment can only be recovered after five to ten years.

To reduce the initial costs of installation, energy geostructures can be considered the consequent evolution of this technology. Heat exchange tube loops are embedded directly in the concrete of those structures that are in contact with ground for a certain depth such as bearing piles, foundations, retaining walls and tunnel linings: thus, it is possible to combine structural function and heat exchange role.

2. ENERGY WALLS

2.1 Energy geostructures

Energy geotechnical engineering is spreading all around the world to tackle the disadvantages of heat exchanger in boreholes or trench, i.e. great initial investment and large occupied space. Energy geostructures can link the structural role to the energy supply, using the principle of a ground source heat pump system. Pipes are directly installed in the reinforced concrete structural element, usually fastened to the steel bars. Thus, a sustainable energy source can be exploited in a cost-effective way, since only elements conventionally designed and realized to perform a structural function are used.

As it is shown in Figure 2.1, a thermo-active system for energy geostructures is composed of a primary closed circuit below ground, embedded in the earth-contact concrete elements, and a secondary circuit in the building. In the primary pipe network a heat carrier fluid, usually antifreeze water, is pumped and exchanges heat between ground and external environment. The secondary pipework is a closed fluid-based circuit embedded in the floors and walls of buildings or bridge decks, road structures, etc. A heat pump connects the two closed circuits, in which heat exchange occurs.

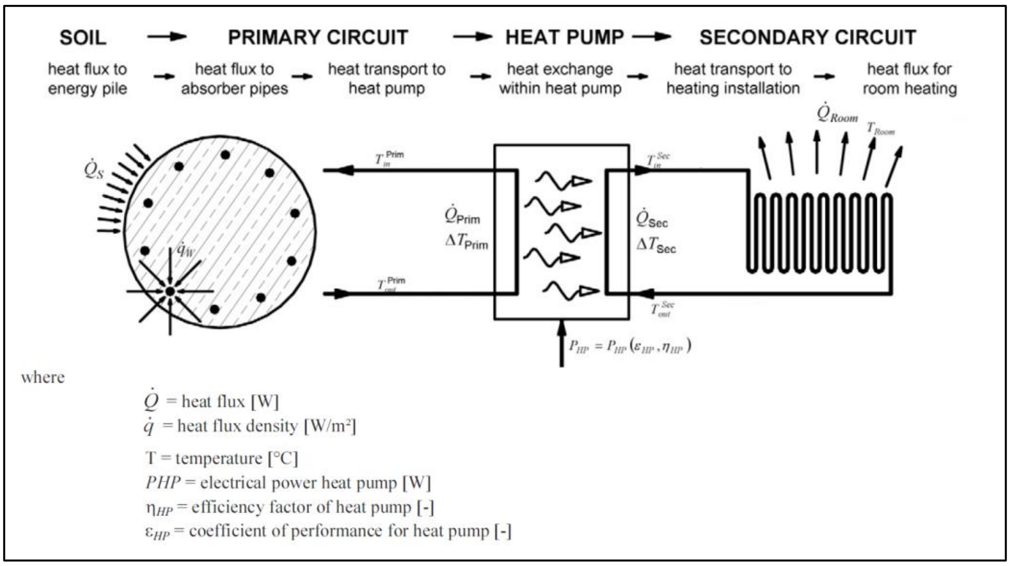

Figure 2.1 Scheme of a heat exchange system with energy piles (Brandl, 2006)

The design procedure for these thermo-active structures is more challenging with respect to conventional projects. Besides the known procedures for the delivery of a geostructure, it is requested to design and dimensioning the geothermal equipment, with particular attention to energy demand and the additional effects induced by temperature variation on the structure itself in terms of stresses and displacements. In this matter, previous experience and existing cases of energy geostructures have the main role. Nowadays, examples of thermo-active structures such as foundations, tunnels, retaining and diaphragm walls can be easily found in Europe, in the USA and in China (Bourne-Webb et al., 2016).

So called *energy piles*, i.e. thermo-activated foundation piles, are the most common energy geostructures, and their application started in Austria in the '80s (Brandl, 2006). In 2013 the number of energy piles has been estimated to be around 100 000, increasing year by year (Brandl, 2016). In the foundation field, also base slabs can be used as heat exchangers, since they have a large area in contact with the ground. Energy pile technology can be also extended to bored piled walls with the function of retaining walls.

The first thermo-activated diaphragm wall, i.e. *energy wall*, is dated to 1996, in Austria (Brandl, 2006): diaphragm walls are widely used in urban excavations for buildings basements and underground works realized by the cut-and-cover method, therefore their use as heat exchangers can be readily exploited.

As it is shown in Figure 2.2, the main difference of this type of geostructure with respect to energy piles is that diaphragm walls are divided into two parts by the excavation line: over the excavation line, the diaphragm wall is surrounded on one side by soil, on the other side by the air of the excavation. There the air conditions in the excavation undertake an important role, mainly in terms of temperature and heat flux and it is necessary to take them into account during analyses and modelling.

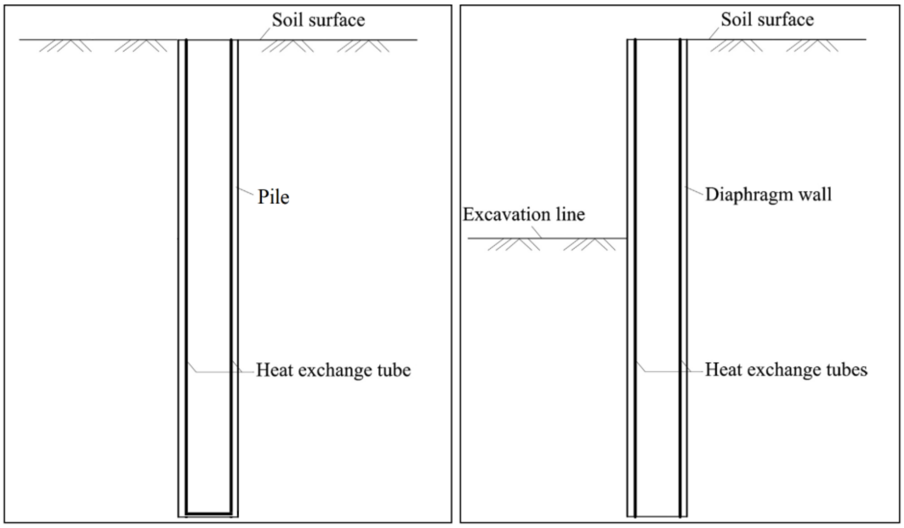

Figure 2.2 Schematic section plan drawing of geothermal heat exchangers embedded in a foundation pile (on the left) and in a diaphragm wall (on the right) (Sun et al., 2013)

More recently, GSHP technology has been used for tunnel application. With respect to building foundations, *energy tunnels* can involve a larger volume of ground and surface for heat exchange. Moreover, in deep tunnels higher ground temperatures can be exploited to heating/cooling the surrounding buildings and much more heat can be absorbed from the air inside the tunnels, heated by traffic.

Different type of geothermal installation has to be considered for conventional method and mechanized method of excavation. Numerical and experimental assessments have been carried out to analysed the feasibility and the efficiency of this type of energy geostructures (Franzius and Pralle, 2011, Zhang et al., 2013, Di Donna and Barla, 2016). However, actual implementations of energy tunnels are very limited, for the moment.

For example, in Austria part of the Lainzer tunnel (New Australian Tunnelling Method) has been equipped with a GSHP system in 2004 (in Figure 2.3, Brandl, 2006, Markiewicz and Adam, 2006) and an experimental geothermal plant has been installed in a lot of the Turin Metro tunnel (Tunnel Boring Machine) in 2017 in Italy (in Figure 2.4, Barla and Perino, 2014, Barla et al., 2016).

Figure 2.3 Detail of the absorber loops with collection pipe in the Lainzer tunnel (Brandl, 2006)

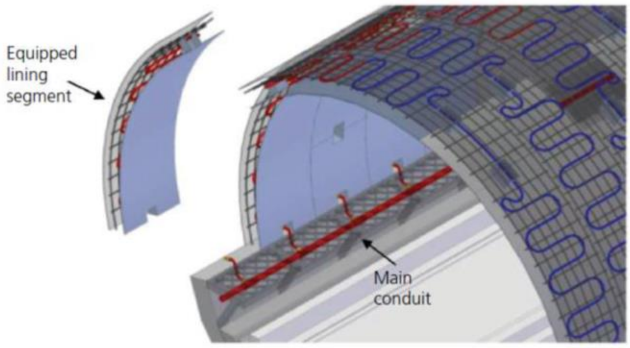

Figure 2.4 An application of tunnel with energy segments (Barla and Perino, 2014)

2.2 Thermal response test (TRT)

In the relatively new field of energy geostructures, design procedures are still mainly based on previous experiences and experimental data. It is possible to have a consistent database of information about energy piles, since existing cases, now significantly widespread, have been studied and monitored since 80's. The situation about different energy geostructures such as thermo active diaphragm walls and tunnels is quite different. Moreover, in these applications it is not suitable to use models and methods for traditional boreholes heat exchangers as it can done, with some flexibility, for energy piles.

These axisymmetric elements present superficial similarities to boreholes, their shorter length being the main difference (Loveridge et al., 2015).

Energy diaphragm walls, together with the dissimilarity in terms of buried depth, are different from BHEs because they are surrounded on one side by the soil, on the other one by the excavation air. Retaining walls do not have an axisymmetric geometry, on the contrary they have a longitudinal dimension much more extended that the transversal one (Sun et al., 2013). Heat transfer occurs mainly along this direction instead of along radial direction as it occurs in piles and BHEs. It is evident that there is still a lot of work to do to disclose how heat exchangers can be correctly designed and how they can affect the structural and energetical response of energy walls.

To predict the thermal performance of energy geostructures, it is fundamental to define thermal conductivity to be used in design and modelling analyses stages. Therefore, in situ tests can play an important role. Laboratory tests can be used to determine some ground thermal properties but it can be questioned whether they are representative, considering a sample of only a few centimetres in dimension. Furthermore, laboratory experiments cannot take into account the complex phenomenon of groundwater that can be identified in field tests such as the Thermal Response Test (TRT), typically used in geothermal applications of BHEs.

Thermal Response Test is a measurement method usually used to determine heat transfer properties of a BHE (for similarities also of an energy pile) and surrounding ground. In particular, thermal conductivity has to be defined since it strongly affects heating/cooling efficiency. It varies by a factor of more than two (1.5 to 3.5 W m^{-1} K^{-1}) for the range of common rocks encountered at the surface and can vary significantly for many superficial deposits (from British Geological Survey, 2011). Imposing a constant heating power in the circuit, inlet and outlet temperature of the fluid can be measured and interpreted through analytical methods (e.g. the line source method) to determine thermal conductivity. In Figure 2.5 typical outputs of a TRT are shown.

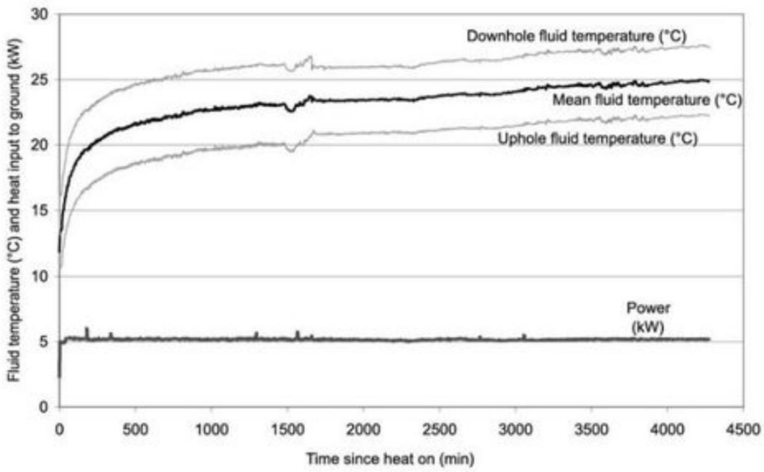

Figure 2.5 Example of output from a TRT (Banks, 2008)

The same TRT with constant power input has been used for energy walls as well. However, there is no reliable methods to interpret these data, due to their many differences with respect to axisymmetric heat transfer systems. Therefore, typical solutions for BHEs or energy piles cannot be used and numerical simulations are generally required to analyse test results.

TRT equipment can also be used to obtain evidence of the actual energy efficiency of a thermo active geostructure, to be checked with the one assessed *a priori*. In this case, a constant inlet temperature is imposed to the fluid circulating in the pipework. Interpreting the inlet temperature with the outcomes in terms of outlet temperatures it is possible to obtain information about heat exchanged rate in the GSHP system. This testing method is usually useful for comparing heat power from different types of ground heat exchangers (Xia et al., 2012).

2.3 Examples of energy walls

Existing cases of retaining walls used as heat exchangers in the UK, in Austria, in Germany and in China can be listed (Bourne-Webb et al., 2016). Scientific publications about these works are important since existing regulations do not provide specific guidelines for energy walls design procedures, that are still mainly based on experience.

Brandl (2006) described the use of piled retaining walls equipped with GSHP system at a rehabilitation centre in Austria and in the Section LT24 of the Lainzer tunnel near Vienna. Remaining in Austria, pioneer in energy geotechnical engineering, different authors (Brandl, 2006 - 2016, Markiewicz and Adam, 2006 - 2009) highlighted the use of different energy geostructures in the realisation of the extension of the Viennese metro line U2, among them energy diaphragm walls. Suckling and Smith (2002) described the first embedded energy piled wall in the UK at Keble College, Oxford, while Amis et al. (2010) dealt with the installation of the first energy diaphragm wall for the new Bvlgari Hotel in London. Moreover, the new underground railway line in London has been equipped with geothermal technology in diaphragm walls (Amis and Loveridge, 2014).

In Frankfurt, Germany, a bored pile type wall was installed in the construction of the Palais Quarter development (Katzenbach et al., 2017) and in the new Shanghai Museum of Natural History diaphragm wall system has been thermo-activated to provide heating and cooling to the museum (Xia et al., 2012).

At present the design of geostructures is still mainly based on empirical values. Thus, a scientific monitoring and a good interpretation of its data are very important to adapting such systems better to future applications. In the following paragraphs we are going to explain in more details some of these listed works and afterwards some previous studies will be reviewed to highlight important developments.

2.3.1 Vienna Metro Line U2 – Austria (Brandl, 2006 - 2016)

The project of the extension of the Viennese Metro Line U2, Austria, has been the first full-scale application of the GSHP technology in Metro engineering in the world. In an initial design stage it was decided to equip four stations and a bored tunnel section with geothermal systems to tackle heating and cooling demand. The construction method was the cut-and-cover, therefore the stations were equipped with absorbers in the diaphragm walls, base slabs and between the primary and the secondary lining of the tunnel support.

Numerical analyses were used to determine the thermal and mechanical effects in the structure, and to find the optimised configuration of the system. However, detailed evidence concerning numerical modelling and calculation for this project cannot be found in literature. Considering all the many uncertainties in the design stage, the observational method has been implemented using monitoring and quality control. To this end, as well as for regulation and to optimise the operation of the geothermal system, all the thermo-activated facilities have been equipped with several measuring devices.

In Figure 2.6 the cross section of the first station (U2/2 – Taborstraße) is shown, where the measuring instruments are indicated. Beside the operational measuring, in this diaphragm wall some temperature and strain gauges as well as an extensometer have been installed to investigate the thermal influence on the deformation behaviour of the underground structure and on the enclosing subsoil. Considering the lack of experimental data referred to thermomechanical behaviour of energy walls, this type of in situ monitoring could be useful in future application. However, it is not possible to find the results of this actual case study, as well as details about the arrangement of the pipework inside the cage.

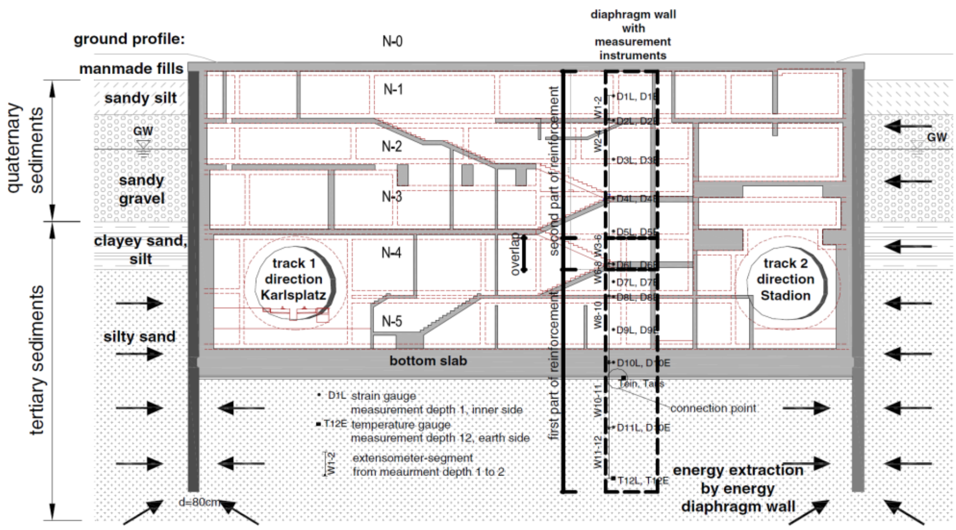

Figure 2.6 Cross section of a typical U2 metro station equipped for geothermal energy use, and monitoring equipment installed in one panel of the diaphragm wall in U2/2 – Taborstraße Station (Brandl, 2006)

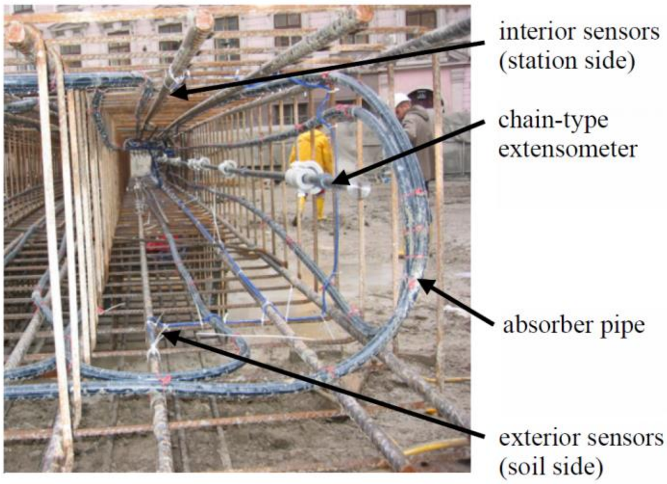

Figure 2.7 Heat exchanger pipe system and monitoring equipment in diaphragm wall reinforcement cage (Markiewicz and Adam, 2006)

2.3.2 Bvlgari Hotel, London – United Kingdom (Amis et al, 2010)

The Bvlgari Hotel project in London is the first one in the UK dealing with energy diaphragm walls. For the realization of the basement of the hotel, that extends for 6 levels underground, to a depth of 25 m under the pavement level, the design defined the construction of a diaphragm wall composed by 39 panels of 800 mm thickness, with the top down method, to be equipped with GSHP system. An additional depth of the diaphragm panel was required to support the high magnitude of the load given by the superstructure, that extends for 10 levels over the pavement level. This increased extension of the wall can be exploited for heat exchange.

In Figure 2.8, a schematic representation of the panel, equipped with the GSHP system, is shown as well as a section with a typical reinforcement and geothermal loop configuration adopted in this project. Taking the experience from previous schemes of pipework installed in piles, designer developed a solution which maximised the ground sourced heating and cooling potential. It can be noticed that adsorbing equipment are installed only in the side of the wall permanently in contact with the ground, on the external face of the reinforcement cage. To accommodate the loops the cover in the soil side was increased. However, no specific details on how this optimizing analysis have been carried out could be found, nor whether numerical analyses have been performed to this purpose.

A two parts study was undertaken to understand the effects of geothermal loops in diaphragm walls.

In particular, it was meant to disclose how thermal conductivity and resistivity change due to excavation of the basement in a diaphragm wall. In Figure 2.9 and Figure 2.10 the conductivity test configurations are shown. The first part of the study was conducted before the excavation. Even though there are no data published from the study, it has been stated that the conservative values of thermal conductivity used in the ground loop design were supported by the outcome of the test. The second part of the study was meant to compare and assess any reduction in the conductivity values due to the excavation, with the purpose to define conductivity parameters to be used in future applications. Nonetheless, these assessments have not been reported yet.

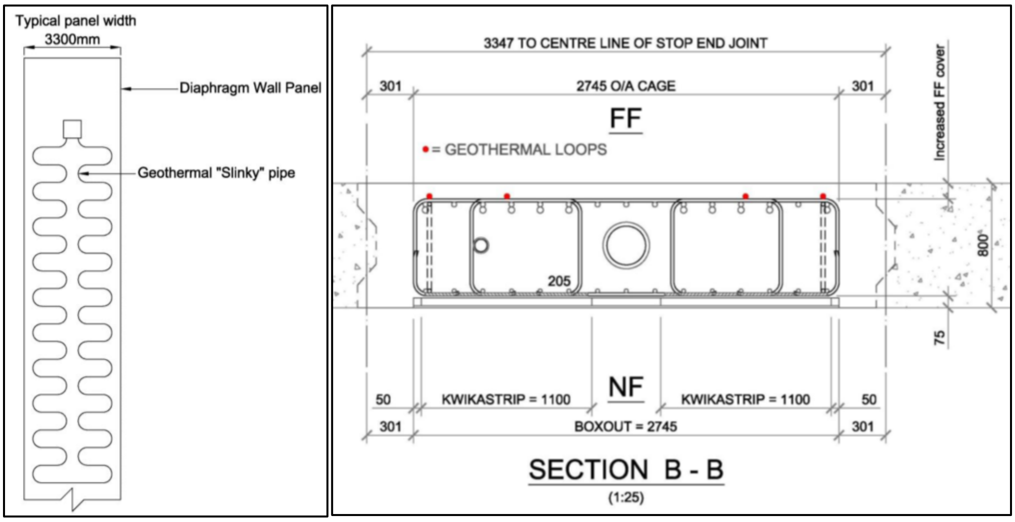

Figure 2.8 On the left, a schematic pipe arrangement in the panel. On the right, a typical reinforcement and geothermal loop configuration in a section of the panel (Amis et al., 2010)

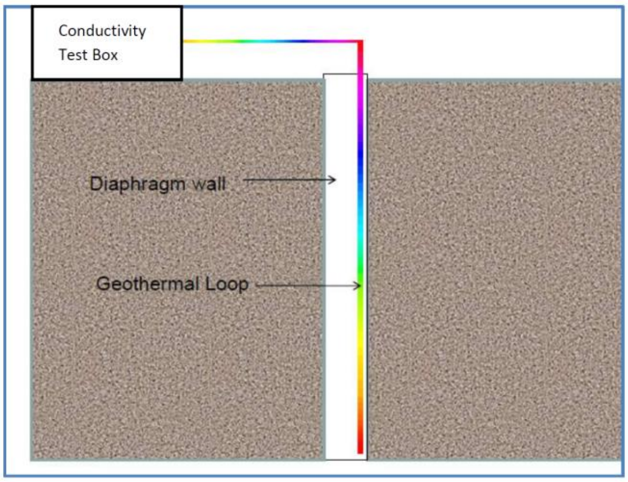

Figure 2.9 Stage one of the conductivity test (Amis et al., 2010)

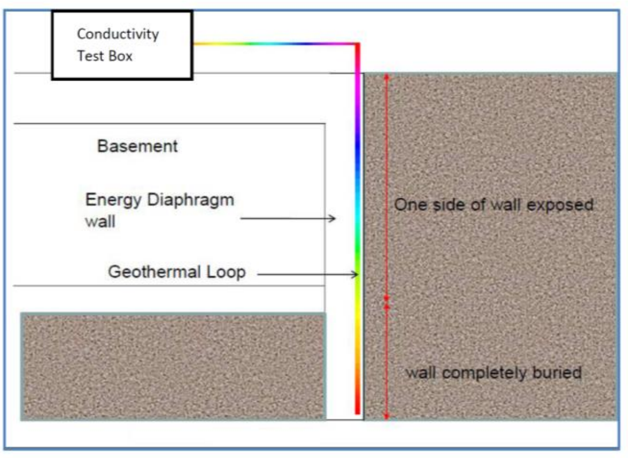

Figure 2.10 Stage two of the conductivity test (Amis et al., 2010)

2.3.3 Shanghai Museum of Natural History, China (Xia et al, 2012)

In the project of the new Shanghai Museum of Natural History a very wide diaphragm wall system was designed. To reduce primary energy consumption, absorber tubes for heat exchange were buried in the concrete elements of the foundations system, as well as in the diaphragm walls of the metro line passing underneath the museum. In those elements, with a depth of 30-38 m, heat exchangers consist in two U-shaped absorber tubes in series connection, one in the earth-contact side, the other in the excavation face. Pipes have 25 mm diameter and 2.3 mm thickness.

To perform an experimental test (TRT - constant temperature method), monitoring sensors were installed in three diaphragm walls. Purpose of the experiment was to evaluate the heat transfer performance according to different configurations of the GSHP system. Varying some influencing factors of heat transfer as it shown in Table 2-1, i.e. heat exchangers type (Figure 2.11), inlet water temperature, water velocity and operation mode, an optimized configuration of the GSHP system for this project was defined, in terms of heat exchange rate.

No.	Influence factors	Factor levels	Other conditions
1	Heat exchanger types	Tubes type (a), (b), (c) (Figure 2.11)	Velocity 0.6 m/s; Inlet temperature 35°C
2	Water velocity [m/s]	0.25, 0.45, 0.6, 0.75, 0.9, 1.05, 1.30, 1.5	Tubes type (b); Inlet temperature 7°C
3	Inlet water temperature [°C]	32.0, 35.0, 38.0	Tubes type (a), (b), (c); Velocity 0.6 m/s
4	Operation modes	Intermittent operation (1:1), Continuous operation	Tubes type (b); Velocity 0.6 m/s; Inlet temperature 35°C

Table 2-1 Experimental schemes of heat transfer test in diaphragm walls (Xia et al., 2012)

The results showed that the heat transfer rate of W-shaped pipework is higher with respect to single U-shaped tube. In addition, enlarging the distance between the branch tubes near the soil face is an effective way to improve the system performance.

Concerning inlet water temperature and velocity, is has been evaluated that heat exchange rate rises with the increasing of the inlet velocity, until a limit of 0.9 m/s, and it changes linearly with the inlet temperature.

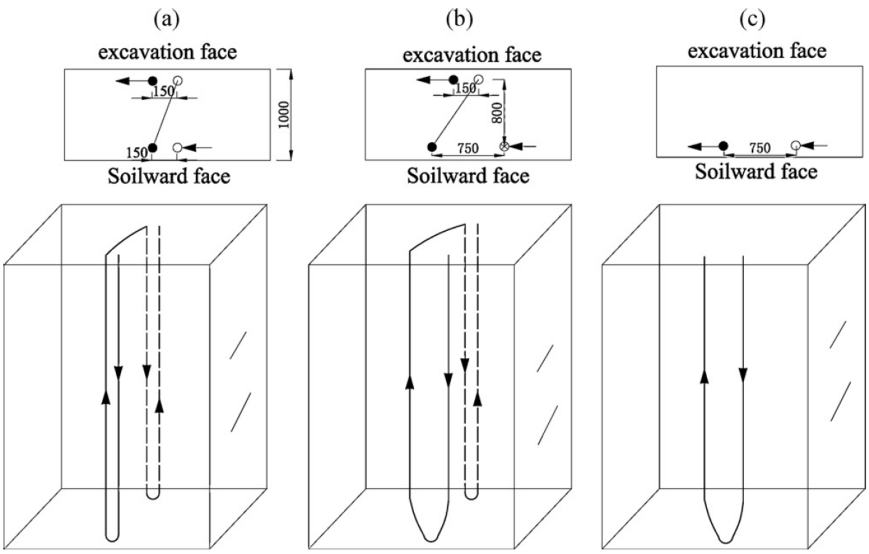

Figure 2.11 Three types of underground heat exchangers investigated (pipe inner diameter, d = 2.04 cm): (a) W-shaped type, (b) improved W-shaped type and (c) single U-shaped type. (Xia et al., 2012)

2.4 Analysis methods for energy walls: Literature Review

Since the ‘90s, several authors started to deal with analyses concerning about energy geostructures, to disclose the influences of the geothermal equipment in the structural element, as well as in the surrounding ground and groundwater.

Bourne-Webb (2013) collected in one work many of these scientific publications with the purpose to provide an overview of the information that is available. However, most of them are referring to energy piles; the knowledge of thermal and thermomechanical performance of thermo-active foundation piles having been deepened over the years.

Otherwise, very little work has been carried out for other energy geostructures. After 2013, a new impulse in this direction has started. Surprisingly, there is a lack of detailed case studies and performance analyses from Austria, Switzerland and Germany, where energy geotechnical engineering originated. Brandl (2006) stated that a value of 30 W/m^2 for the potential heat flow can be used in workability studies for diaphragm and piled walls. Following observations from the Lainzer tunnel showed however that this is achievable only in particular conditions. Therefore, the potential heat exchange must be assessed carefully according to every specific case. Some other authors tried to analyse the energy performance of a diaphragm wall, influenced by different factors.

A finite element analysis was performed by Sterpi et al. (2014). The results show that to optimise heat exchange the ideal layout of the embedded pipework should reduce the development of high temperature gradients between different portions of the tube itself. It is important then to allow for a gradual temperature changes of the fluid, using a slinky pipe arrangement. The same results are obtained in Barla et al. (2017), where a similar analysis was carried out to disclose the optimisation of the loop configuration. In both papers the influence of the heat exchange on the subsoil temperature distribution has been investigated, as well as some possible temporary and permanent effects. The outcome proved the soil to be an efficient heat storage mass, but to avoid long term permanent temperature variations it is necessary to provide a proper balance between the heating and the cooling operating modes throughout the year.

Di Donna et al. (2016) run a parametric analysis for the energy assessment of diaphragm walls with respect to the optimisation of their energy efficiency. It has been stated that pipe spacing is the most influencing factor for short-term concerns, while in the long term temperature difference between the soil and the excavation is the most important element affecting energy efficiency. Some other important considerations concerning the modelling, geometry and boundary conditions, have been presented and they will be reviewed later in this dissertation for the numerical analyses (see Chapter 4).

Xia et al. (2012) presented an experimental study to highlight the influence of different heat exchanger configurations can have on the efficiency of an energy diaphragm wall, referring to the measuring instruments installed in the Shanghai Museum of Natural History. Referring to the same case study, Sun et al. (2013) developed a two dimensional design method for geothermal heat exchanger in diaphragm walls. It seems to have good correspondence with the experimental data, even though plane configuration might be not representative of the real 3D problem (Bourne-Webb et al., 2016). Moreover, the model was tested in short term only, without an appropriate long term analysis, nor an operational validation. Thus, its applicability has some limits.

Concerning thermal only performance, it has been evaluated through numerical computations that the temperature field in the diaphragm wall is uniform around the heat exchange pipes, and the temperature in the diaphragm continuous wall can be considered as constant in the ground (Xia et al., 2014). The temperature stress changed at a small range near the pipes and should be taken into account in the structure analysis, while in the structure far from the absorbers stress field is small and can be neglected (Gong et al., 2015).

From the mechanical point of view, in energy piles equipped as heat exchangers the main concern seems to be the occurrence of the internal stresses that can be induced by external restraints. The same problem can be even worse for diaphragm walls, since they have perhaps more constraints with respect to potential thermally induced movement. Bourne-Webb dealt with this thermomechanical problem.

He reviewed some data from Brandl (2006) that include both mechanical bending strain and thermally induced stain (Bourn-Webb, 2013) and performed some numerical analyses (Bourne-Webb et al., 2015, 2016). The impact of heating/cooling operations on the mechanical performance of the wall proved to be largely benign, since the major changes can be related to climatic variations in the ground and in the external environment that will take place anyway. The same conclusion is reported in Barla et al. (2018), where mechanical effects induced on the wall by its thermal activation are investigated through a numerical analysis. The results show that stress variations computed are largely compatible with strength limits.

Bourne-Webb focused particularly on the conditions of the excavation environment. He ran some numerical simulations using different types of boundary conditions to model the excavation-wall interface that appears to have an important role in heat transfer for these geostructures. He pointed out that applications with "hot" excavation spaces such as rail tunnels and metro station, may be more suitable for heat extraction. This issue has been also confirmed in Di Donna et al. (2016) study. The parametric analysis showed how the temperature different between excavation and soil is the most influencing factor in the long term energy efficiency of diaphragm walls. However, this potentially source of heat may be unfavourable for applications in heat disposal.

It is evident that very little work has been done with respect to preliminary design procedure for energy walls, in terms of energy assessment. It can strongly depend on the specific site ground conditions (both soil and groundwater) and on the intended use of the excavation. The purpose of the following chapters is therefore to analyse the influence of different affecting factors on the energy efficiency of a diaphragm wall and to provide preliminary design charts. A similar study has already carried out for energy tunnels (Di Donna and Barla, 2015), where the extension of the Turin Metro tunnel (Italy) under construction has been considered as reference case for the simulation.

2.5 The role of ground conditions on energy tunnels

Thermo hydraulic properties of the ground, as well as groundwater conditions, have an important role on the exchanged heat of geostructures. With a 3D numerical model of the Turin Metro Line 1 tunnel, it was possible to evaluate how exchanged heat varies under different ground thermo-hydro scenarios. A parametric study was then carried out to assess the influence of the ground conditions on the energy efficiency of energy tunnels, varying the parameters as it follows:

- Ground temperature: 8 – 18°C;
- Groundwater flow velocity: 0 – 2 m/d;
- Thermal conductivity: 0.9 – 3.9 W/mK.

The effect of the affecting parameters was then illustrated in some graphs. In Figure 2.12 the influence of ground temperature on the energy efficiency in winter and in summer is shown. In winter the extracted heat power increases with the increasing of soil temperature, in summer the opposite trend can be noticed. Independently of groundwater flow and thermal conductivity, the exchanged heat shows an increasing by about 25% with respect to the initial value (at T = 8°C) per degree Celsius of soil temperature in winter and a decreasing by about 5% per degree Celsius in summer.

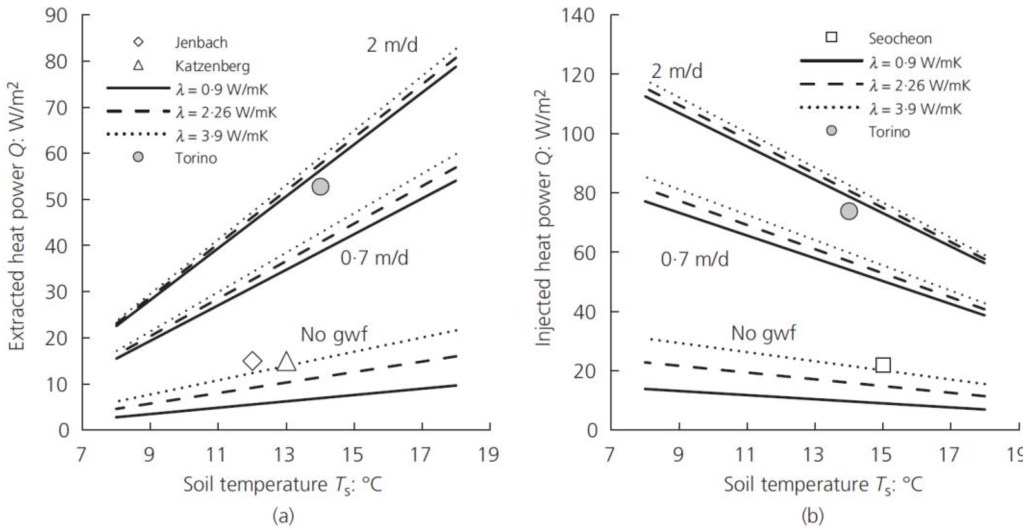

Figure 2.12 Effect of temperature on the energy performance (the numbers near the curves indicate groundwater flow velocities (gwf)): (a) winter mode and (b) summer mode (Di Donna and Barla, 2015)

Figure 2.13 illustrates the effect of groundwater flow velocity on the exchanged heat in summer and in winter. In both cases heat power rises up with the increasing of the velocity of the aquifer. For the same thermal conductivity, the increase in exchanged heat with the increasing of the groundwater velocity is the same with respect to the initial value (i.e. groundwater flow velocity = 0 m/d), irrespective of the ground temperature. For different values of thermal conductivity the rise of heat power is higher with lower values of thermal conductivity, thus when the conductive component is less important.

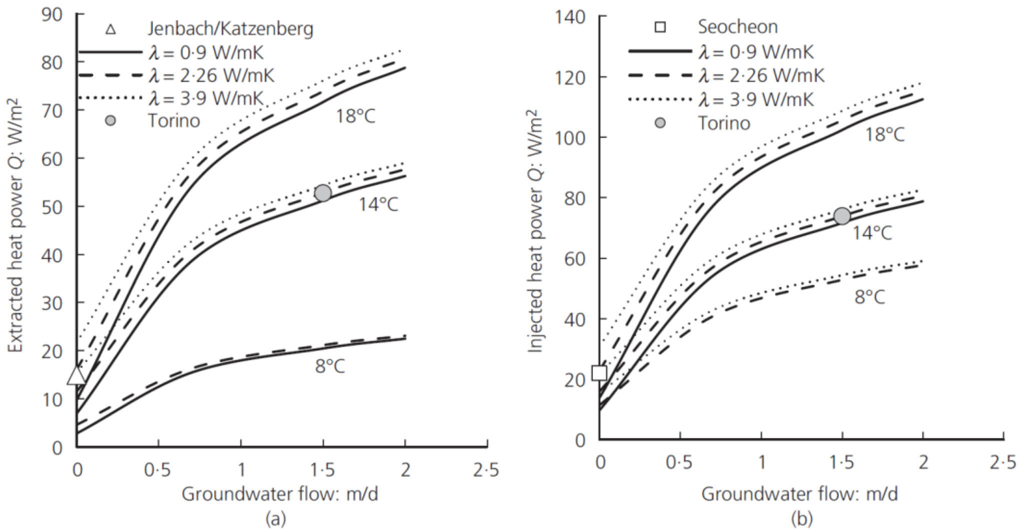

Figure 2.13 Effect of groundwater flow velocity on the energy performance (the numbers near the curves indicate soil temperature (T)): (a) winter mode and (b) summer mode (Di Donna and Barla, 2015)

The results in terms of thermal conductivity are shown in Figure 2.14. As the thermal conductivity grows, exchanged heat increases both in winter and in summer. However, this effect becomes more evident as the groundwater flow velocity reduces. Heat power grows by about 25% with respect to the initial value (λ = 0.9 W/mK) per unit increment of thermal conductivity if no water flow is present and only by 1% in the case of 2 m/d groundwater flow velocity.

In general, the parametric analysis pointed out that in heating mode (winter) high groundwater flow velocity and ground temperature are the more suitable conditions for energy tunnel, in terms of energy efficiency of the geothermal system. Reasonable values of extracted heat vary in the range 10 – 70 W/m^2. In cooling mode (summer), high groundwater flow velocity and colder ground are more convenient, with achievable values of injected heat in the range of 10 – 100 W/m^2.

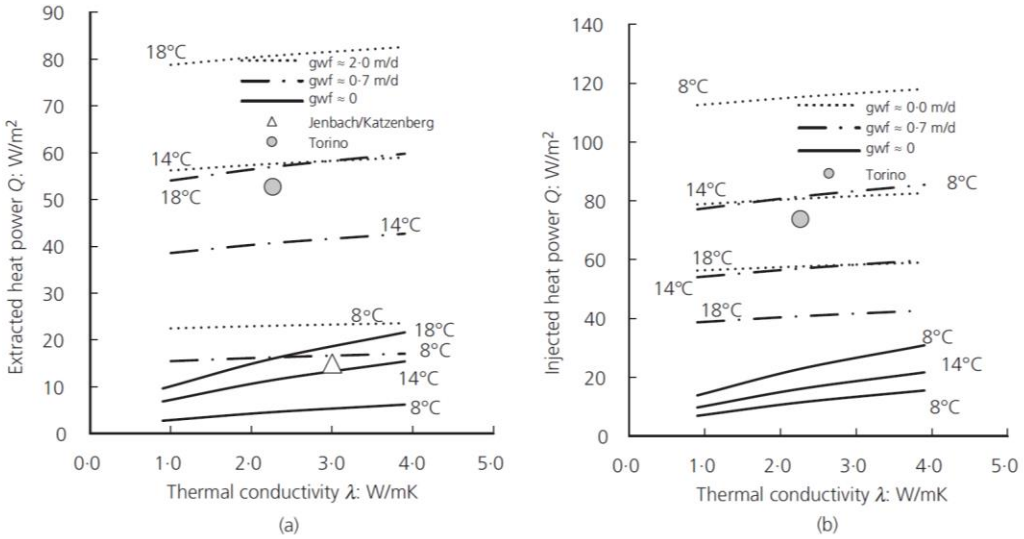

Figure 2.14 Effect of thermal conductivity on the energy performance (the numbers near the curves indicate soil temperature (T)): (a) winter mode and (b) summer mode (Di Donna and Barla, 2015)

3. THE NUMERICAL MODEL

The study of energy geostructures involves different processes at the same time. Dealing with heat flux, often groundwater flow cannot be neglected and both thermal and hydraulic processes have impacts on the mechanical behaviour of the earth-structure system. This is the reason why it is usually referred to be a thermo hydro mechanical (THM) problem. A fully coupled analysis can be remarkably complicated, therefore it is often convenient to uncouple the problem to simplify the computation. Anyhow, analytical solutions are not achievable, thus numerical methods are used to solve these systems and they are introduced in Chapter 3. To simulate the operation of a GSHP system, a thermo-hydraulic (TH) approach can be appropriate. This formulation, presented in the Chapter 3.2, is implemented in the finite element package FEFLOW. The software has been selected to evaluate the efficiency of energy walls through a parametric analysis. Thus, in Chapter 3.3 the principles of the code are reviewed and a validation analysis is performed to assess the appropriateness of its use.

3.1 The finite element method

As it often happens in engineering applications, the set of differential equations defining a thermo hydro mechanical problem cannot be easily solved through analytical solutions. When it is not possible, in issues of practical concern approximate solutions may be found using computer based numerical methods. In this field, the finite element method (FEM) can be considered as the leading mean for analysis of complex systems.

In the finite element method the problem domain is subdivided into discrete elements which provide a physical approximation to the continuity of some quantities, e.g. temperature and pressure head, within the continuum. The governing equations are written and solved exactly for points, or nodes, at which adjacent elements are connected, in terms of a principle variable. Within every single element, the variable is then computed by approximating functions, the so called shape functions. Thus, the finite element method gives an exact solution to a differential approximation of the problem.

Some steps have to be followed to get to a FE solution. At the beginning it is requested to pass from the real model to the discretised one through a mesh generation. This means that the whole domain of our geotechnical model has to be subdivided into small regions, i.e. finite elements. The propriety of the mesh is of fundamental importance because mesh generation plays a great role in the computed solution. It is then necessary to define the primary variable and how it should vary over a finite element.

It is frequently a polynomial law and the higher the polynomial degree, the better the approximation. Then, element equations can be derived and combining them it is possible to form the global equations. They can be modified introducing boundary conditions that are indispensable to solve the equations system. They can specify the values in which a solution is applied within the boundary of the domain, in terms of a function (Dirichlet or first-type BC), its derivative (Neumann or second-type BC) or both (Cauchy BC or third-type BC). Finally, the solution at the nodes can be determined in terms of the principle variable, from which secondary quantities can be derived.

In a THM problem, equilibrium equations have to be defined, as well as compatibility equations and constitutive laws for the mechanical analysis. Hydraulic process in porous media are governed by mass conservation equations and Darcy's velocity law. Heat transfer is controlled instead by energy conservation equations. A schematic representation of a THM problem is shown in Figure 3.1: besides the definition of the whole set of equations, it is necessary to determine several additional properties and parameters to characterise the materials involved.

To focus on some specific aspects regarding a GSHP system, such as energy efficiency, an uncoupled approach (TH) can be used to simplify the calculations.

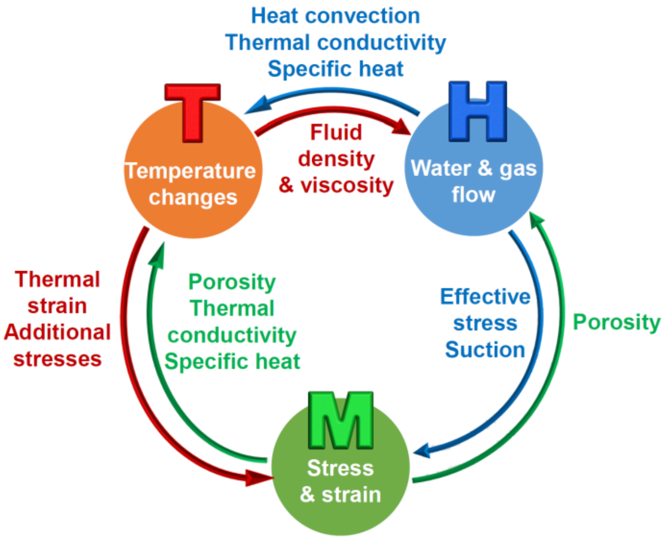

Figure 3.1 Schematic representation of a thermo hydro mechanical coupled problem

3.2 Thermo hydro (TH) coupling problem

In thermo hydraulic coupled problem, the simultaneous action of both fluid and heat transport is investigated. Dealing with porous media such as the ground, the equations that govern the problem are:

- The mass conservation equation;
- The Darcy's law;
- The energy conservation equation.

3.2.1 Hydraulic process

The principle of the mass conservation states that the rate of change of water mass over time equals water inflow minus outflow for a unit control volume, as it is expressed by the equation:

$$\frac{\partial}{\partial t}(n\rho_w S) = -\nabla(\rho_w \boldsymbol{v}) - \rho_w w \tag{1}$$

where

- t: time;
- ∇: divergence and ∂: time derivative;
- $\boldsymbol{v}$: water velocity in m s^{-1};

- ρ_w: water density in kg m^{-3};
- n: ground porosity and S: degree of saturation;
- w: source term in s^{-1} (injection/extraction of water volume per unit volume of porous medium per unit time).

In shallow geothermics with restricted temperature changes, temperature dependence of water density can be disregarded. If we assume w null and saturated soil ($S = 1$), the equation simplifies:

$$-\nabla \boldsymbol{v} = \frac{\partial n}{\partial t} \tag{2}$$

Flow in saturated porous media with constant water density is usually described by Darcy's law. It states that the flow rate is proportional to the head gradient and Darcy's postulation is:

$$\boldsymbol{v} = -\boldsymbol{K}\nabla h \tag{3}$$

where

- h: hydraulic head in m, defined as: $h = z + \frac{p}{\rho_w g}$;
- z: elevation in m and p: pressure in Pa;
- ρ_w: fluid's density in kg m^{-3};
- ∇: gradient operator;
- $\boldsymbol{K}$: hydraulic conductivity in m s^{-1}.

Hydraulic conductivity **K** usually exhibits strong spatial variability due to non-homogeneity of porous media. Moreover, it may show a directional behaviour thus causing anisotropic conditions. Such conditions prevail in aquifers where horizontal layering is observed, thus reducing the hydraulic conductivity components to two, the horizontal and vertical hydraulic conductivities.

Combining the two previous equations we can obtain:

$$\nabla \cdot (\boldsymbol{K}\nabla h) = \frac{\partial n}{\partial t}. \tag{4}$$

3.2.2 Heat transfer process

Concerning to energy conservation, it is necessary to recall that heat transport can occur through three main mechanisms: conduction, convection and radiation.

The third one, that is basically heat transmission through electromagnetic waves, can be neglected when dealing with shallow geothermal energy. Temperatures involved are quiet low and energy radiated is proportional to the fourth power of the absolute temperature (Stefan-Boltzmann, 1884):

$$E = \sigma T^4 \tag{5}$$

where:

- E: energy radiated in W m^{-2};
- σ: Stefan-Boltzmann constant (5.67×10^{-8} W m^{-2} K^{-4});
- T: temperature, in K.

Otherwise, heat conduction is the main mechanism and it describes the process by which heat diffuses through a solid, liquid or gas by processes of molecular interaction. It occurs when there is contact between two bodies at different temperature, and it is strictly linked to thermal conductivity. It describes how good the medium is at conducting heat. Typical values for rocks and other geological materials stay in the range 1 – 3 W m^{-1} K^{-1}. Heat transfer can be defined as Fourier's law statement:

$$q_{cond} = -\lambda \nabla T \tag{6}$$

where:

- q_{cond}: heat transfer by conduction in W m^{-2};
- λ: thermal conductivity in W m^{-1} K^{-1};
- ∇T: temperature gradient in K.

Convection is not negligible in media characterised by high permeability in presence of fluid. Fluids such as water store heat, thus moving water means moving heat.

In this case heat transfer can be considered as:

$$q_{conv} = c_w \rho_w \boldsymbol{v} \Delta T \tag{7}$$

where:

- q_{conv}: heat transfer by convection in W m^{-2};
- c_w: water specific heat capacity in J kg^{-1} K^{-1};
- ρ_w: water density in kg m^{-3};
- $\boldsymbol{v}$: water velocity in m s^{-1};
- ΔT: temperature difference in K.

The principle of energy conservation states that the rate of change of energy content equals the energy inflow minus the outflow over a unit control volume increased by the energy production in that volume. Assuming that the mean temperatures of the water and the solid phase are the same within the control volume, the energy balance for a unit volume of saturated porous medium can be formulated as:

$$c\rho \frac{\partial T}{\partial t} = \nabla \cdot (\lambda \nabla T) - c_w \rho_w \nabla \cdot (\boldsymbol{v}T) \tag{8}$$

- $c\rho \frac{\partial T}{\partial t}$: heat storage in transient regime;
- $c\rho$: heat capacity of the ground, including solid (s) and water (w) values following the expression: $c\rho = nc_w\rho_w + (1-n)c_s\rho_s$; (8a)
- λ: thermal conductivity of the ground, including solid (s) and water (w) values following the expression: $\lambda = n\lambda_w + (1-n)\lambda_s$. (8b)

3.3 Finite element based software FEFLOW

FEFLOW code is a finite element based software that allows geotechnical modelling analyses involving complicated conditions, such as groundwater flow, contaminant, groundwater age and heat transport simulations. Thus, FEFLOW software has been selected to the development of this project and in the following chapters its features and functioning will be described, carrying on a validation analysis. In the software the thermo-hydro mathematical formulation implemented is implemented by the following equations (Diersch, 2009), being the previous ones of a more general nature. They are written in the Eulerian coordinate system for a saturated medium composed of a solid skeleton and a liquid (water) phase.

- The mass conservation equation

$$S\partial_t p - n\beta_w \partial_t T + \nabla \cdot (nv_{w,i}) - nv_{w,i}\beta_w \nabla T = 0 \tag{9}$$

where ∂_t, $\nabla \cdot$ and ∇ denote the time derivative, the divergence and the gradient operators respectively; $S = [nY_w + (1-n)Y_s]$ is the specific storage coefficient; n is the porosity; Y_w and Y_s are the water and the solid compressibilities respectively; p is the pressure; β_w is the water thermal expansion coefficient; T is the temperature; $v_{w,i}$ is the vector of water velocity with respect to the solid skeleton.

- Darcy's velocity ($v_{f,i}$) law

$$v_{f,i} = nv_{w,i} = -\frac{\boldsymbol{k}_{ij}\rho_w \boldsymbol{g}_i}{\mu}\nabla h = -\boldsymbol{k}_{ij}\nabla h \tag{10}$$

where $\boldsymbol{k}_{ij}$ is the intrinsic hydraulic conductivity tensor (expressed in square metres), ρ_w is the water density, $\boldsymbol{g}_i$ is the gravity vector, μ is the water dynamic viscosity and h is the hydraulic head defined as

$$h = \frac{p}{\rho_w \boldsymbol{g}_i} + z \tag{11}$$

where z is the vertical coordinate.

- The energy conservation equation

$$[n\rho_w c_w + (1-n)\rho_s c_s]\partial_t T + n\rho_w c_w v_{w,i}\nabla T - \nabla \cdot \left(\lambda_{ij}\nabla T\right) = 0 \tag{12}$$

where c_w and c_s are the water and solid phase heat capacities and ρ_s is the solid phase density. The term λ_{ij} includes the heat conduction and the dispersion components as

$$\begin{aligned}\lambda_{ij} &= [n\lambda_w + (1-n)\lambda_s]\delta_{ij} \\ &+ \rho_w c_w \left[\alpha_T\sqrt{q_{f,i}q_{f,j}}\delta_{ij} + (\alpha_L - \alpha_T)\frac{q_{f,i}q_{f,j}}{\sqrt{q_{f,i}q_{f,j}}}\right]\end{aligned} \tag{13}$$

where λ_w and λ_s are the water and solid phase thermal conductivities, δ_{ij} is the Kronecker delta, α_T and α_L are the transverse and longitudinal thermo dispersivities respectively and $q_{f,i}$ is the fluid flux along direction i.

3.3.1 Model validation

Whilst dealing with numerical analysis, it is important to validate the model with respect to real data, to confirm the appropriateness of the results. Few experimental data exist in the literature concerning energy diaphragm walls. During the construction of the Shanghai Museum of Natural History an experimental test (TRT – constant temperature method) was carried out and the obtained results are shown in Xia et al. (2012). This case study, in particular experimental scheme 1 and tube layout (c) in Table 2-1 in Chapter 3, will be re produced in a FEFLOW model and the numerical outcomes will be compared with the experimental data for the validation assessment.

The thermo activated element is shown in Figure 3.2: a 38 m depth energy diaphragm wall with a 18.5 m excavation, 2.25 m width and 1 m thickness. The model is 40 m high, 10 m long and 2.25 m wide and it is composed of 178 290 nodes, 318 258 triangular prismatic six-node elements. For 3D models, FEFLOW applies a layer-based approach. The triangular mesh is extended to the third dimension by extruding the 2D mesh, resulting in prismatic 3D elements. In FEFLOW terminology, all vertically adjacent 3D elements comprise one layer, while a slice is either the interface between two horizontally adjacent layers. All mesh nodes are located on slices.

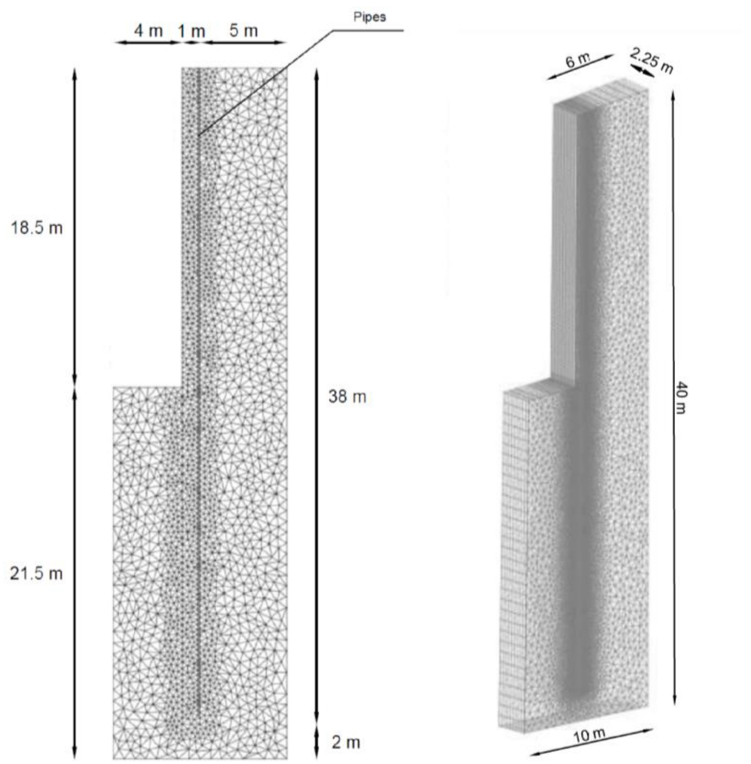

Figure 3.2 2D (on the left) and 3D (on the right) finite element model of the validation test

The temperature of the external air and of the soil, measured before the test, were 10.6°C and 16.3°C respectively. The average temperature of the wall was 23°C. According to the information given in the paper, constant external air temperature has been fixed on the top boundary, excavation plane and the right side of the wall, towards the excavation. As it is shown in Figure 3.3, on the bottom, right and left boundaries constant soil temperature has been applied. To have no groundwater flow in the simulation, it is necessary to impose the same hydraulic head on the right and the left boundaries of the model.

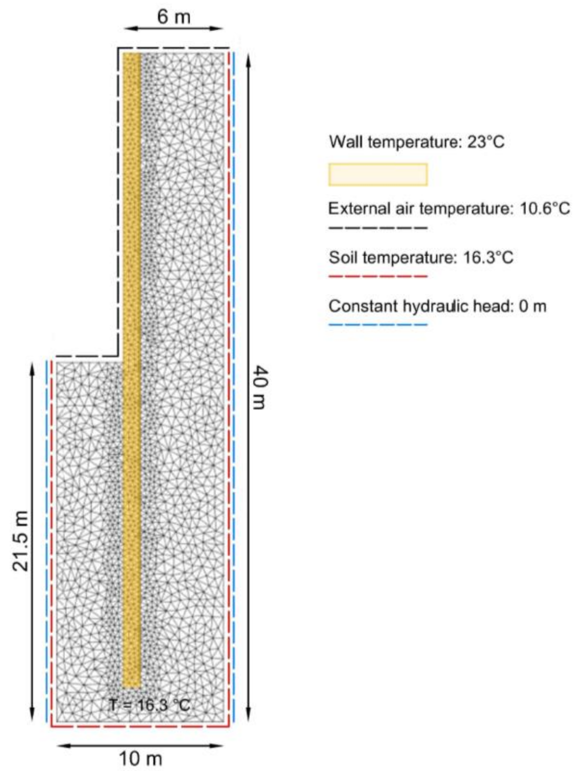

Figure 3.3 Boundary conditions adopted in the validation analysis

The configuration of the pipework embedded in the wall is represented in Figure 3.4. The U-pipe equipment is installed on the soil side only, with a spacing of 75 cm and a concrete cover of 10 cm. The pipe extends along the depth of the wall until about 0.5 m from the bottom. It has an external diameter of 25 mm and a thickness of 2.3 mm.

In FEFLOW it is possible to model the pipework through special one dimensional elements, called “Discrete Features”. The user can choose between three different flow laws:

- Darcy, that describes the flow of a fluid through a porous medium.
- Hagen-Poiseuille, that describes the laminar flow of a Newtonian fluid through a long cylindrical pipe of constant cross section.
- Manning-Strickler, that is an empirical formula estimating the average velocity of a liquid flow in open channels or in partially full conduits.

To represent the water circulating in the GSHP loop, Hagen-Poiseuille law is the most suitable. In these elements, the thermal resistance of the plastic pipes is neglected.

However, the error that occurs in making this assumption has been proved to be very small and good results can be obtained, in agreement with analytical solutions (Diersch, 2009).

In Diersch (2009) it is possible to find the complete formulation implemented in the software for the Hagen-Poiseuille law in the “Discrete Features”.

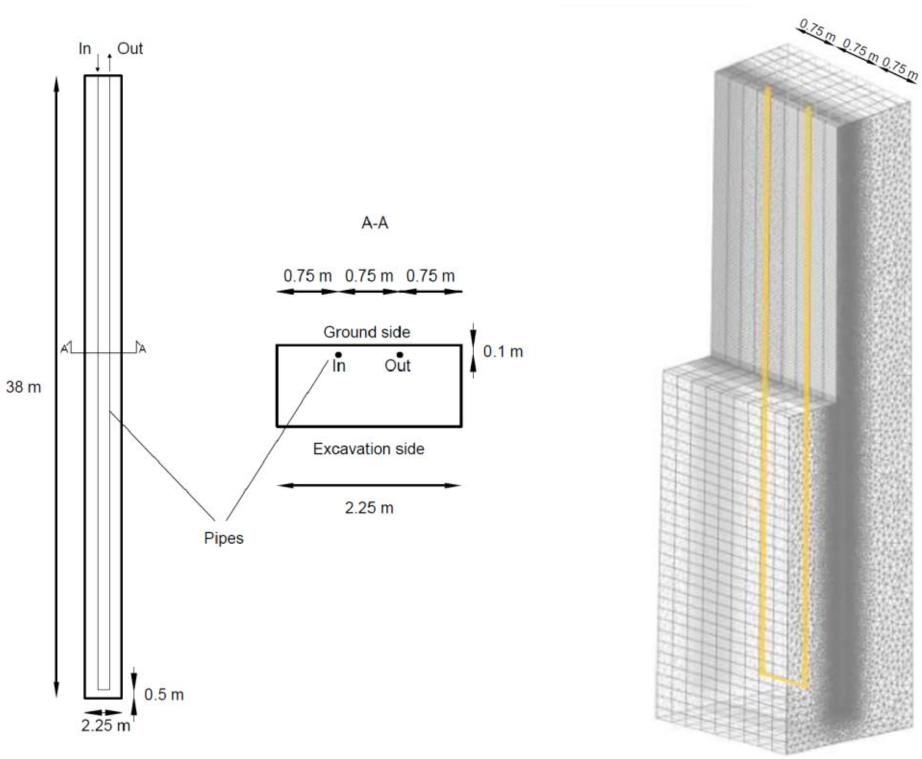

Figure 3.4 Geometry and pipe configuration of the wall for the validation test (the third dimension has been stretched for a clearer representation)

For the axisymmetric flow in a circular tube (Figure 3.5), the average velocity for the Hagen-Poiseuille law is:

$$v_z = -\frac{r_{hydr}^2}{2\mu}\left(\frac{dp}{dz} - \rho g_z\right) \tag{14}$$

where:

- v_z: velocity of the fluid along z-axis in m s^{-1};
- r_{hydr}: hydraulic radius in m;
- μ: viscosity of the fluid in Pa s;
- p: fluid pressure in Pa;
- ρ: fluid density in kg m^{-3} and g_z: gravity along z-axis in m s^{-2}.

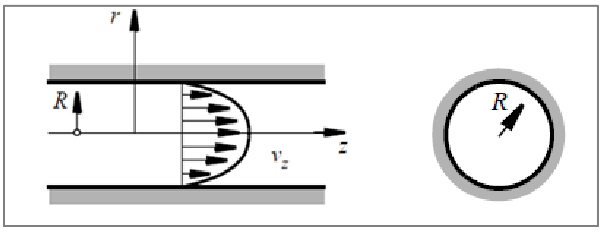

Figure 3.5. Axisymmetric Poiseuille flow

The hydraulic radius is defined as the flow cross-sectional area divided by the wetted perimeter and for a circular tube with radius R (Figure 3.5) it is defined as:

$$r_{hydr} = \frac{\pi R^2}{2\pi R} = \frac{R}{2} \tag{15}$$

Therefore, it is required to assign some geometrical features to the 1D elements (Table 3-1) and the thermal properties of the carrier fluid circulating in the pipes (Table 3-2). Thermo-hydro properties used to characterise the ground, the wall and the pipework are shown in Table 3-2.

External diameter, d [mm]	25
Tube thickness, s [mm]	2.3
Effective section, A [mm^2]	326.8
Hydraulic radius, r_{hydr} [mm]	5.1

Table 3-1 Pipe geometrical properties

To simulate the fluid circulating in the pipes, a fluid velocity of 0.6 m/s has been fixed on the inlet and outlet points in the model (negative value for the entrance, positive for the exit). These significant points are identified as "Observational Points": with this function of the software it is possible to record and monitor data from the calculation (e.g. local temperature and pressure) as the computation proceeds. It is important to check the pressure in these points, since it can indicate the possible presence of errors (usually a bad connection between the *discrete elements* of the pipe loop).

Property	*Concrete*	*Soil*	*Pipework*
Bulk thermal conductivity, λ [W/(mK)]	2.3	1.74	0.58
Bulk specific heat capacity, c [J/(kgK)]	1 046	1 690	4 200
Bulk density, ρ [kg/m^3]	2 500	1 800	1 000
Porosity, n [-]	0	0.25	-
Specific storage, S [1/m]	10^{-4}	10^{-4}	10^{-4}
Hydraulic conductivity, K_{ij} [m/s]	0	10-4	-
Longitudinal dispersivity, α_L [m]	-	5	1
Transversal dispersivity, α_T [m]	-	0.5	-

Table 3-2 Properties of materials involved in validation analysis (Di Donna et al., 2016)

To apply thermal proprieties of the soil, the software requires a distinction between the solid phase and the fluid phase and their values (Table 3-3) can be obtained from the bulk values through the equations (8a) and (8b) in Chapter 3.2.2.

Property	*Water*	*Solid*
Thermal conductivity, λ [W/(mK)]	0.65	2.10
Heat capacity, cρ [MJ/(m^{3}K)]	4.2	2.65

Table 3-3 Properties of the fluid phase and the solid phase of the soil

The test was carried out for three days. A constant inlet temperature (T_{in}) of 35°C is applied at the inlet point and outlet temperatures (T_{out}) are the outcomes of the calculation, shown in Figure 3.6.

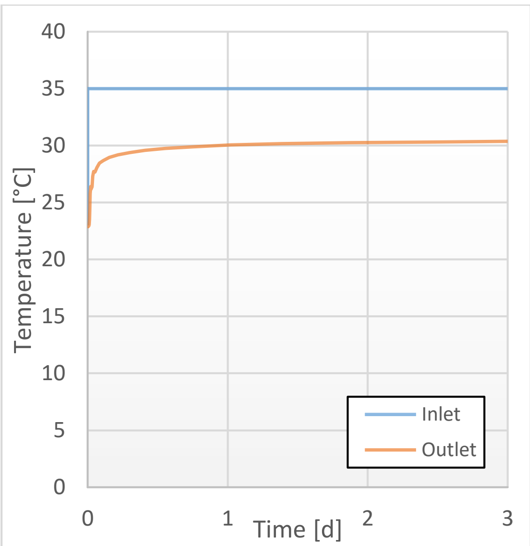

Figure 3.6 Imposed inlet and computed outlet temperatures for the validation model

From these values it is possible to get the exchanged power Q (measured in W) with the formulation:

$$Q = mc_w \cdot (T_{in} - T_{out}) \tag{16}$$

where m is the mass flow rate in the pipe, defined as: $m = A \cdot v \cdot \rho$ in kg/s. The results are then compared with the experimental data in Figure 3.7. The heat exchange rate, q [W/m], is expressed in terms of heat transfer per unit pipe length against time.

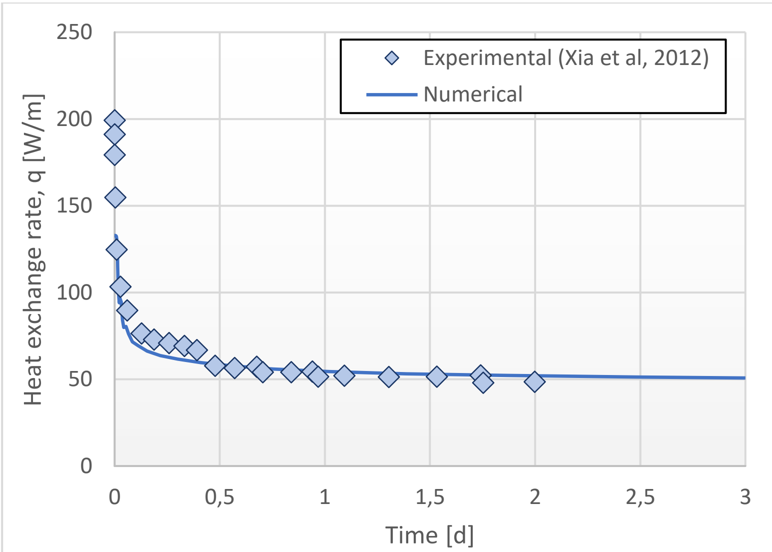

Figure 3.7 Validation of numerical approach

The domain borders (size 40×10×2.25 m) were proved to be far enough not to affect the results. As it is shown in Figure 3.8, heat transfer process around the wall does not influence the initial fixed temperature of 16.3 °C at the edges of the domain.

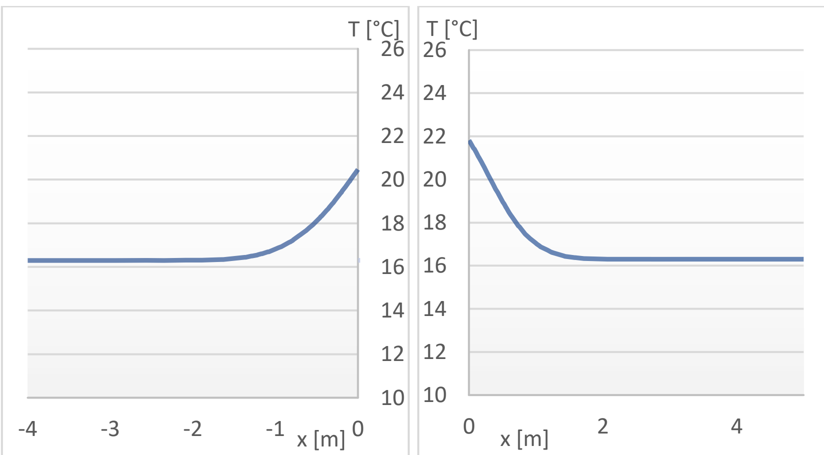

Figure 3.8 Variation of the temperature throughout the domain. The origin of the x-axis is fixed at the border of the wall.

The discretisation plays an important role in the simulation, therefore a mesh sensitivity analysis has been carried out.

The area around the pipes is the most sensitive, because the temperature gradient is higher. As it is illustrated in Figure 3.9, to reduce the oscillations in the very first time steps of the calculation it was required to increase the mesh density around the heat exchangers, while in long terms convergence is reached. In Table 3-4 details of the different types of mesh adopted are listed. The target element size is the size that has to be obtained in critical regions, while the gradation of the refinement defines the rapidity of the increased density around them. The higher is the grade, the smoother is the variation of the elements size while the target size is reached.

N° Mesh	*Gradation of refinement*	*Target element size [m]*	*N° elements per layer*
1	4	0.4	5 695
2	6	0.2	13 421
3	8	0.1	35 362

Table 3-4 Different mesh refinements for the model

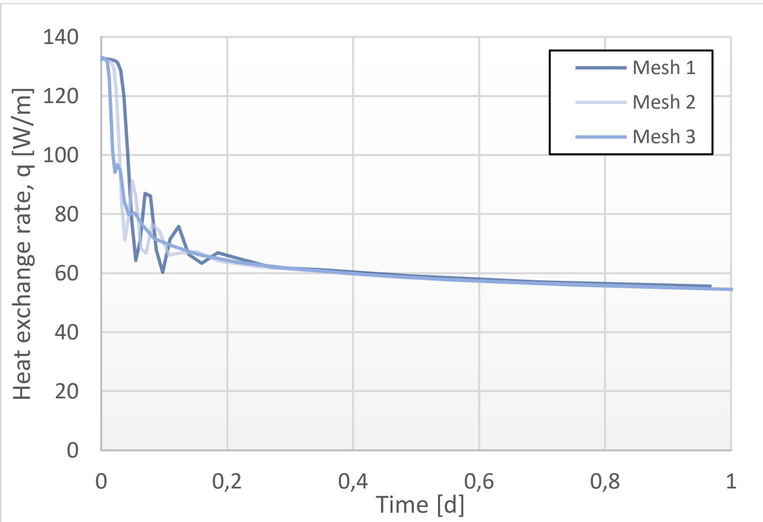

Figure 3.9 Comparison between the results for different types of the mesh, defined in Table 3-4 (the time in the x-axis stops at 1 day to clearly appreciate the very early results of the analyses).

The discretisation along the third dimension proved to be the most influencing feature in the model validation. It consists in subdividing the extension, 2.25 m, in a number of layers and slices, defined in terms of spacing between slices. In Figure 3.10 the comparison between different values of the spacing between slices are shown and the variability can be easily appreciated.

The solution with a spacing of 0.25 m well reproduces the experimental data and does not show high fluctuations. While further increasing the density of elements in the third dimension, in terms of spacing between the slices, the heat exchanged rate keeps lowering down, without reaching convergence in the simulations results. Moreover, oscillations in the very first values are larger as the discretisation increases. This can be explained with a bad configuration of the mesh that occurs when the size of elements is reduced only in one direction. Refining the mesh only in one dimension leads to distorted triangular elements that have to be avoided. Around the pipe the element size in the plane is about 0.1 m, while at the edges of the domain it has an averaged value of 0.6 m. Thus, a spacing in the third dimension of 0.25 m can be a reasonable agreement and it will be adopted in the parametric analysis as first setting for the model. However, it will be checked again for mesh sensitivity since it proved to significantly influence the results.

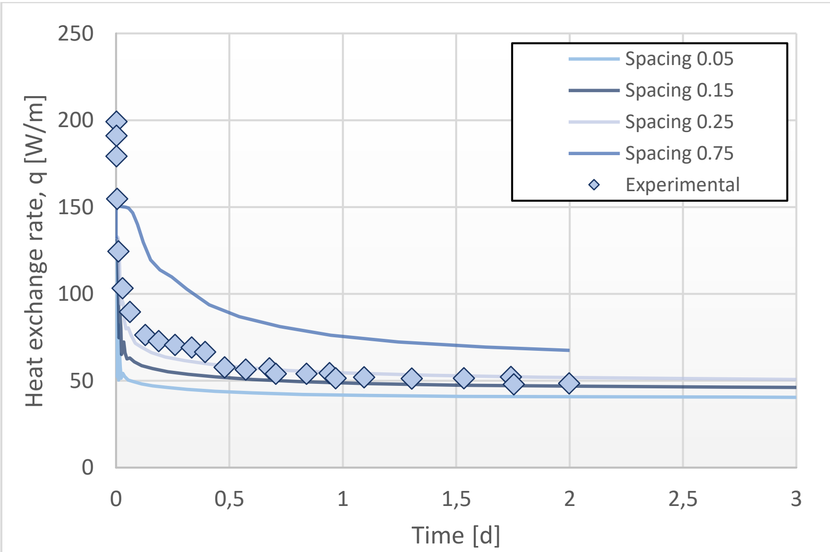

Figure 3.10 Comparison between the results for different discretisations in the third dimension, in terms of spacing [m] between the slices

4. PARAMETRIC ANALYSIS

In this dissertation a parametric analysis will be performed to assess the influence of the ground conditions on the energy efficiency of diaphragm walls. It is important therefore to define the geometry of the problem, as well as the boundary conditions and the properties of the materials involved. Since it is not dealing with an existing case nor a specific project, the purpose of the next chapters is to collect information from previous examples of energy diaphragm walls and GSHP systems (real or numerically simulated) and represent a general model for the successive calculations. In accordance with Di Donna and Barla (2016) that deals with energy tunnels, ground conditions of Torino (Italy) will be taken into account as reference case. Considering that, it will be possible to have a comparison between results obtained for thermo active tunnels and diaphragm walls.

Two preliminary distinctions have to be made whilst dealing with GSHP equipped diaphragm walls. These energy geostructures are in contact with the ground on one side, while they are exposed to the excavation air for some of their total depth on the other side. Heat exchange performance can be significantly affected by the excavation conditions that play an important role (Bourne-Webb et al., 2016 and Di Donna et al., 2016). It is then fundamental to understand how heat exchange can occur on that face and to correctly reproduce it in the numerical model. In this report distinct parametric analyses will be performed with two different types of boundary conditions adopted to the wall-excavation side: heat transfer flux or constant temperature (see Chapter 4.3).

The other important element in the heat exchange performance is the presence of groundwater flow. It is well known that heat efficiency significantly increases thanks to the convective contribution of water flow. Diaphragm walls are shallow structures and it is quite unlikely for them to be completely below the water table. It might be interesting to evaluate how changing the water table level can influence the results in term of energy efficiency. In this study, to reduce the affecting variables in the analyses, one case only will be considered. The whole domain of the model will be completely saturated, with groundwater table at the surface. Since water flow significantly influences the energy transfer process, the velocity of groundwater will vary in the parametric analysis (see Chapter 4.2.2).

4.1 Thermo active diaphragm wall

4.1.1 Geometry

From literature, the geometry of a generic diaphragm wall, shown in Figure 4.1, can be deduced. In Table 4-1 some geometrical characteristics of existing constructed cases of energy walls are listed. Typical depths vary in the range of 10 – 40 m, while thickness is usually 0.8 – 1.2 m (Di Donna et al., 2016). Thus, the mean values have been selected for the model, 20 m depth and 1 m thickness (*D* and *W* in Figure 4.1, respectively).

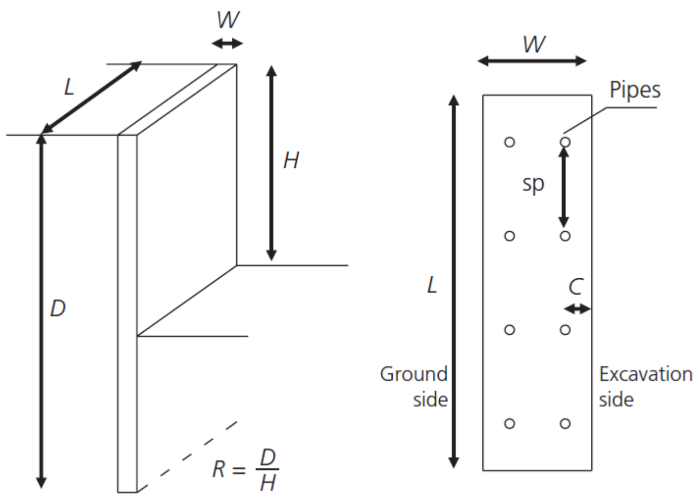

Figure 4.1 Geometry parameters (Di Donna et al., 2016)

Case and source	*Wall depth, D [m]*	*Embedment depth, D-H [m]*	*Panel width, W [m]*
U2 Taborstrasse Station, Vienna (Brandl et al., 2010; Markiewicz, 2004)	31	10.45	0.8
Shanghai Museum of Natural History (Sun et al., 2013; Xia et al., 2012)	30-38	12-20	1.0
Bvlgari Hotel, London (Amis et al., 2010)	Up to 36	11.65	0.8
Dean Street Station, London (Rui, 2014)	41	12	1.0
Tottenham Court Road Station, London (TRT data)	15.3	8.7	1.0
Moorgate Shaft, London (*source not available*)	48.5 to 52.4		1.2
Arts Centre, Bergenz, Austria (Brandl, 1998)	Up to 28	Up to 17	0.5 to 1.2

Table 4-1 Geometric information from constructed energy diaphragm walls (reviewed from Di Donna et al., 2016)

This type of retaining geostructures are characterised by a portion of the whole length exposed to the air of the excavation environment. Di Donna et al. (2016) highlighted that the ratio between the panel height and the excavation depth (R in Figure 4.1) has not a main role in the energy performance of the system. The choice then was made for simplicity to be $R = 2$, i.e. $H = 10$ m.

As it is shown in Table 4-2, the variability of L, length of wall panels is about 1 – 4 m. It has to be noticed however that the lowest values (1 – 1.5 m) have been used for generic numerical simulations, where the size of the model can strongly affect the complexity and the duration of the computation. It is possible to reduce the length of the panel when the pipe configuration is symmetric. For real applications of diaphragm walls bigger values (2.25 – 4 m) are used, being unlikely to be designed based on energy considerations. For the parametric analysis a 2.5 m length panel has been modelled.

After all these observations, in Figure 4.2(a) the designated geometry of the diaphragm wall is represented.

Case and source	*Panel length, L [m]*
Shanghai Museum of Natural History (Xia et al., 2012)	2.25
Bvlgari Hotel, London (Amis et al., 2010)	3.9
Tottenham Court Road Station, London (TRT data)	3.25
Underground car park, Torino (Di Donna, 2016)	2.5
Residential building, Varese, Italy (Mauri and Sterpi, 2015)	2.4
General numerical analysis:	
Sterpi et al., 2014	1.2
Mauri, 2014	1.2
Callagaro, 2017	1.0
Di Donna et al., 2016	1.5

Table 4-2 Panel length values adopted in previous studies

4.1.2 Pipes configuration

The shape of the pipework installed in energy walls are quite standards and from literature the U-shape (single or in a double W-shape) can be defined to be the most common. In the majority of previous works, for example Mauri (2014), Di Donna et al. (2016), Markiewicz (2004) and Xia et al (2012), the authors considered this loop system type. However, it can be noticed that in some cases (Sterpi et al, 2014, Amis et al., 2011, Di Donna, 2016, Barla et al., 2017) a "slinky" shape of the tube system has been chosen after optimisation analyses. Sterpi et al. (2014) justified this result with evidences coming out from a numerical analysis, stating that it possible with this configuration to reduce gradients of temperature between successive portions of the pipe itself.

In Amis et al. (2011) the constructed case of the Bvlgari Hotel was described and the choice of the pipe configuration was justified through an optimisation study, as well as in Di Donna (2016) where a real (but not yet constructed) energy wall is modelled and studied. The limits for this type of tube arrangement are only of practical concern. In particular, slinky pipework is practicable only if there are no cage joints, otherwise fusion weld is required to join the pipes every cage splice. Therefore, as a result of a compromise between construction feasibility and optimization of heat exchange, the U-shape configuration is still the most common and it has been selected for this analysis.

Moreover, a single U-shape configuration allows a reduction of the panel length, due to symmetry. However, a double W-shape will be adopted in this report to take into account a total length of the pipe of about 80 m, typical for these applications.

Even though some previous studies indicated that installing heat exchangers also on the excavation side can be useful (Di Donna et al., 2016 and Xia et al., 2012), in this numerical simulation it has been chosen not to consider the pipework on the external face. This arrangement might enable a bigger heat extraction exploiting the excess of temperature in the excavation environment but this can be a downside for heat injection. The geothermal loop will be considered on the sideward only side, consisting in tubes of 25 mm external diameter and 2.3 mm thickness. It is then important that heat absorbers are installed as close as can be practically achieved to the soil. Thus, the concrete cover will be 50 mm.

The pipe spacing proved to have a main role in the energy performance (Di Donna et al., 2016) and in particular reducing the distance between tube branches is a good way to improve the heat exchange rate. This might disagree with Xia et al. (2012) where it has been showed that enlarging the spacing can be effective. However, in that case study the authors considered a tube configuration installed on both sides of the wall during an in-situ test, while Di Donna et al. (2016) assessments are based on a generic numerical simulation. ICConsulten (2005) suggested, for long terms and a balanced heating/cooling operation mode, an optimal pipe spacing of 40 – 60 cm. The mean value of 50 cm has been chosen for this model. In Figure 4.2 (b) the above defined pipework configuration is represented.

As already mentioned (see Chapter 3.3.1), in FEFLOW code pipework is reproduced with 1D element called "Discrete Features" and the suitable flow law to model their behaviour is the Hagen-Poiseuille law for laminar flow in conduits. To simulate the heat exchange process through the GSHP loop, it is requested to assign a fluid flux circulating in the 1D features, in terms of fluid velocity, and a fluid inlet temperature.

Sterpi et al. (2014) show that the dependence of the heat transfer rate on the fluid velocity is not linear and for every pipe configuration an optimal velocity exists.

From the experimental test conducted in Xia et al. (2012), an optimal velocity of 0.6 – 0.9 m/s has been evaluated for the geothermal systems installed in the diaphragm walls of the Shanghai Museum of Natural History. However, Di Donna et al. (2016) analysis shows that this parameter does not have a significant effect on energy performance and typical values are 0.2 – 1.2 m/s. In the tunnel parametric analysis in Di Donna and Barla (2016) a fluid velocity of 0.4 m/s (*Fluid Flux BC*, i.e. Neumann BC) has been used. Accordingly the same value, low but conservative, will be adopted in this study.

Regarding fluid temperature, it should vary according to the external temperature, for a heating/cooling balanced mode throughout the year. The air at the surface varies seasonally, with a summer peak and a winter peak. The seasonal variation can strongly differ among different locations. In accordance with Di Donna and Barla (2016), the imposed inlet temperature in the operating conditions will be equal to 4 and 28°C for winter (heating mode) and summer (cooling mode) respectively.

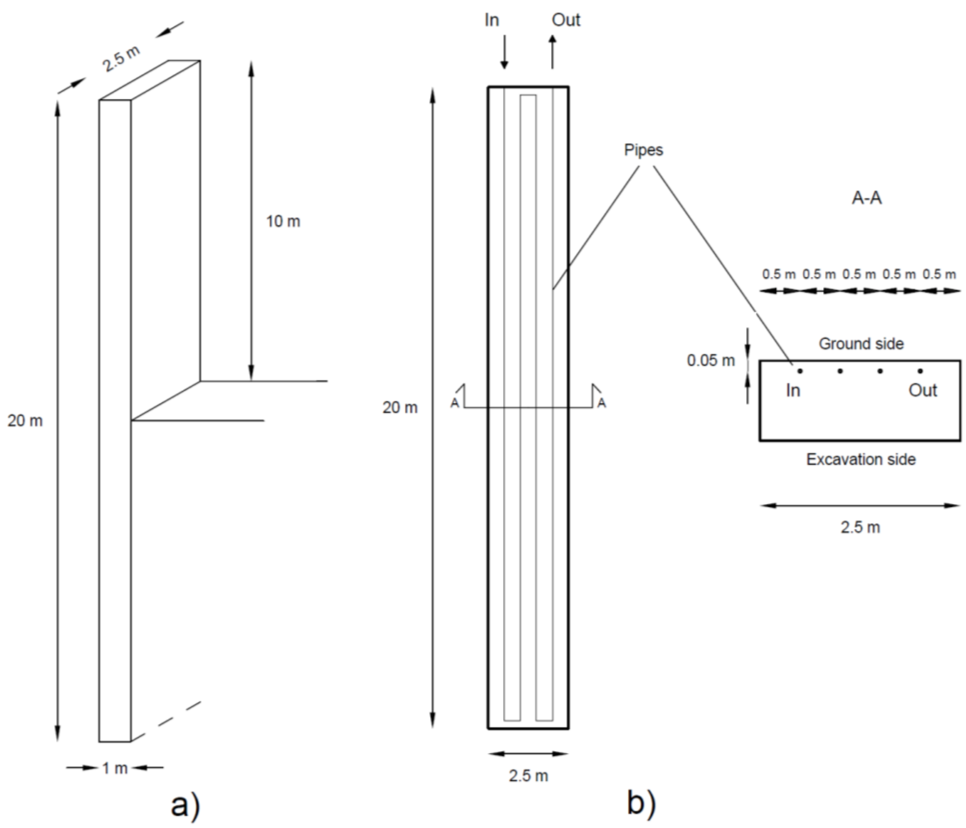

Figure 4.2 Problem geometry for parametric analysis: a) Geometry of the wall; b) vertical and horizontal cut of the wall panel with pipe configuration

4.2 Characterisation of adopted materials

4.2.1 Materials properties

The materials to be considered in this analysis are soil, concrete, fluid in the pipes and in the ground. The properties of the concrete and the fluid will be kept fixed in all the simulations, while some of the soil parameters will be varying in the parametric analysis. To allow a comparison with the outcomes of the similar work on energy tunnels (Di Donna and Barla, 2016), the underground conditions of Torino have been selected as reference case and its thermo-hydro properties are shown in Table 4-3.

Property	*Soil*
Horizontal hydraulic conductivity, k_x=k_z [m/s]	4.15×10^{-3}
Vertical hydraulic conductivity, k_y [m/s]	2.1×10^{-4}
Specific storage coefficient, S [1/m]	10^{-4}
Porosity, n [-]	0.25
Bulk heat capacity, ρc [MJ/(m^{3}K)]	2.55
Bulk thermal conductivity, λ [W/(mK)]	2.26
Longitudinal dispersivity, α_L [m]	3.1
Transversal dispersivity, α_T [m]	0.3

Table 4-3 Soil thermo-hydro properties for the reference case (Di Donna and Barla, 2016)

In the parametric analysis, numerical simulations will be performed, varying the following factors, that mostly influence energy transfer process:

- The ground temperature, in the range 8 – 18°C (typical of continental regions).
- The bulk thermal conductivity, in the range 0.9 – 3.9 W/mK (which correspond to solid particle thermal conductivities of 1 – 5 W/mK in presence of groundwater in the voids).

In Table 4-4 thermo-hydro properties of the other materials adopted are listed. In FEFLOW it is required to define the ground properties in terms of fluid and solid phase. The fluid phase in the voids of the porous medium in saturated conditions is the water, whose thermal properties are standard and reported in Table 4-4.

Thermal properties of the concrete, in particular its thermal conductivity, proved to significantly influence energy performance in Di Donna et al. (2016).

Therefore, it has been suggested to engineer the concrete mix to maximize thermal conductivity using silica-rich aggregates and reducing application of admixtures. However, to consider a general application, in the range of typical values for concrete thermal conductivity (1.5 – 3 W/(m K)), in Table 4-4 a mean value has been chosen, the same used in Di Donna and Barla (2016) for tunnels, as well as the others thermo-hydro features listed.

Property	*Concrete*	*Water*	*Pipework*
Hydraulic conductivity, K_{ij} [m/s]	10^{-16}	-	-
Specific storage coefficient, S [1/m]	10^{-4}	10^{-4}	10^{-4}
Porosity, n [-]	0	-	-
Heat capacity, ρc [MJ/(m^{3}K)]	2.19	4.2	4.2
Thermal conductivity, λ [W/(mK)]	2.3	0.65	0.65

Table 4-4 Thermo-hydro properties of the materials adopted

To reproduce the pipes, it is requested to characterised the “Discrete Features”. Their properties (thermal ones in Table 4-4 and geometrical ones in Table 4-5) are quite standard for energy geostructure applications. Pipework thermal conductivity and heat capacity are the ones of the fluid (water) circulating in the pipes, since the thermal resistance of the plastic tubes is neglected.

External diameter, d [mm]	25
Tube thickness, s [mm]	2.3
Effective section, A [mm^2]	326.8
Hydraulic radius, r_{hyd} [mm]	5.1

Table 4-5 Pipe geometrical properties

4.2.2 Groundwater

Groundwater has a great role in heat transfer between soil and the wall, because it allows a continuous thermal recharge of the ground with great benefit to heat extraction and injection efficiency. Thus, groundwater is introduced in the model and the influence of different water flow velocities will be investigated. Water flow is imposed in FEFLOW code by applying different hydraulic head gradients between the two lateral borders of the numerical model domain. Accordingly, it is necessary to initialize the model to evaluate water flow, determined by the Darcy’s law.

Thus, hydraulic conductivity (Table 4-3) is indirectly taken into account. Groundwater flow velocity can be significantly variable, based on the specific local conditions. Taking into account Torino as reference case, groundwater flow can reach in some areas a velocity of about 1.5 m/d. In accordance with Di Donna and Barla (2015), the parametric analyses will be performed with a water flow velocity variation in the range 0 – 2.0 m/d.

The direction of groundwater flow can be perpendicular or parallel to the longitudinal extension of the wall. Only few cases in literature include in the model the presence of aquifer, often neglected because it can complicate the numerical computation. Di Donna and Barla (2015) and Di Donna (2016) take into account groundwater flow with perpendicular direction to the tunnel axis and to the wall panel, respectively. These papers deal with existing cases study in the urban area of Torino and this assumption has been justified by the real conditions of the water flow in Torino subsoil. It is well known that under the city the water flows towards the Po river (Di Donna and Barla, 2015). Nonetheless, to take into account parallel water flow it is required to enlarge the domain in the third dimension. The longitudinal dimension of the wall is usually reduced to the length of a single panel and in such a short extension the influence of the flowing groundwater may not be correctly reproduce.

Thus, for simplicity and with accordance with energy tunnel case study (Di Donna and Barla, 2015) water flow perpendicular to the wall will be considered. It may be of interest to examine in further investigation how parallel water flow can influence the efficiency of energy walls.

4.3 Initial conditions and boundary conditions

4.3.1 Initial conditions

Initial conditions in the model concern temperature field and groundwater. As it has been stated in Chapter 1.1, the temperature in the soil remains quite constant in the shallow geosphere, in a typical range of 8 – 18°C.

Thus, the same value of temperature is imposed to all the nodes of the domain, according to parametric analysis schemes, and it is free to vary where influenced by the activation of the GSHP system and by the external air temperature.

Groundwater is taken into account in terms of hydraulic head. Accordingly, correspondent hydraulic heads have to be assigned to the left and to the right boundaries.

To reproduce groundwater flow, it is required to initialise the model before activating the geothermal loop. According to the Darcy's law, water flow in a porous medium occurs when there is a hydraulic head difference between left and right boundaries of the model and it is directly linked to the hydraulic conductivity of the soil (Table 4-3). The model has to be completely saturated, therefore hydraulic head on the left boundary will be fixed at the ground level for the analyses, while on the right will be varying, following the scheme in Table 4-6. The values in the table have been determined considering a domain length of 120 m (see Chapter 4.4), according to the Darcy's law equation: $v_x = -k_x \frac{\Delta H}{\Delta x}$.

N°	*Hydraulic head difference, ΔH [m]*	*Groundwater flow velocity [m/d]*
1	0	0
2	0.23	0.7
3	0.67	2.0

Table 4-6 Hydraulic head boundary conditions for different values of groundwater flow velocity

4.3.2 Boundary conditions

Concerning temperature boundary conditions, different environments are in contact with the model. If the diaphragm wall is surrounded by the soil on one side, it is partially exposed to the excavation air on the other side. Moreover, the top of the model is in contact with the external air. Temperature boundary conditions have to be accordingly applied to the borders of the domain.

On the earth-wall side the temperature is the one of the soil, depending on the scheme of the parametric analysis. The temperature on the ground level varies between day and night, day by day, season by season. For simplicity, in this paper a constant value for winter and a constant value for summer will be adopted.

Feasible values of external temperatures in Torino are 30°C in summer and 2°C in winter (from the weather monitoring database ARPA Piemonte - *Agenzia Regionale per la Protezione dell'Ambiente*).

The temperature of the air inside the excavation area can vary significantly according to many factors, e.g. intended use and external temperature. To take into account a general case, the temperature in the excavation should be lower in summer and higher in winter than the outside, since the environment is usually confined and not directly exposed to the external air. Thus, a reasonable temperature of 20°C for summer and 10°C for winter will be adopted.
In Figure 4.3 all the boundary conditions adopted in the model are recapped.

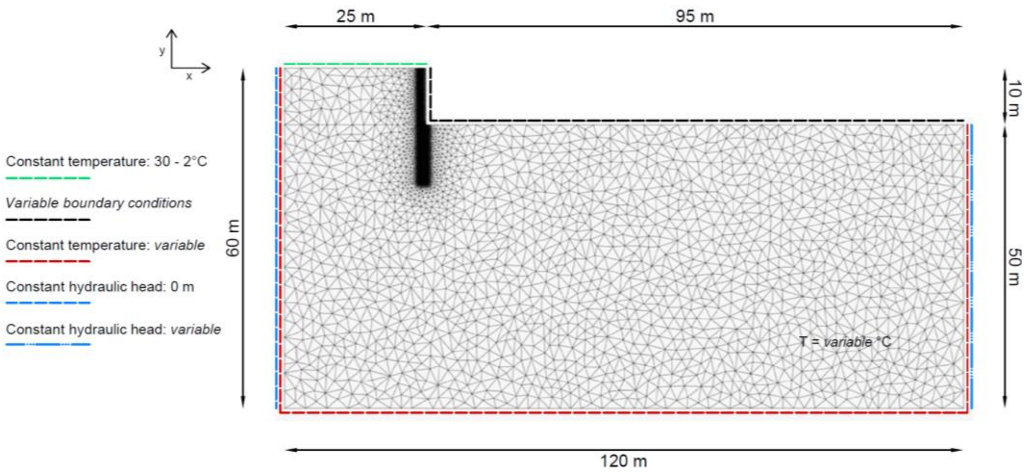

Figure 4.3 The 2D model of the wall and a schematic representation of the boundary conditions adopted

4.3.3 Excavation environment

On the excavation side of the wall it is possible to apply a constant temperature boundary condition (*Temperature BC,* i.e. Dirichlet BC) only or to combine it with a convective heat transfer boundary condition (*Heat Transfer BC,* i.e. Cauchy BC). The first one can be more effective while dealing with tunnels and metro stations, where the air flow inside the excavation can reach high values (> 3-5 m/s, Bourne-Webb et al., 2016)). On the other hand, a convective heat transfer, determined by a heat transfer coefficient and the temperature difference between the wall and the space, should be more suitable in other applications where air flow is not significant.

Bourne-Webb et al. (2016) performed some simulations on tunnels considering different values of heat transfer coefficient applied on the face of the wall towards the excavation space, while Sterpi et al. (2014), Di Donna et al. (2016), Di Donna (2016) and Mauri (2014) applied a constant temperature boundary condition, justifying it with reasons of computational simplicity. Sterpi et al. (2014) and Di Donna et al. (2016) considered general application of energy walls, while Di Donna (2016) focused on an underground car park and Mauri (2015) dealt with a basement.

Some justifications for the convective heat flux approach can be found in BS EN ISO 13789:2017, where some values for heat transfer coefficient are suggested, used in Bourne-Webb et al. (2016). Other applications dealing with different boundary conditions are collected in Di Donna et al. (2016), in Table 4-7. However, they concern tunnels (Nicholson et al., 2014 and Zhang et al., 2013) or in one case basements (Kürten, 2014) where the velocity of the airflow is high and a constant temperature boundary condition might be conservative and thus acceptable. Only in Kürten et al. (2015) the adopted value is verified through a laboratory test, whilst in the other cases no rational justifications have been given to explain the choices.

Case and source	*Scenario*	*Heat transfer coefficient, h [W/m²K]*
Lainzer tunnel, Austria. Sensitivity analysis (ICConsulten, 2005)	Metro tunnel and stations	10-15
Generic case. General sensitivity analysis only (Bourne-Webb et al., 2015,2016)	Not specified	2.5-25
Mongolian road tunnel. Field study and analytical model (Zhang et al., 2013)	Road tunnel	15
Bored tunnel, London. Analysis only (Nicholson et al., 2014)	Rail tunnel	5
Laboratory experiment. Analytical and numerical studies (Kürten, 2014)	Basements	7.7

Table 4-7 Heat transfer coefficients adopted in energy geostructure analysis (Di Donna et al., 2016)

A more conservative approach is to use an adiabatic condition on the excavation side. Heat transfer is forced to only occur between wall and ground and nothing happens on the excavation-wall side. However, although conservative, this condition is unlikely to occur in a real situation, therefore this option will be neglected in this analysis.

To run the parametric analysis, two different boundary conditions at the excavation side will be used in this study, to make a distinction between tunnels and metro stations, i.e. high values of airflow velocity, and basements and underground car parks, i.e. near-zero value of airflow velocity. Thus, in terms of boundary conditions respectively a constant *Temperature BC* and a *Heat transfer BC*, with a heat transfer coefficient of 2.5 W/m^2K (BS EN ISO 13789:2017) will be adopted. In absence of specific monitoring data on airflow velocity in the excavation environment, the above mentioned conditions can be considered as the limits of these applications, in terms of potential heat flux. A parametric analysis with a variation of adopted heat transfer coefficients might be performed in further investigation. Furthermore, it should be based on the relation between heat transfer coefficient and airflow velocity in underground environments that has to be more deeply investigated.

4.4 The numerical model

All features being defined, the model shown in Figure 4.4 is built. Differently of the validation analysis, it is required to enlarge the domain to allow water flow to occur. Thus, the model is 60 m high, 120 m long and 2.5 m wide.

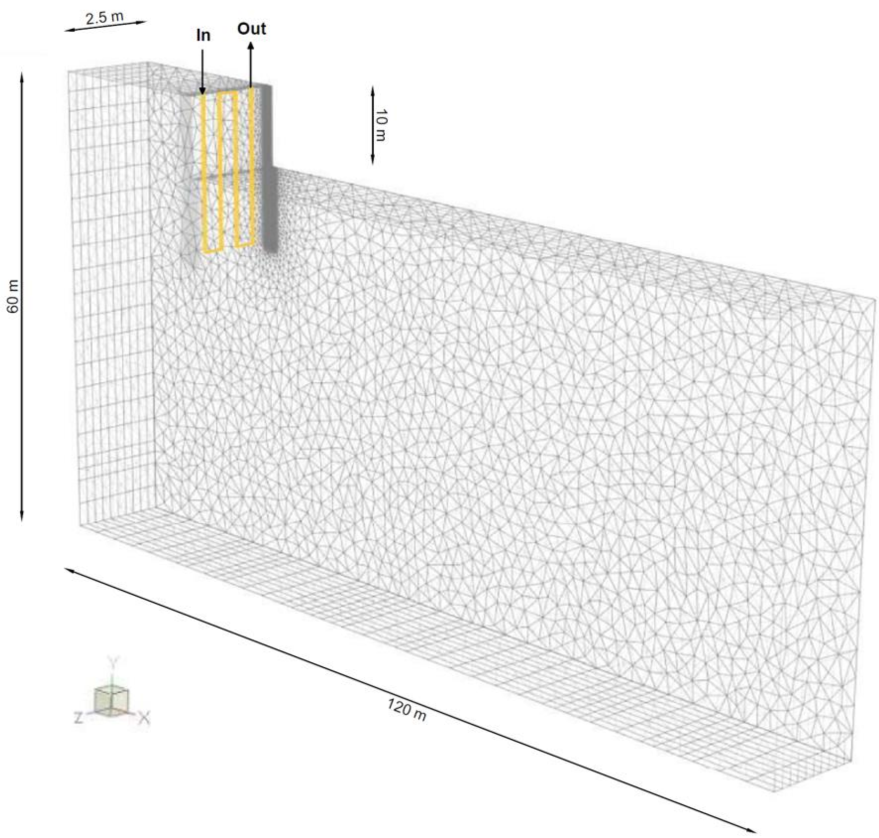

Figure 4.4 3D model for the parametric analysis (Case I). The third dimension has been stretched for a clearer representation

A constant temperature boundary condition will be referred as Case I, whilst Case II concerns a heat transfer boundary condition. A mesh sensitivity analysis of the model will be performed in the following chapter.

Geometry and boundary conditions being kept fixed, in the parametric analysis the three affecting parameters, listed again in Table 4-8, will be varying throughout the analyses, with a total of 108 runs.

Parameter	*Range*		
Soil temperature, T [°C]	8	14	18
Soil thermal conductivity, λ [W/mK]	0.9	2.26	3.9
Groundwater flow velocity, gwf [m/d]	0	0.7	2.0

Table 4-8 Variation of the parameters for the analysis

4.4.1 Model validation

It is fundamental to check the model and for simplicity only a value for each affecting parameters is used, i.e. $\lambda = 3.9$ W/mK, T = 14°C and gwf = 0 m/d.

As it is shown in Figure 4.5, the domain borders have been checked to be far enough not to affect the results. In this case, the results with different values of groundwater flow velocity are included, since moving water favours the heat propagation. To evaluate the influence of heat exchange around the pipes in the temperature field of the model, on the slab of the excavation the same temperature of the soil has been applied. Otherwise, the temperature in the excavation would have interfered in the results.

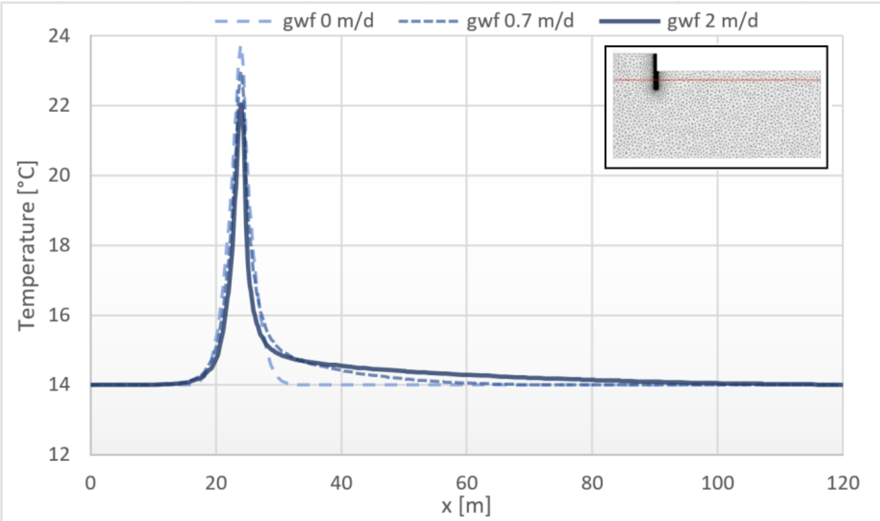

Figure 4.5. Variation of the temperature throughout the domain (values measured along the red line indicated in the model on the top right, at 15 m depth form the ground level)

The mesh configuration of the diaphragm wall-soil system has been initially defined based on the validation model, with 405 460 triangular prismatic six-node elements, 224 191 nodes and a spacing between the slices in the third dimension of 0.25 m. Then, the mesh has been checked through a mesh sensitivity analysis. In terms of outlet temperature, different solutions obtained varying the discretisation in the plane (i.e. in the layer, listed in Table 4-9) and in the third dimension are illustrated in Figure 4.6 and Figure 4.7 respectively. To appreciate the differences with the variation of the discretisation, it is necessary to reproduce the results in a logarithmic plane. The analysis validates mesh and discretisation of the model.

N° Mesh	Gradation of refinement	Target element size [m]	N° elements per layer
1	4	0.4	7 538
2	6	0.2	16 413
3	8	0.1	40 546

Table 4-9 Different mesh refinements for the model

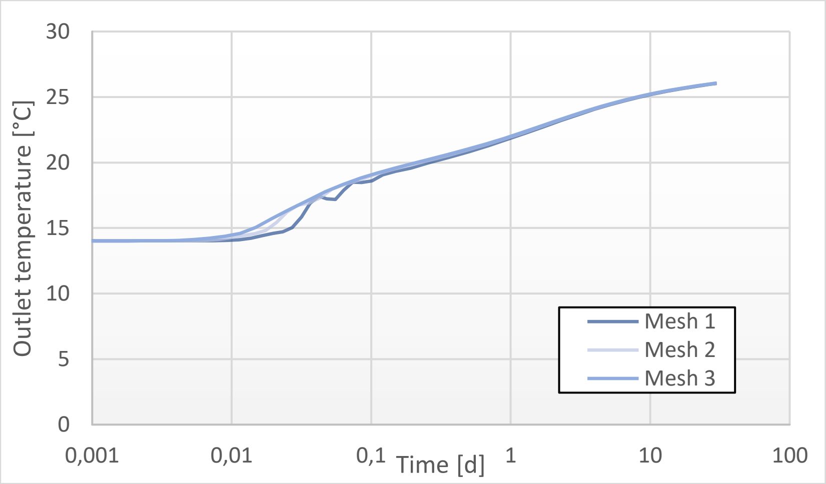

Figure 4.6 Comparison between the results for different types of the mesh, defined in Table 4-9 (the time in the x-axis is in logarithmic scale)

It is possible to notice in Figure 4.6 that increasing the mesh density in the critical area around the pipes, i.e. refining the target element size, reduces the oscillations in the first steps of the simulations.

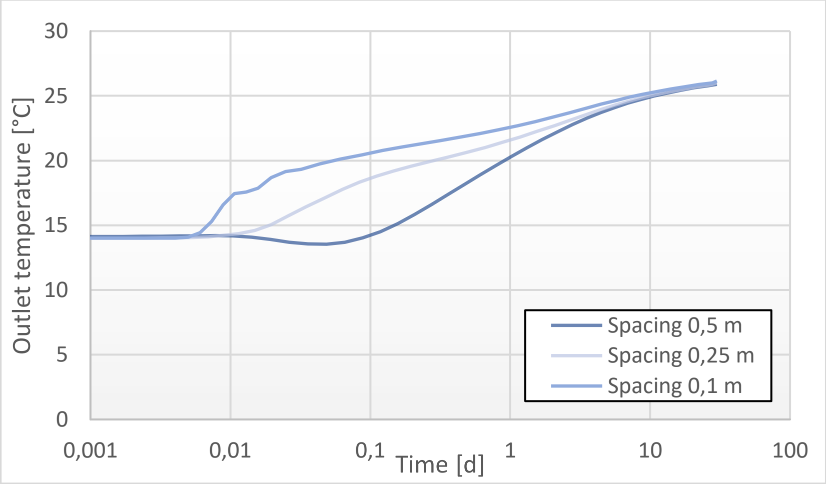

Figure 4.7 Comparison between the results for different discretisations in the third dimension, in terms of spacing [m] between the slices (the time in the x-axis is in logarithmic scale)

Differently in Figure 4.7 the discretisation in the third dimension, in terms of spacing between the slices, has to be a reasonable compromise between the largest and the shortest size of elements, to avoid distort prisms in the model that lead to wavy solutions at the beginning of the performance. In any case, convergence is reached in long terms.

The model being checked, the parametric analyses will be performed with a simulated time of one month (30 days) in cooling mode (summer) and one month in heating mode (winter).

5. RESULTS AND DISCUSSION

In this chapter the outcomes of simulations will be interpreted and discussed, focusing on the affecting parameters. Firstly the case with a constant temperature boundary condition (Case I) at the excavation borders will be studied, then the case with a heat transfer coefficient (Case II) will be introduced and compared with the previous results. Thus, the influences of different underground and boundary conditions on the energy efficiency are investigated. Finally, a direct comparison with the tunnel case study (Di Donna and Barla, 2015) will be carried out.

5.1 Initialisation of the model

The model being built, it is required to initialise it to simulate the target groundwater flow before activating the geothermal loop. To reproduce a null groundwater flow velocity (gwf = 0 m/d) the initialisation is not necessary, since the water in the aquifer is in quiet. Applying the same hydraulic head at the lateral borders, no movement of the water occurs, paying attention to have the domain completely saturated (hypothesis of the study). Thus, the water table has to be located on the top of the model. Differently, in the other two cases (gwf = 0.7 m/d, gwf = 2 m/d) the model has to be initialised to reach the steady state in terms of water flow velocity in the domain. In the following pictures (Figures 5.1 – 5.3), the different initialisation stages are shown. According to Darcy's law, a difference of hydraulic head has been applied at the lateral boundaries (see Table 4-6) and groundwater flow has been computed and verified.

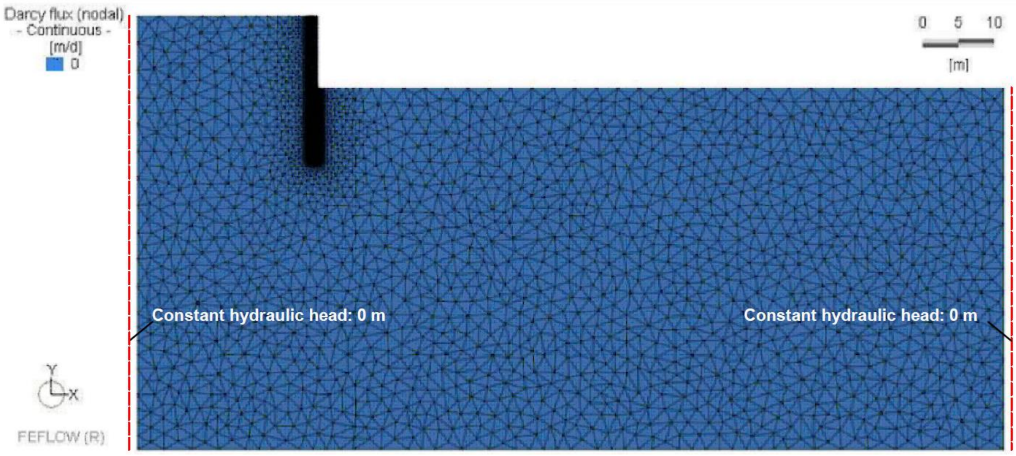

Figure 5.1 Initial groundwater condition (gwf = 0 m/d) before the thermal activation

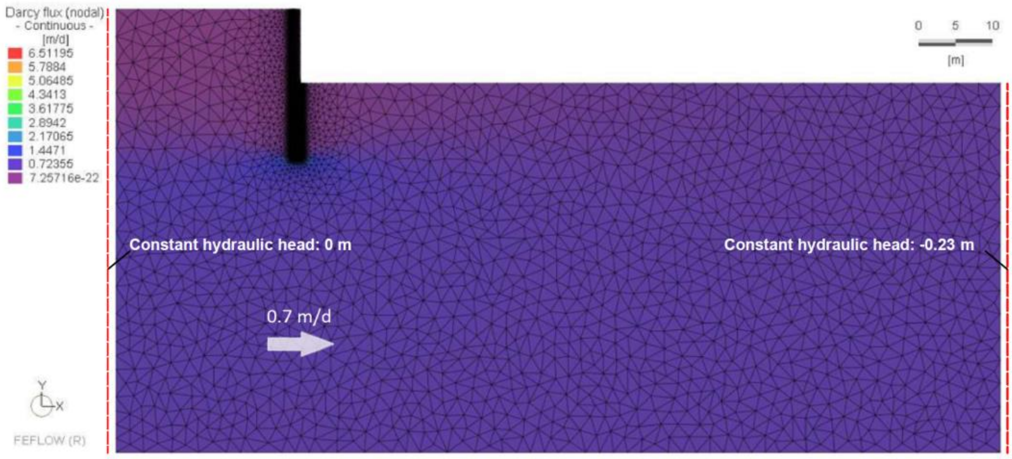

Figure 5.2 Initial groundwater condition (gwf = 0.7 m/d) before the thermal activation

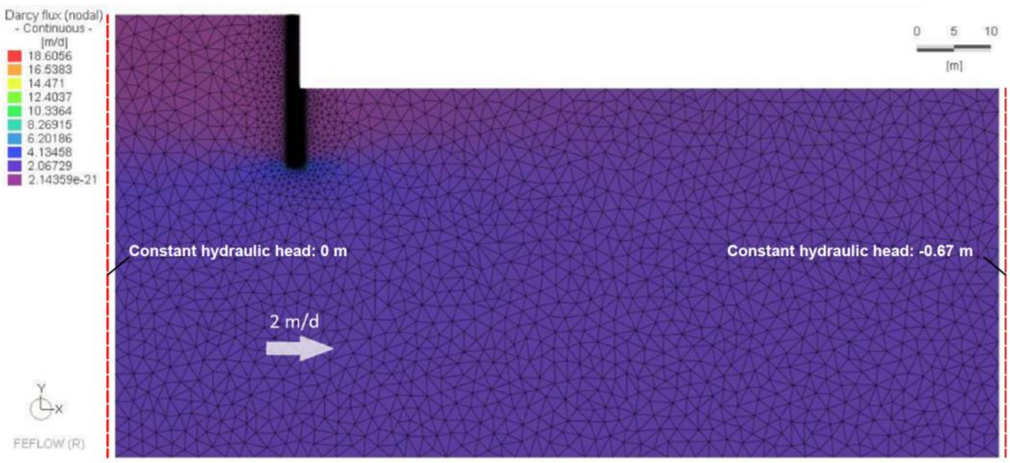

Figure 5.3 Initial groundwater condition (gwf = 2 m/d) before the thermal activation

5.2 Case I

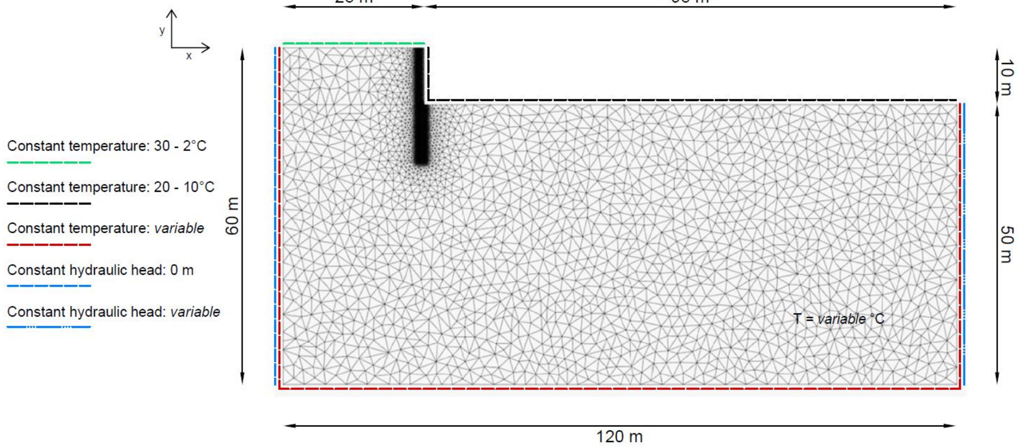

Figure 5.4 2D model of the energy wall with boundary conditions and ground properties (Case I)

The reference model, with boundary conditions and ground properties, is illustrated in Figure 5.4. In absence of specific monitoring data, a constant temperature BC adopted for the excavation borders is more suitable for metro stations or tunnels where very large air flow velocity is expected (Bourne – Webb et al., 2016). The choice of the temperature value to be applied on the excavation side of the wall is however sensitive, because it proved to strongly affect the heat exchange. In further investigation this aspect should be deepened. In this study, for simplicity, it has been left out from the parametric analysis and reasonable values of 20°C (summer) and 10°C (winter) have been used then in the simulations (see Chapter 4.3.2).

After the initialisation, when it is required, the geothermal system can be activated, running the simulation with the variation of the affecting parameters step by step. The fluid circulates in the pipes with the imposed velocity of 0.4 m/s and the heat exchange occurs. At the end of the simulation (30 days) the temperature in the domain has changed due to the effect of the thermal activation and of the influence of the external temperatures. The results depend on the parameters adopted in each computation, that are recapped in Table 5-1:

Parameter	*Range*		
Soil temperature, T [°C]	8	14	18
Soil thermal conductivity, λ [W/mK]	0.9	2.26	3.9
Groundwater flow velocity, gwf [m/d]	0	0.7	2.0

Table 5-1 Variation of the parameters for the analysis

Figures 5.5 – 5.7 show some examples of how the temperature field modifies (only one layer is reported but it is the same for all the slices), with the increasing of groundwater flow rate, the most appreciable change coming out from a preliminary overview of the pictures. In the details, it is possible to notice how the temperature changes just on the sides of the wall, due to the presence of moving water. The influence of the parameters will be deeply investigated through the computed data in the following chapters.

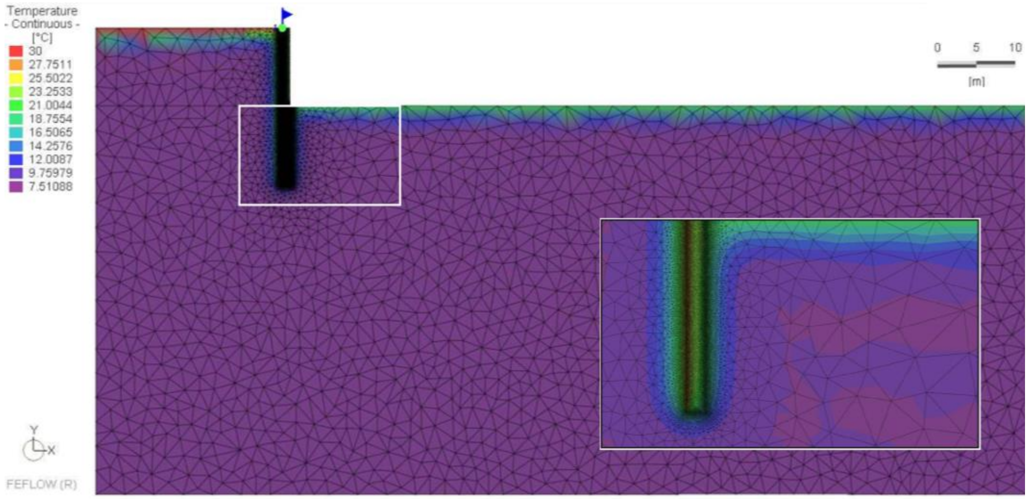

Figure 5.5 Temperature at t = 30 d (gwf = 0 m/d, T = 8°C, λ = 0.9 W/mK), with detail (Case I)

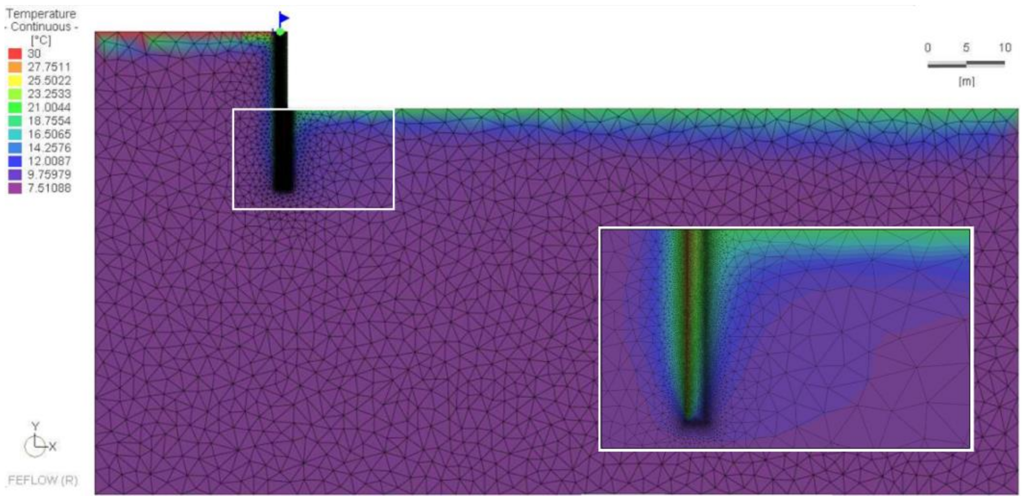

Figure 5.6 Temperature at t = 30 d (gwf = 0.7 m/d, T = 8°C, λ = 0.9 W/mK), with detail (Case I)

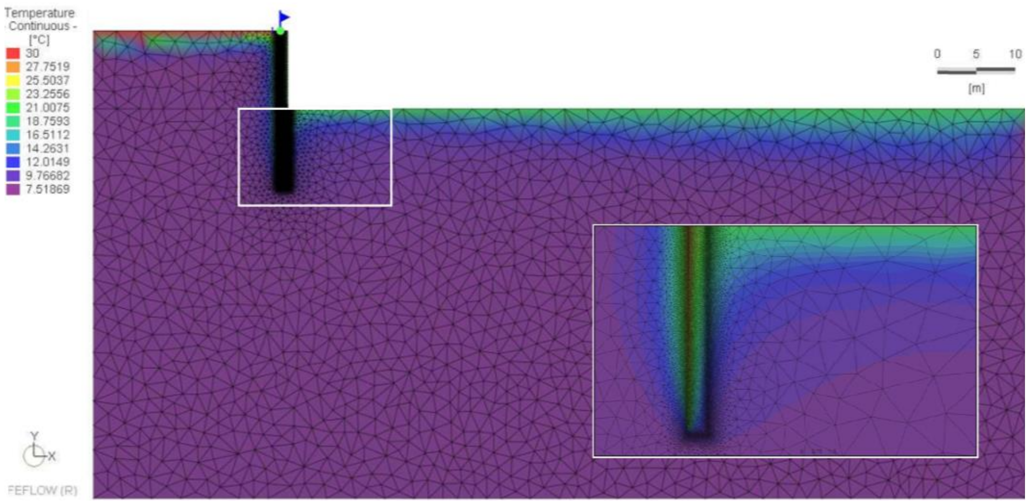

Figure 5.7 Temperature at t = 30 d (gwf = 2 m/d, T = 8°C, λ = 0.9 W/mK), with detail (Case I)

5.2.1 Outlet temperature

After the initialisation, it is possible to activate the geothermal system. The local temperatures at the inlet and outlet points of the circuit are displayed and collected for every run of the parametric analysis. Then, all the results are assembled in some graphs, both for winter conditions and for summer conditions, where inlet and outlet temperatures versus time are plotted. In summer (Figure 5.8), it is possible to notice that as the soil temperature increases, the difference between inlet and outlet temperature decreases. It has to be expected then that the injected heat will decrease too, being in function of the temperature difference. In winter (Figure 5.9), the opposite trend is shown: as the temperature of the ground enhances, the outlet temperature moves away from the inlet line.

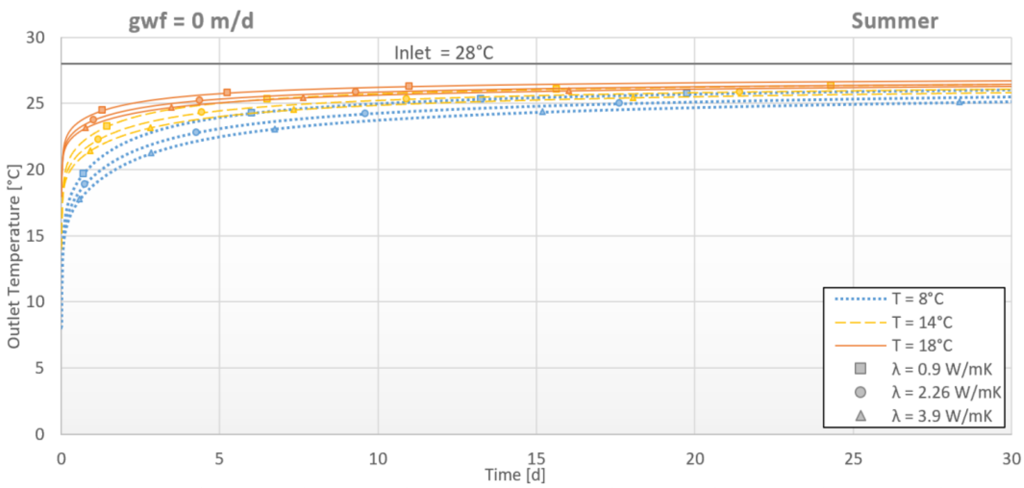

Figure 5.8 Imposed inlet and computed outlet temperatures for summer conditions with gwf = 0 m/d (Case I)

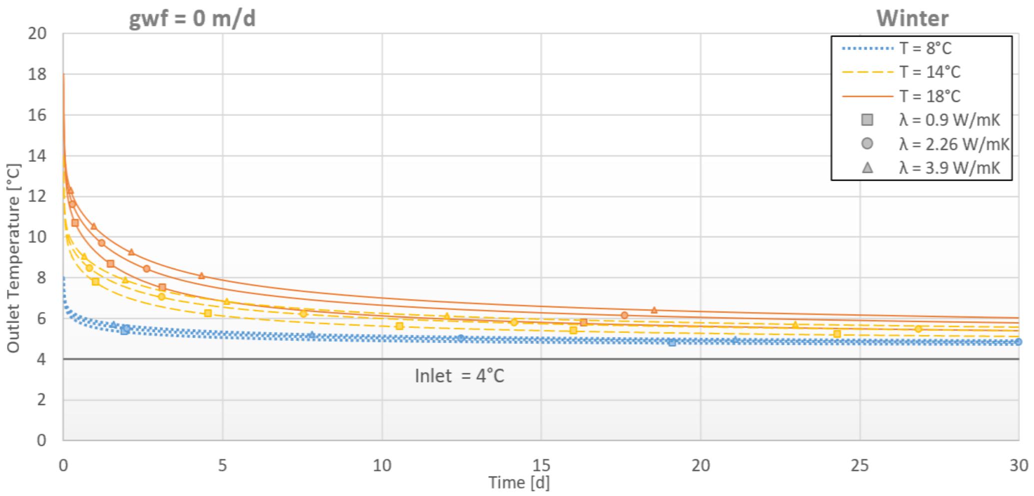

Figure 5.9 Imposed inlet and computed outlet temperatures for winter conditions with gwf = 0 m/d (Case I)

While different soil temperatures are represented with different colours, the distinct values of thermal conductivity are taken into account in the graphs with three different curves, referring to the same soil temperature. Both in cooling and heating mode, the increasing of thermal conductivity leads to a rising in terms of temperature difference, as in summer the outlet temperature lowers down and in winter it rises up.

The same trends can be obtained also in presence of groundwater flow. In Figures 5.10 – 5.13Figure 5.13 the relative charts are displayed.

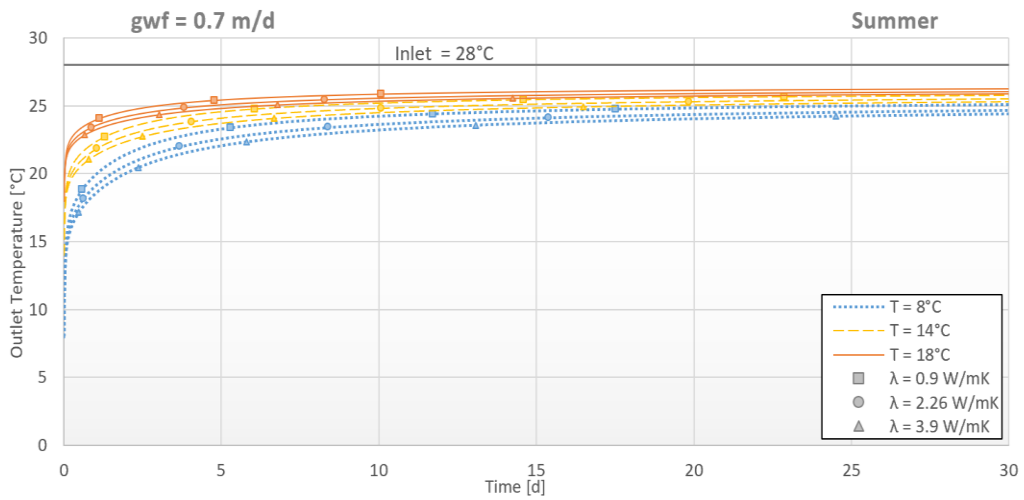

Figure 5.10 Imposed inlet and computed outlet temperatures for summer conditions with gwf = 0.7 m/d (Case I)

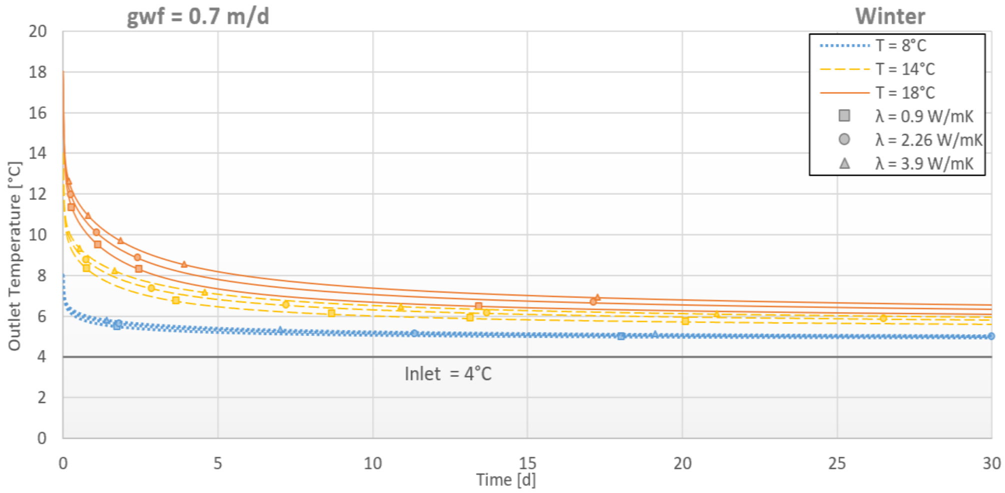

Figure 5.11 Imposed inlet and computed outlet temperatures for winter conditions with gwf = 0.7 m/d (Case I)

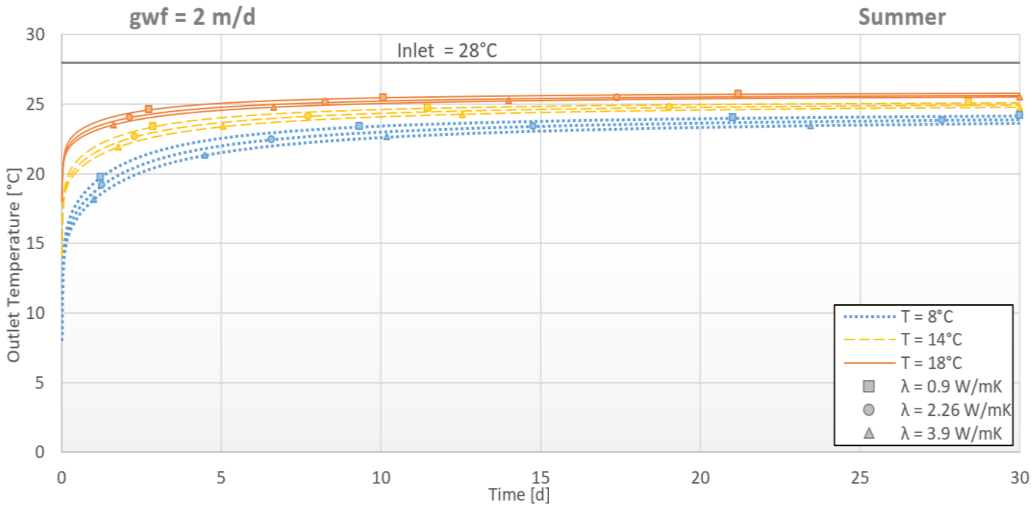

Figure 5.12 Imposed inlet and computed outlet temperatures for summer conditions with gwf = 2 m/d (Case I)

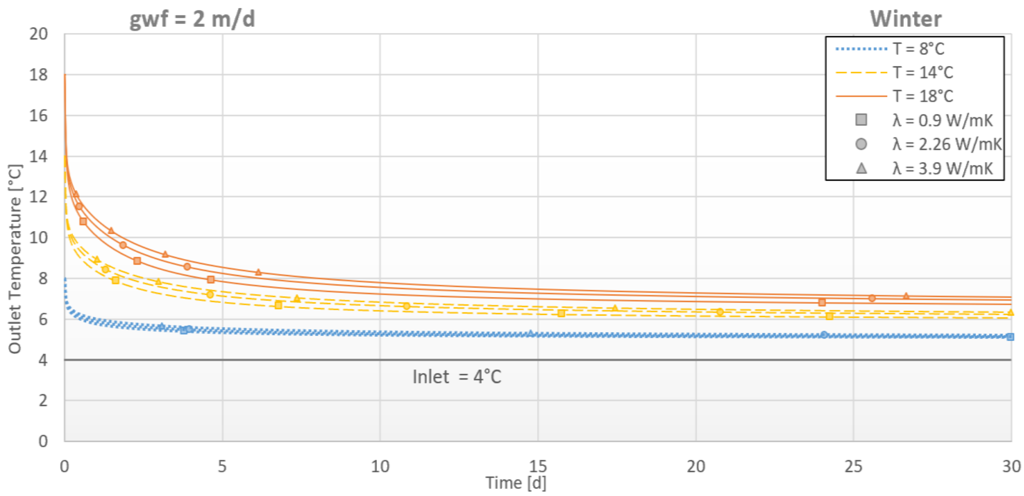

Figure 5.13 Imposed inlet and computed outlet temperatures for winter conditions with gwf = 2 m/d (Case I)

As the groundwater flow velocity increases, the distinction between the curves is clearer, while in the case without water flow the different lines are overlapped. The separation between different soil temperatures becomes larger, especially in the case with gwf = 2 m/d, where the outlet temperature are clearly assembled in groups according to the ground temperature. As it was expected, due to the contribution of the convective heat transfer process linked to the movement of the groundwater, the outlet temperatures increase in winter, and decrease in summer, with the increment of groundwater flow velocity. The moving water supplies the soil more rapidly with heat, that can be extracted with the GSHP loop in heating mode. Accordingly, in cooling mode the moving heat due to the groundwater flow increases the heat injection of the geothermal system.

For a direct comparison between the varying parameters, only the outlet temperatures obtained at t = 30 days (horizontal axis) are collected in the graphs in Figure 5.14 and Figure 5.15, where groundwater flow velocity is on the vertical axis. Different colours and hatchings represent different soil temperatures, whilst different shaped pointers express different thermal conductivities. In Table 5-2 the results are listed (only the outlet temperatures at t = 30 days of simulation). It is possible to notice in these conclusive charts all the considerations made previously.

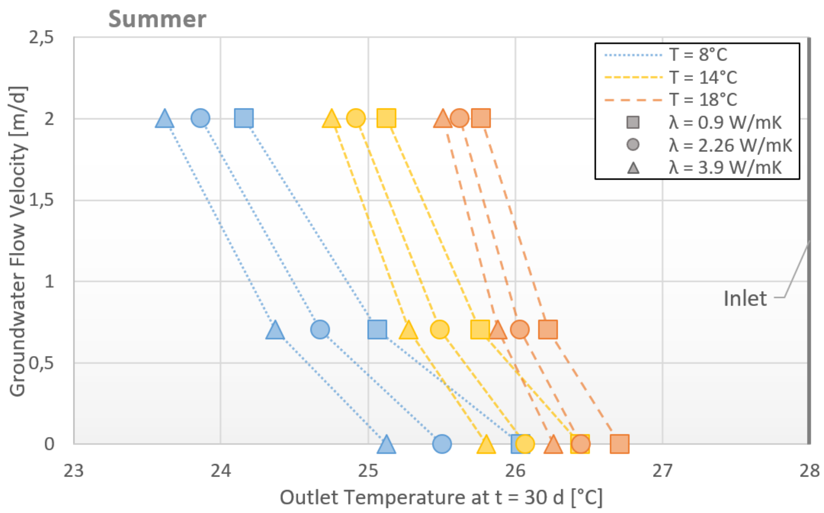

Figure 5.14 Outlet temperatures at t = 30 d of the simulations in summer, as the parameters of the analysis vary (Case I)

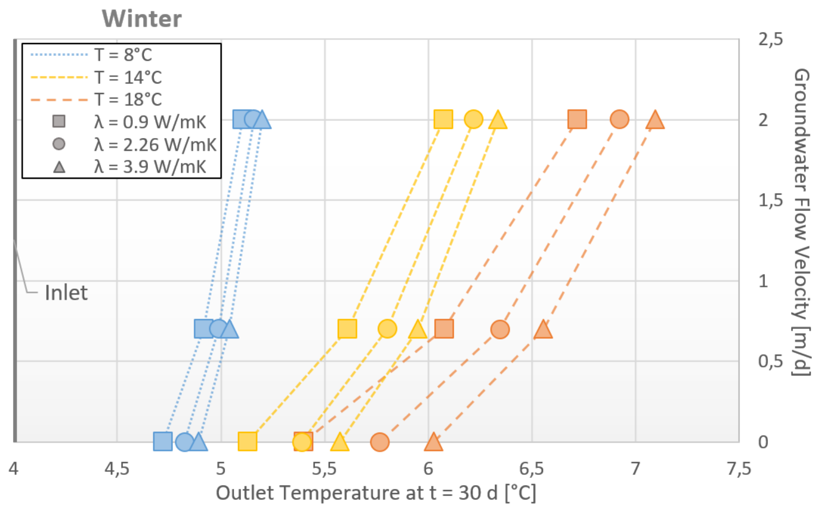

Figure 5.15 Outlet temperatures at t = 30 d of the simulations in winter, as the parameters of the analysis vary (Case I)

	T = 8°C			T = 14°C			T = 18°C			
	λ = 0.9 W/mK	λ = 2.26 W/mK	λ = 3.9 W/mK	λ = 0.9 W/mK	λ = 2.26 W/mK	λ = 3.9 W/mK	λ = 0.9 W/mK	λ = 2.26 W/mK	λ = 3.9 W/mK	
S	26,04	25,51	25,13	26,44	26,07	25,81	26,71	26,45	26,26	gwf = 0 m/d
W	4,72	4,82	4,89	5,13	5,39	5,57	5,40	5,77	6,03	
S	25,07	24,68	24,37	25,76	25,49	25,28	26,23	26,03	25,89	gwf = 0.7 m/d
W	4,92	4,99	5,04	5,61	5,80	5,95	6,08	6,35	6,56	
S	24,16	23,86	23,62	25,13	24,92	24,76	25,77	25,63	25,51	gwf = 2.0 m/d
W	5,11	5,16	5,20	6,07	6,22	6,34	6,72	6,93	7,09	

Table 5-2 Outcomes of the parametric analyses, in terms of outlet temperatures [°C] at t = 30 d (Case I)

5.2.2 Heat power

Based on the results of the parametric analysis at the end of simulations, in terms of outlet temperature T_{out} of the GSHP system, it is possible to quantify the extractable/injectable heat power Q of the energy wall (expressed in W) through the equation (16). The imposed inlet temperature is 4°C and 28°C in winter and in summer, respectively. The exchanged heat power will be presented also in W per square metre and in W per metre, normalising the results with respect to the wall panel surface (50 m^2) and its length (20 m) respectively. In Table 5-3 the results are listed in a concise representation, whilst in Appendix a more comprehensive table is added. It is possible to produce some charts relating to the exchanged heat power and they are shown in Figure 5.16 and Figure 5.17.

		T = 8°C			T = 14°C			T = 18°C			
		λ = 0.9 W/mK	λ = 2.26 W/mK	λ = 3.9 W/mK	λ = 0.9 W/mK	λ = 2.26 W/mK	λ = 3.9 W/mK	λ = 0.9 W/mK	λ = 2.26 W/mK	λ = 3.9 W/mK	
S	*ΔT [°C]*	1,96	2,49	2,87	1,56	1,93	2,19	1,29	1,55	1,74	gwf = 0 m/d
	Q [W]	1,08	1,37	1,58	0,86	1,06	1,20	0,71	0,85	0,96	
	q [W/m²]	21,55	27,40	31,55	17,12	21,20	24,08	14,16	17,06	19,10	
	q [W/m]	53,89	68,49	78,87	42,79	52,99	60,20	35,40	42,65	47,76	
W	*ΔT [°C]*	0,72	0,82	0,89	1,13	1,39	1,57	1,40	1,77	2,03	
	Q [W]	0,40	0,45	0,49	0,62	0,76	0,86	0,77	0,97	1,11	
	q [W/m²]	7,94	9,05	9,80	12,39	15,27	17,28	15,36	19,41	22,27	
	q [W/m]	19,85	22,63	24,50	30,97	38,17	43,21	38,39	48,52	55,68	
S	*ΔT [°C]*	2,93	3,32	3,63	2,24	2,51	2,72	1,77	1,97	2,11	gwf = 0.7 m/d
	Q [W]	1,61	1,82	1,99	1,23	1,38	1,49	0,97	1,08	1,16	
	q [W/m²]	32,19	36,47	39,81	24,56	27,55	29,86	19,48	21,60	23,22	
	q [W/m]	80,49	91,17	99,54	61,41	68,87	74,66	48,69	53,99	58,05	
W	*ΔT [°C]*	0,92	0,99	1,04	1,61	1,80	1,95	2,08	2,35	2,56	
	Q [W]	0,50	0,54	0,57	0,89	0,99	1,07	1,14	1,29	1,40	
	q [W/m²]	10,07	10,87	11,44	17,71	19,81	21,41	22,80	25,77	28,06	
	q [W/m]	25,17	27,17	28,60	44,28	49,52	53,54	57,01	64,41	70,16	
S	*ΔT [°C]*	3,84	4,14	4,38	2,87	3,08	3,24	2,23	2,37	2,49	gwf = 2.0 m/d
	Q [W]	2,11	2,27	2,40	1,58	1,69	1,78	1,22	1,30	1,37	
	q [W/m²]	42,19	45,43	48,08	31,57	33,81	35,62	24,48	26,06	27,31	
	q [W/m]	105,48	113,57	120,20	78,92	84,52	89,05	61,21	65,14	68,26	
W	*ΔT [°C]*	1,11	1,16	1,20	2,07	2,22	2,34	2,72	2,93	3,09	
	Q [W]	0,61	0,64	0,66	1,14	1,22	1,28	1,49	1,61	1,70	
	q [W/m²]	12,15	12,74	13,19	22,78	24,38	25,67	29,87	32,13	33,98	
	q [W/m]	30,37	31,86	32,96	56,95	60,95	64,16	74,67	80,33	84,96	

Table 5-3 Extracted/injected heat at t = 30 d of the simulations, in winter and in summer (Case I)

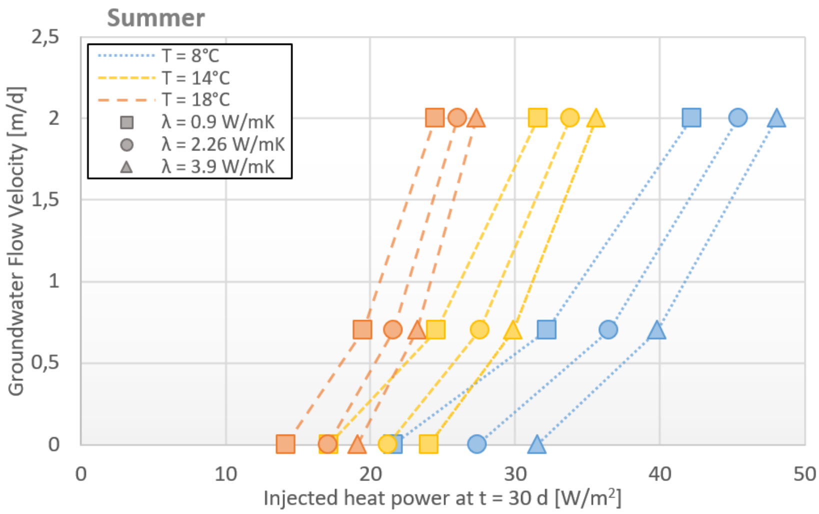

Figure 5.16 Injected heat power at t = 30 d of the simulations in summer, as the parameters of the analysis vary (Case I)

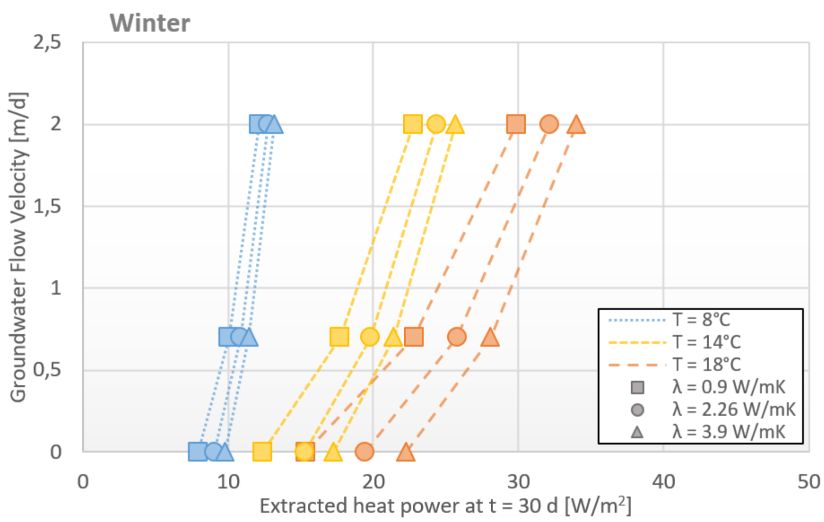

Figure 5.17 Extracted heat power at t = 30 d of the simulations in winter, as the parameters of the analysis vary (Case I)

The maximum efficiency is shown in summer (48 W/m^2), as the difference between inlet and outlet temperatures reaches the highest values in the operational mode with respect to winter case. In summer the injected heat power decreases with the increasing of the ground temperature, while in winter the opposite trend is shown. Furthermore, the chart indicates that in heating mode and with a cold ground (T = 8°C) the efficiency of the system is remarkably lower with respect to the other cases (around 10 W/m^2), thus the effects of thermal conductivity and groundwater flow velocity are less appreciable.

Even though less evident, the same trend can be appreciated in summer with T = 18°C. Reasonably, when the temperature of the ground is similar to the inlet temperature the efficiency of the system reduces.

Focusing separately on the influence of the ground features under investigation, the interpretation of these data leads to some graphs that are analysed in the following paragraphs. For tunnels and metro/rail stations, on the specific site conditions (i.e. ground temperature, soil thermal conductivity and groundwater flow velocity) the charts can give the designer a reasonable idea of the potential energy exploitation both in winter and in summer conditions, expressed in watts per square metre of diaphragm wall.

5.2.2.1 Influence of ground temperature

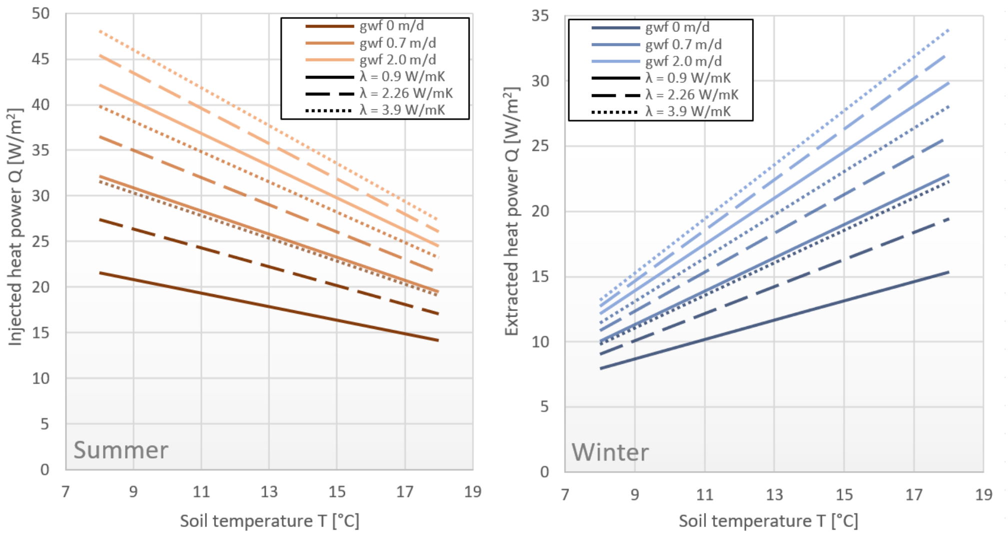

Figure 5.18 Effect of soil temperature on the energy performance, Case I (different colors = groundwater flow velocities (gwf), different hatching = bulk thermal conductivities (λ)): on the left summer mode, on the right winter mode

Based on the results of the parametric analyses, in Figure 5.18 it is possible to appreciate the linear variation with ground temperature of the injected/extracted heat both for summer and winter. In summer, the difference between the inlet and the outlet temperature decreases with the increase in soil temperature, as a result of which the efficiency decreases. The opposite trend is shown in winter mode. When groundwater flow velocity increases, energy performance becomes more sensitive to ground temperature, as the slope of the straight lines enhances.

Differently, the influence of thermal conductivity reduces with the increasing of flow velocity, as the gap between the lines decreases. Reasonably, when the convective component (groundwater flow) is less important, the conductive process of heat transfer (thermal conductivity) is predominant.

5.2.2.2 Influence of groundwater flow velocity

Figure 5.19 illustrates the effect of groundwater flow velocity on the energy efficiency of the system for winter and summer modes. Both in heating and cooling mode, the exchanged heat increases in a non-linear way with the increasing of groundwater flow velocity. As the groundwater flow velocity increases, the ratio between the convective and the conductive contributions of the heat transfer changes.

As the two processes intervene in different ways in the transfer, the variation of the exchanged heat power is not linear with the increasing of the groundwater flow velocity.

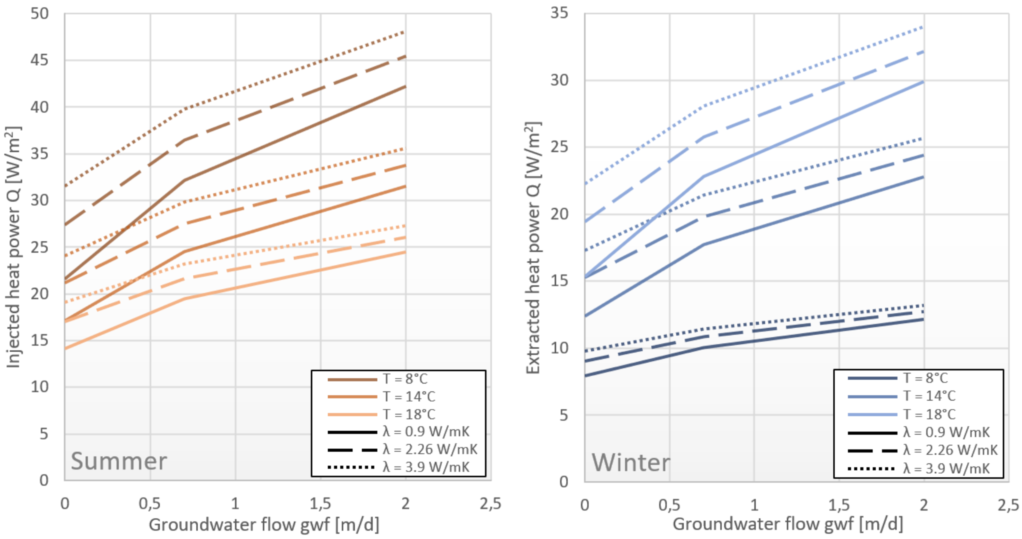

Figure 5.19 Effect of groundwater flow velocity on the energy performance, Case I (different colors = soil temperatures (T), different hatching = bulk thermal conductivities (λ)): on the left summer mode, on the right winter mode

It is possible to appreciate again indeed how, both for summer and winter, the effect of the thermal conductivity reduces as the groundwater flow velocity increases. Furthermore, the energy performance is strongly influenced by the ground temperature when the water in the aquifer is moving more rapidly, in both cooling and heating mode.

5.2.2.3 *Influence of thermal conductivity*

The influence of thermal conductivity on the energy performance is shown in Figure 5.20, for summer and winter. In both cases, the increasing of exchanged heat power with the variation of the thermal conductivity is non-linear. However, non-linearity slightly reduces with the increasing of groundwater flow velocity. In winter, it is possible to notice that the effects of thermal conductivity (average slope of the lines) and groundwater flow velocity (gap between the lines) enhance as the ground temperature rises up. Differently, the opposite trend is appreciated in summer. In both operational modes, as the groundwater flow velocity grows, the influence of thermal conductivity reduces.

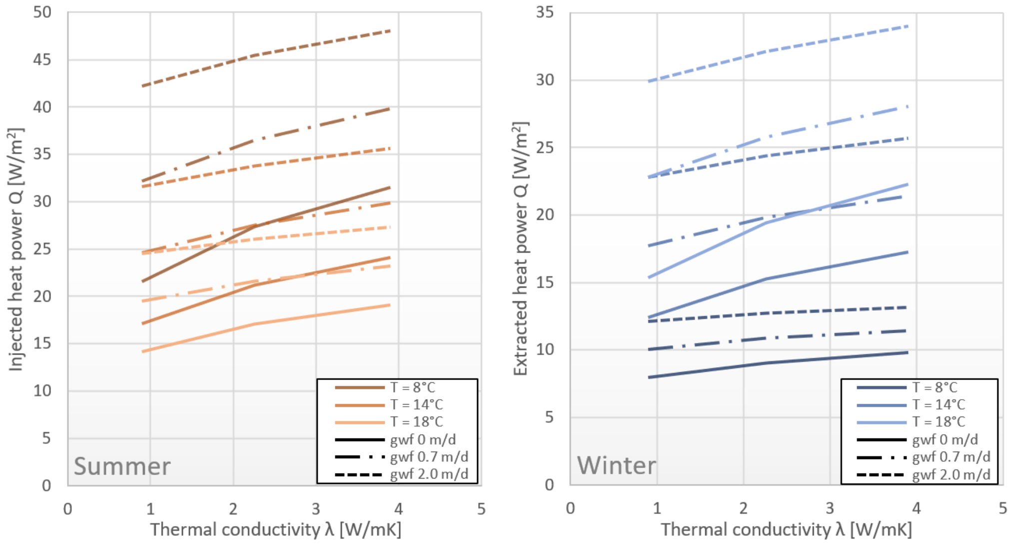

Figure 5.20 Effect of soil thermal conductivity on the energy performance, Case I (different colors = soil temperatures (T), different hatching = groundwater flow velocities (gwf)): on the left summer mode, on the right winter mode (Case I)

5.3 Case II

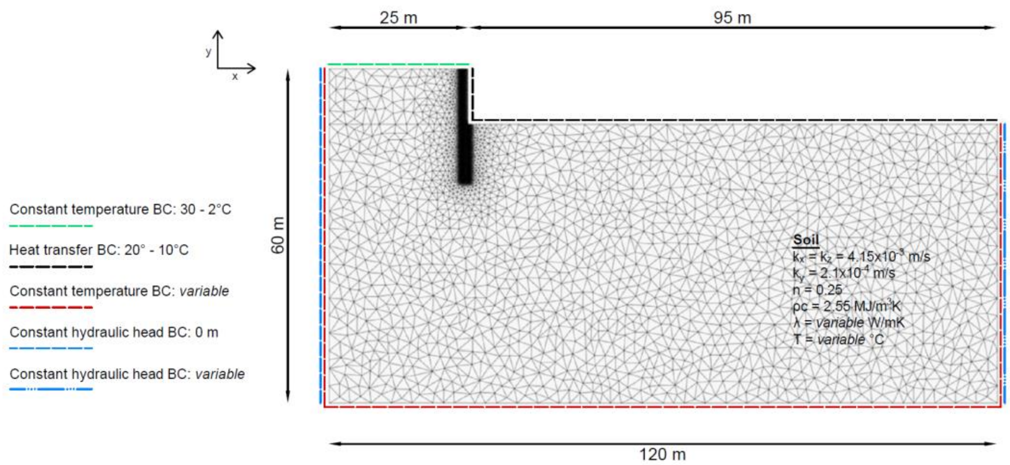

Figure 5.21 2D model of the energy wall with boundary conditions and ground properties (Case II)

In Figure 5.21 the model with its boundary conditions, as well as the ground properties, for the Case II are recapped. In absence of specific monitoring data, a heat transfer BC can be a suitable condition to simulate a heat transfer process that occurs when a very low air flow velocity is present in the excavation side (Bourne-Webb et al., 2016). Thus, Case II is intended to reproduce basements or underground car parks equipped with energy wall.

The air flow velocity influence is taken into account in terms of heat transfer coefficient, accordingly to Bourne-Webb et al. (2016).

In particular, ISO suggests a value of 2.5 W/m^{2}K for horizontal heat from internal surfaces (walls) and it is related to a nearly zero air-speed. It is then necessary to assign the value of 2.5 W/m^{2}K as a material property, that in FEFLOW is defined as In/Out – transfer rate. At the excavation sides a temperature as to be applied, in this case a Heat Transfer BC, with a value of 20°C and 10°C for summer and winter respectively, following the same considerations of Case I.

After the initialisation, when it is required, the geothermal system can be activated, running the simulation with the variation of the affecting parameters step by step. The fluid circulates in the pipes with the imposed velocity of 0.4 m/s and the heat exchange occurs. At the end of the simulation (30 days) the temperature in the domain has changed due to the effect of the thermal activation and of the influence of the external temperatures.

The results depend on the parameters adopted in each computation, that are recapped in Table 5-1. Figures 5.22 – 5.24 show some examples of how the temperature field modifies (only one layer is reported but it is the same for all the slices), with the increasing of groundwater flow rate. In the details, it is possible to notice how the temperature changes just on the sides of the wall, due to the presence of moving water. The influence of the parameters will be deeply investigated through the computed data in the following chapters.

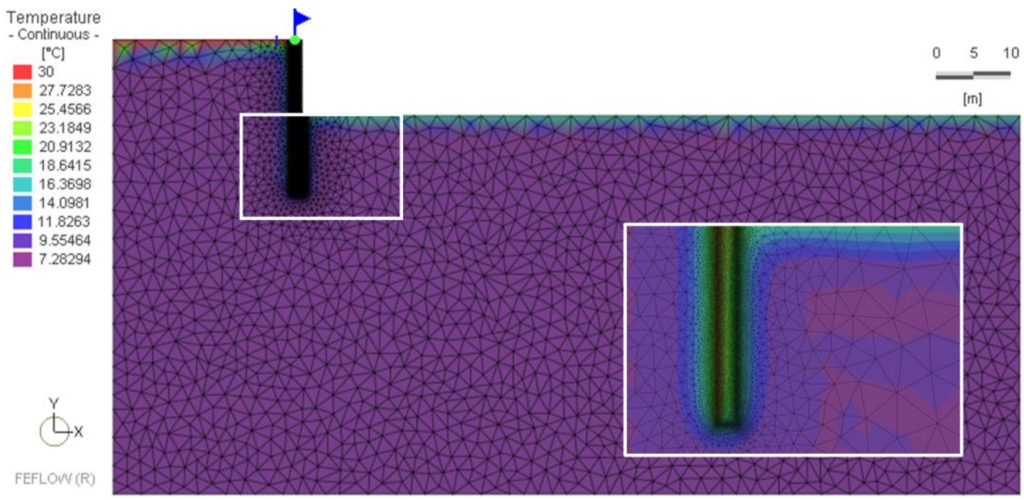

Figure 5.22 Temperature at t = 30 d (gwf = 0 m/d, T = 8°C, λ = 0.9 W/mK), with detail (Case II)

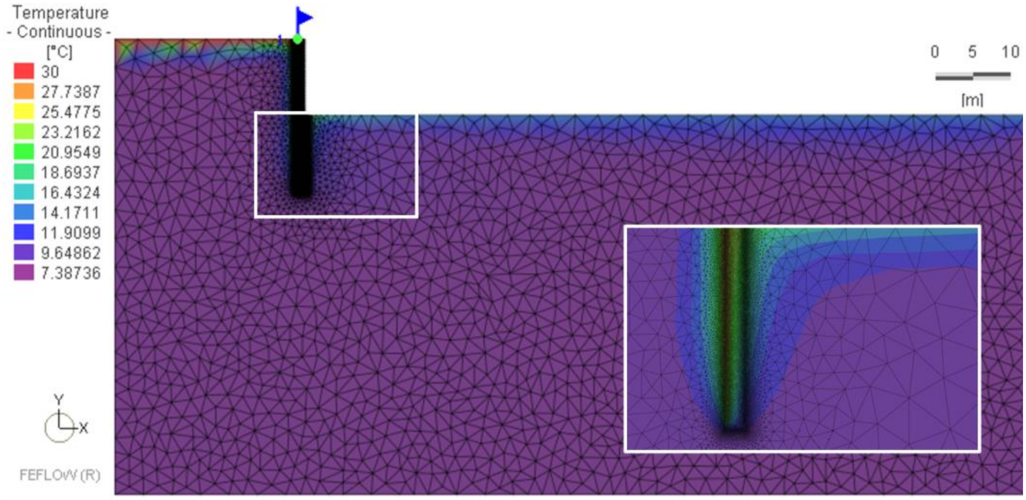

Figure 5.23 Temperature at t = 30 d (gwf = 0.7 m/d, T = 8°C, λ = 0.9 W/mK), with detail (Case II)

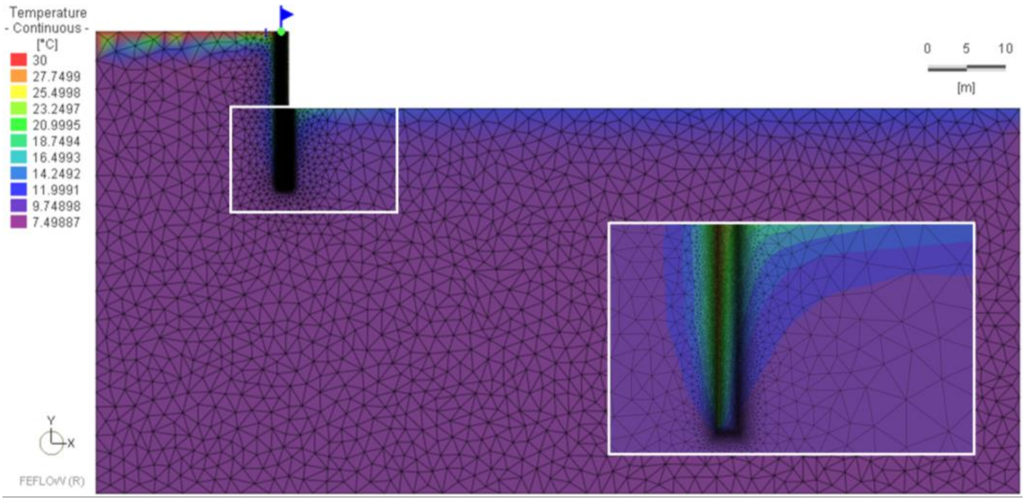

Figure 5.24 Temperature at t = 30 d (gwf = 2 m/d, T = 8°C, λ = 0.9 W/mK), with detail (Case II)

5.3.1 Outlet temperature

After the initialisation, it is possible to activate the geothermal system. The local temperatures at the inlet and outlet points of the circuit are displayed and collected for every run of the parametric analysis. Then, all the results are assembled in some graphs, both for winter conditions and for summer conditions, where inlet and outlet temperatures versus time are plotted. In summer (Figure 5.25), it is possible to notice that as the soil temperature increases, the difference between inlet and outlet temperature decreases. It has to be expected then that the injected heat will decrease too, being in function of the temperature difference. In winter (Figure 5.26), the opposite trend is shown: as the temperature of the ground enhances, the outlet temperature moves away from the inlet line.

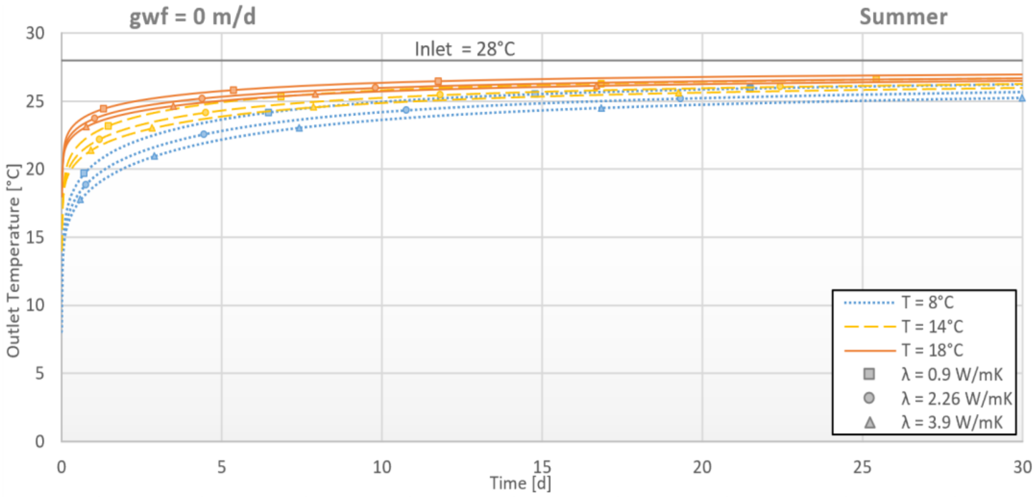

Figure 5.25 Imposed inlet and computed outlet temperatures for summer conditions with gwf = 0 m/d (Case II)

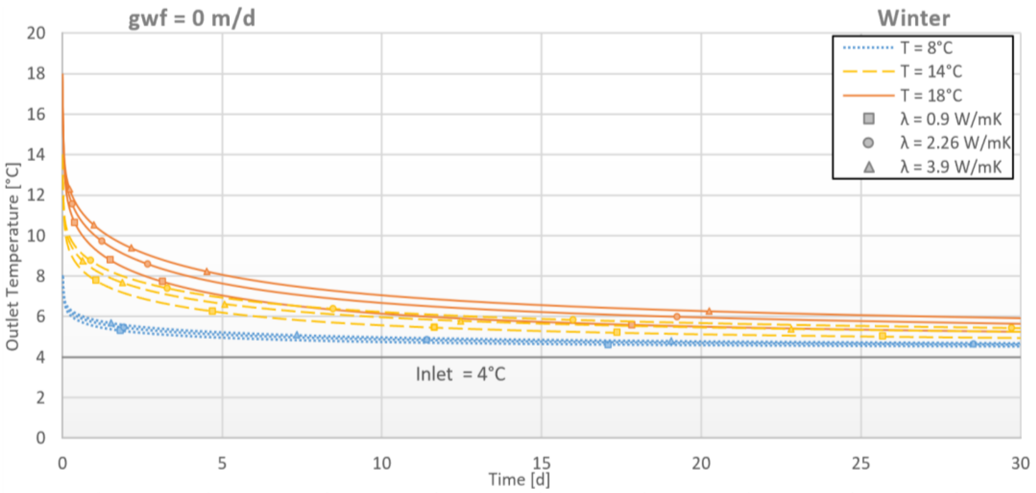

Figure 5.26 Imposed inlet and computed outlet temperatures for winter conditions with gwf = 0 m/d (Case II)

While different soil temperatures are represented with different colours, the distinct values of thermal conductivity are taken into account in the graphs with three different shaped pointers, referring to the same soil temperature. Both in cooling and heating mode, the increasing of thermal conductivity leads to a rising in terms of temperature difference, as in summer the outlet temperature lowers down and in winter it rises up.

The same trends can be obtained also in presence of groundwater flow. In Figures 5.27Figure 5.27 – 5.30Figure 5.30 the relative charts are displayed.

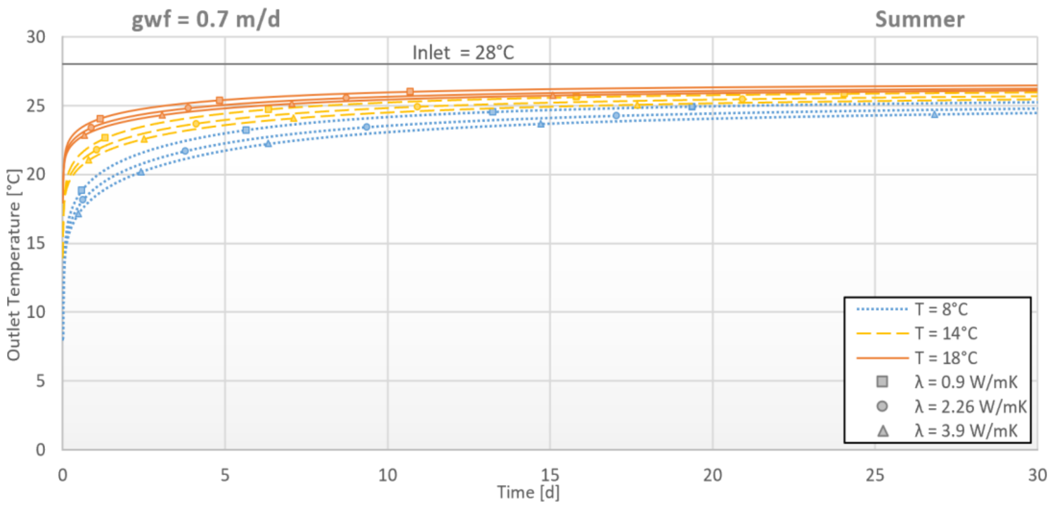

Figure 5.27 Imposed inlet and computed outlet temperatures for summer conditions with gwf = 0.7 m/d (Case II)

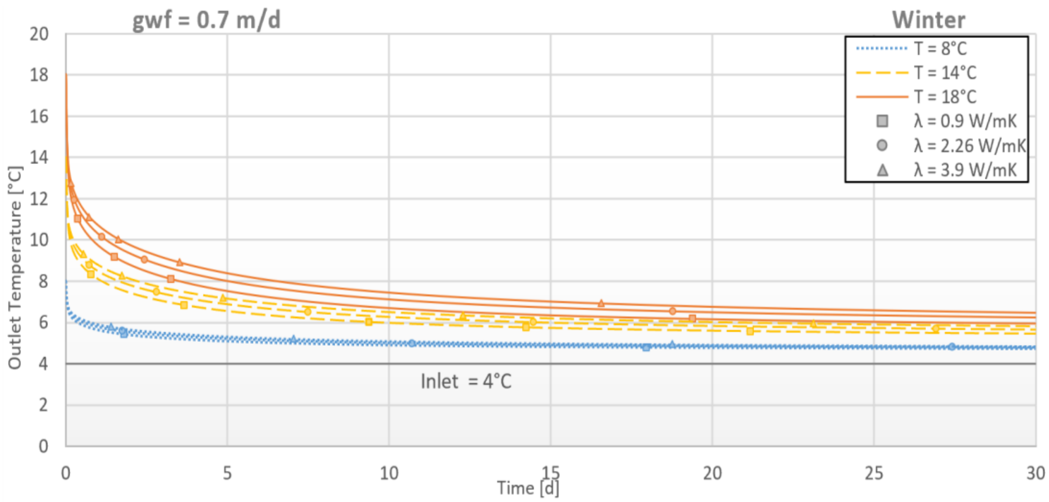

Figure 5.28 Imposed inlet and computed outlet temperatures for winter conditions with gwf = 0.7 m/d (Case II)

As the groundwater flow velocity increases, the distinction between the curves is clearer, while in the case without water flow the different lines are overlapped. The separation between different soil temperatures becomes larger, especially in the case with gwf = 2 m/d, where the outlet temperature are clearly assembled in groups according to the ground temperature. As it was expected, due to the contribution of the convective heat transfer process linked to the movement of the groundwater, the outlet temperatures increase in winter, and decrease in summer, with the increment of groundwater flow velocity.

The moving water supplies the soil more rapidly with heat, that can be extracted with the GSHP loop in heating mode. Conversely, in cooling mode the moving heat due to the groundwater flow increases the heat injection of the geothermal system.

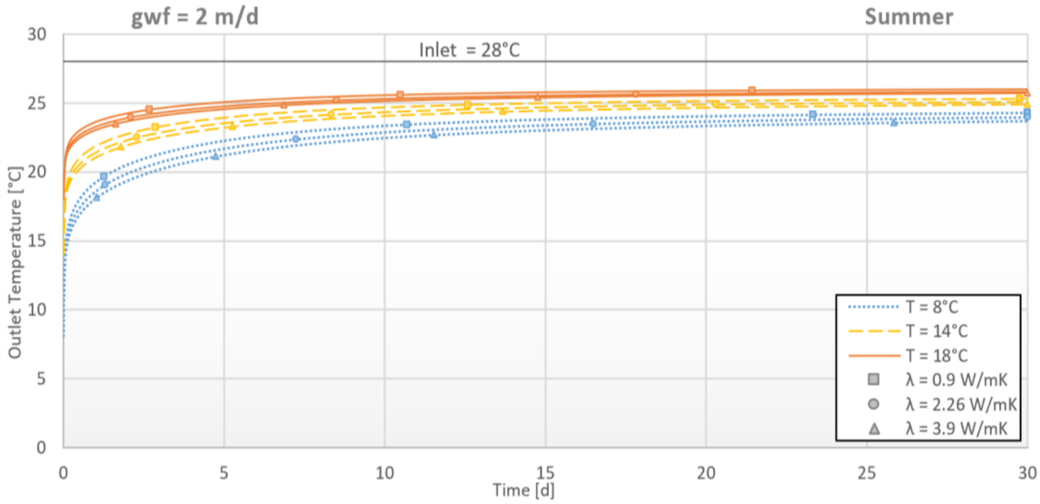

Figure 5.29 Imposed inlet and computed outlet temperatures for summer conditions with gwf = 2 m/d (Case II)

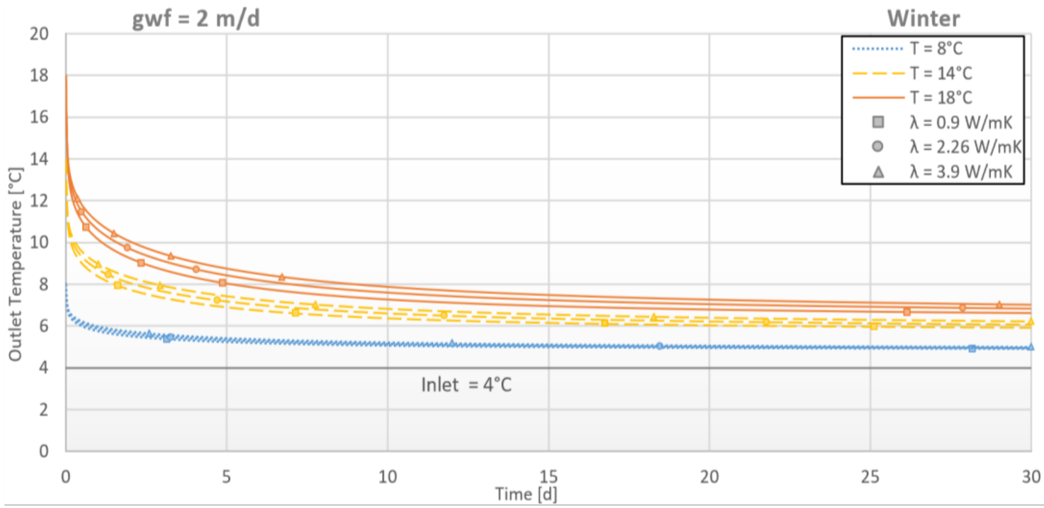

Figure 5.30 Imposed inlet and computed outlet temperatures for winter conditions with gwf = 2 m/d (Case II)

For a direct comparison between the varying parameters, only the outlet temperatures obtained at t = 30 days (horizontal axis) are collected in the graphs in Figure 5.31 and Figure 5.32, where groundwater flow velocity is on the vertical axis. Different colours and hatchings represent different soil temperatures, whilst different shaped pointers express different thermal conductivities. In Table 5-4 the results are listed (only the outlet temperatures at t = 30 days of simulation).

It is possible to notice in these conclusive charts all the considerations made previously.

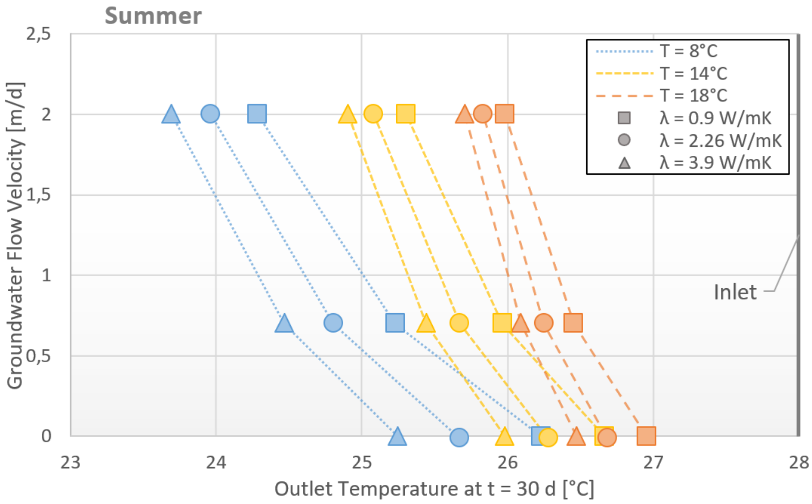

Figure 5.31 Outlet temperatures at t = 30 d of the simulations in summer, as the parameters of the analysis vary (Case II)

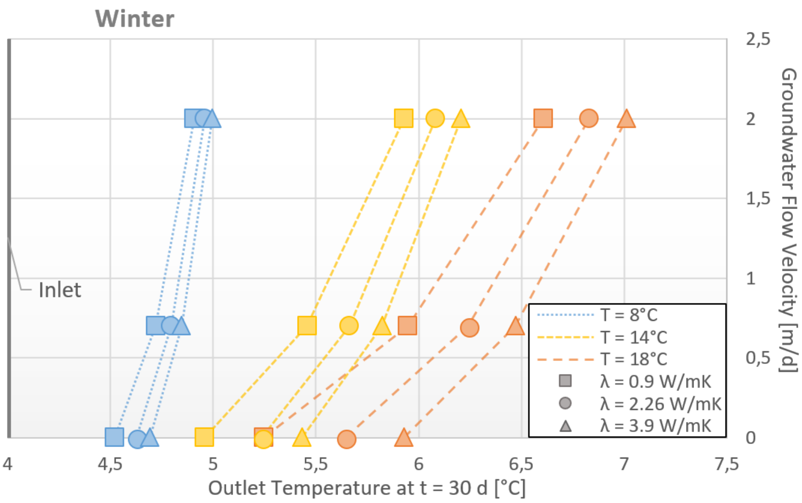

Figure 5.32 Outlet temperatures at t = 30 d of the simulations in winter, as the parameters of the analysis vary (Case II)

	T = 8°C			T = 14°C			T = 18°C			
	λ = 0.9 W/mK	λ = 2.26 W/mK	λ = 3.9 W/mK	λ = 0.9 W/mK	λ = 2.26 W/mK	λ = 3.9 W/mK	λ = 0.9 W/mK	λ = 2.26 W/mK	λ = 3.9 W/mK	
S	26,23	25,66	25,25	26,66	26,27	25,98	26,95	26,67	26,48	gwf = 0 m/d
W	4,52	4,62	4,69	4,96	5,24	5,43	5,25	5,64	5,93	
S	25,23	24,80	24,47	25,96	25,67	25,44	26,45	26,25	26,09	gwf = 0.7 m/d
W	4,72	4,79	4,85	5,46	5,66	5,82	5,95	6,24	6,47	
S	24,29	23,96	23,70	25,30	25,08	24,90	25,98	25,83	25,71	gwf = 2.0 m/d
W	4,91	4,96	5,00	5,93	6,08	6,21	6,61	6,83	7,01	

Table 5-4 Outcomes of the parametric analyses, in terms of outlet temperatures [°C] at t = 30 d (Case II)

5.3.2 Heat power

Based on the results of the parametric analysis at the end of simulations, in terms of outlet temperature T_{out} of the GSHP system, it is possible to quantify the extractable/injectable heat power Q of the energy wall (expressed in W) through the equation (16). The imposed inlet temperature is 4°C and 28°C in winter and in summer, respectively. The exchanged heat power will be presented also in W per square metre and in W per metre, normalising the results with respect to the wall panel surface (50 m^2) and its length (2.5 m) respectively. In Table 5-5 the results are listed in a concise representation, whilst in Appendix more comprehensive tables are added. It is possible to produce some charts relating to the exchanged heat power and they are shown in Figure 5.33 and Figure 5.34.

		T = 8°C			T = 14°C			T = 18°C			
		λ = 0.9 W/mK	λ = 2.26 W/mK	λ = 3.9 W/mK	λ = 0.9 W/mK	λ = 2.26 W/mK	λ = 3.9 W/mK	λ = 0.9 W/mK	λ = 2.26 W/mK	λ = 3.9 W/mK	
S	*ΔT [°C]*	1,77	2,34	2,75	1,34	1,73	2,02	1,05	1,33	1,52	gwf = 0 m/d
	Q [W]	0,97	1,29	1,51	0,73	0,95	1,11	0,57	0,73	0,84	
	q [W/m²]	19,45	25,72	30,25	14,68	19,02	22,13	11,49	14,56	16,73	
	q [W/m]	389,06	514,36	604,93	293,53	380,46	442,64	229,78	291,14	334,55	
W	*ΔT [°C]*	0,52	0,62	0,69	0,96	1,24	1,43	1,25	1,64	1,93	
	Q [W]	0,29	0,34	0,38	0,53	0,68	0,79	0,69	0,90	1,06	
	q [W/m²]	5,72	6,86	7,62	10,52	13,58	15,75	13,71	18,05	21,17	
	q [W/m]	114,43	137,25	152,42	210,30	271,58	315,01	274,22	361,10	423,42	
S	*ΔT [°C]*	2,77	3,20	3,53	2,04	2,33	2,56	1,55	1,75	1,91	gwf = 0.7 m/d
	Q [W]	1,52	1,75	1,94	1,12	1,28	1,40	0,85	0,96	1,05	
	q [W/m²]	30,43	35,08	38,76	22,36	25,57	28,08	16,98	19,22	20,96	
	q [W/m]	608,52	701,66	775,26	447,10	511,43	561,62	339,55	384,50	419,16	
W	*ΔT [°C]*	0,72	0,79	0,85	1,46	1,66	1,82	1,95	2,24	2,47	
	Q [W]	0,40	0,44	0,46	0,80	0,91	1,00	1,07	1,23	1,36	
	q [W/m²]	7,92	8,72	9,30	16,00	18,26	20,00	21,40	24,61	27,13	
	q [W/m]	158,35	174,49	185,99	320,06	365,19	400,01	427,95	492,28	542,58	
S	*ΔT [°C]*	3,71	4,04	4,30	2,70	2,92	3,10	2,02	2,17	2,29	gwf = 2.0 m/d
	Q [W]	2,04	2,22	2,36	1,48	1,60	1,70	1,11	1,19	1,26	
	q [W/m²]	40,79	44,34	47,26	29,60	32,03	34,00	22,14	23,81	25,15	
	q [W/m]	815,85	886,77	945,27	591,97	640,53	679,98	442,76	476,25	503,04	
W	*ΔT [°C]*	0,91	0,96	1,00	1,93	2,08	2,21	2,61	2,83	3,01	
	Q [W]	0,50	0,53	0,55	1,06	1,14	1,21	1,43	1,55	1,65	
	q [W/m²]	9,97	10,53	10,94	21,18	22,86	24,22	28,65	31,09	33,07	
	q [W/m]	199,33	210,60	218,73	423,50	457,29	484,38	572,95	621,71	661,44	

Table 5-5 Extracted/injected heat at t = 30 d of the simulations, in winter and in summer (Case II)

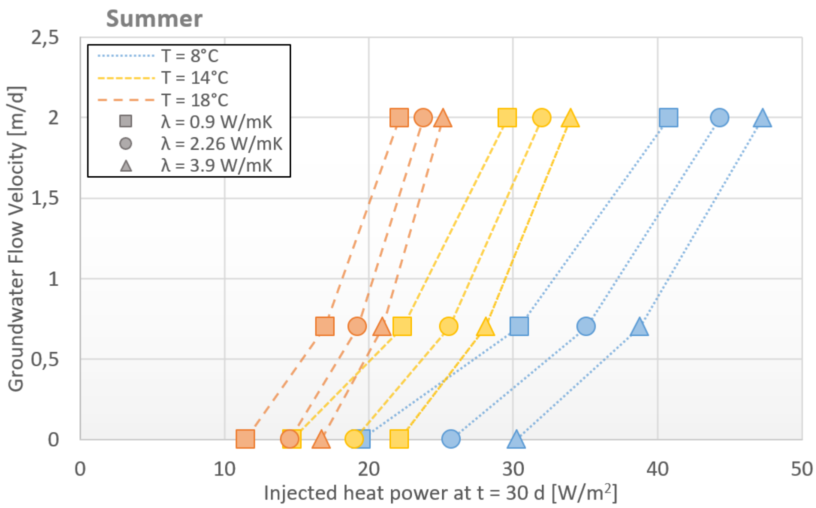

Figure 5.33 Injected heat power at t = 30 d of the simulations in summer, as the parameters of the analysis vary (Case II)

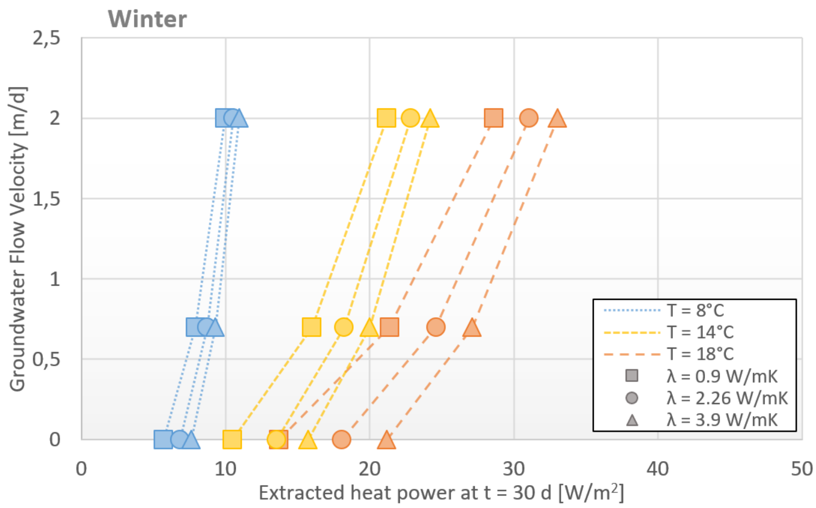

Figure 5.34 Extracted heat power at t = 30 d of the simulations in winter, as the parameters of the analysis vary (Case II)

The maximum efficiency is shown in summer (47 W/m^2), as the difference between inlet and outlet temperatures reaches the highest values in the operational mode with respect to winter case. In summer the injected heat power decreases with the increasing of the ground temperature, while in winter the opposite trend is shown. Furthermore, the chart indicates that in heating mode and with a cold ground (T = 8°C) the efficiency of the system is remarkably lower with respect to the other cases (around 9 W/m^2), thus the effects of thermal conductivity and groundwater flow velocity are less appreciable.

Even though less evident, the same trend can be appreciated in summer with T = 18°C. Reasonably, when the temperature of the ground is similar to the inlet temperature the efficiency of the system reduces.

Focusing separately on the influence of the ground features under investigation, the interpretation of these data leads to some graphs that are analysed in the following paragraphs. For basements and underground car parks, on the specific site conditions (i.e. ground temperature, soil thermal conductivity and groundwater flow velocity) the charts can give the designer a reasonable idea of the potential energy exploitation both in winter and in summer conditions, expressed in watts per square metre of diaphragm wall.

5.3.2.1 *Influence of ground temperature*

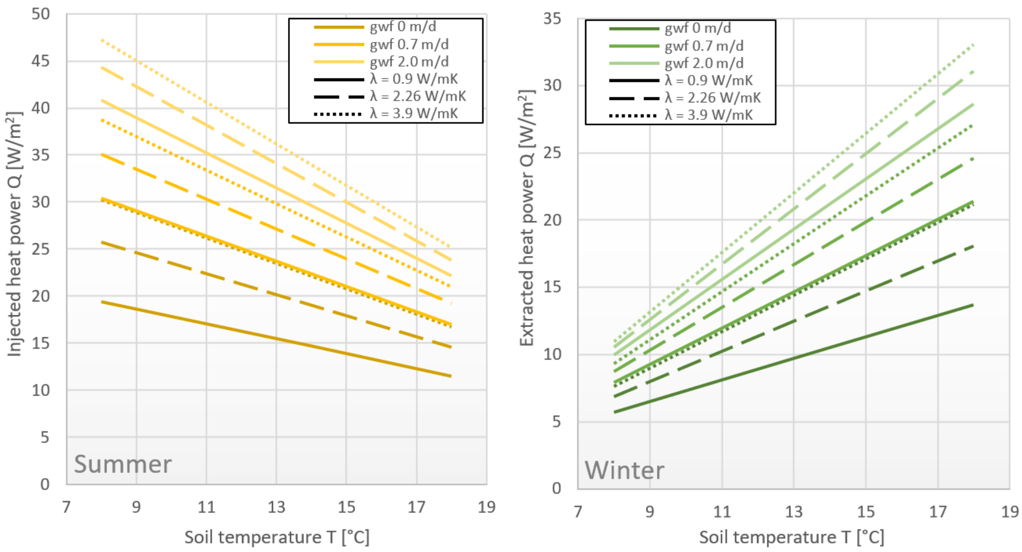

Figure 5.35 Effect of soil temperature on the energy performance, Case II (different colors = groundwater flow velocities (gwf), different hatching = bulk thermal conductivities (λ)): on the left summer mode, on the right winter mode

Based on the results of the parametric analyses, in Figure 5.35 it is possible to appreciate the linear variation with ground temperature of the injected/extracted heat both for summer and winter. In summer, the difference between the inlet and the outlet temperature decreases with the increase in soil temperature, as a result of which the efficiency decreases. The opposite trend is shown in winter mode. When groundwater flow velocity increases, energy performance becomes more sensitive to ground temperature, as the slope of the straight lines enhances.

Differently, the influence of thermal conductivity reduces with the increasing of flow velocity, as the gap between the lines decreases. Reasonably, when the convective component (groundwater flow) is less important, the conductive process of heat transfer (thermal conductivity) is predominant.

5.3.2.2 Influence of groundwater flow velocity

Figure 5.36 illustrates the effect of groundwater flow velocity on the energy efficiency of the system for winter and summer modes. Both in heating and cooling mode, the exchanged heat increases in a non-linear way with the increasing of groundwater flow velocity. As the groundwater flow velocity increases, the ratio between the convective and the conductive contributions of the heat transfer changes. As the two processes intervene in different ways in the transfer, the variation of the exchanged heat power is not linear with the increasing of the groundwater flow velocity.

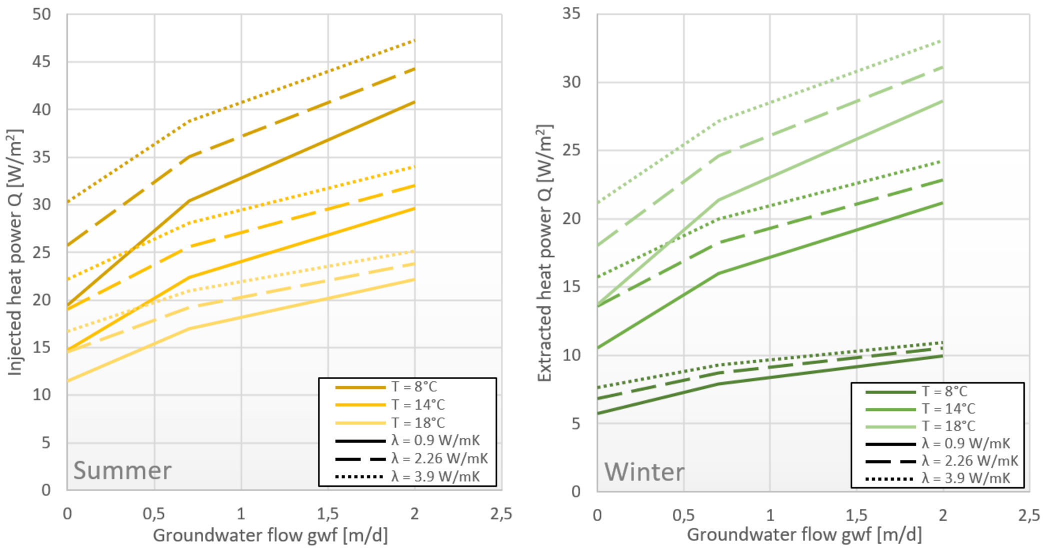

Figure 5.36 Effect of groundwater flow velocity on the energy performance, Case II (different colors = soil temperatures (T), different hatching = bulk thermal conductivities (λ)): on the left summer mode, on the right winter mode

5.3.2.3 Influence of thermal conductivity

The influence of thermal conductivity on the energy performance is shown in Figure 5.37, for summer and winter. In both cases, the increasing of exchanged heat power with the variation of the thermal conductivity is non-linear. However, non-linearity slightly reduces with the increasing of groundwater flow velocity.

In winter, it is possible to notice that the effects of thermal conductivity (average slope of the lines) and groundwater flow velocity (gap between the lines) enhance as the ground temperature rises up. Differently, the opposite trend is appreciated in summer. In both operational modes, as the groundwater flow velocity grows, the influence of thermal conductivity reduces.

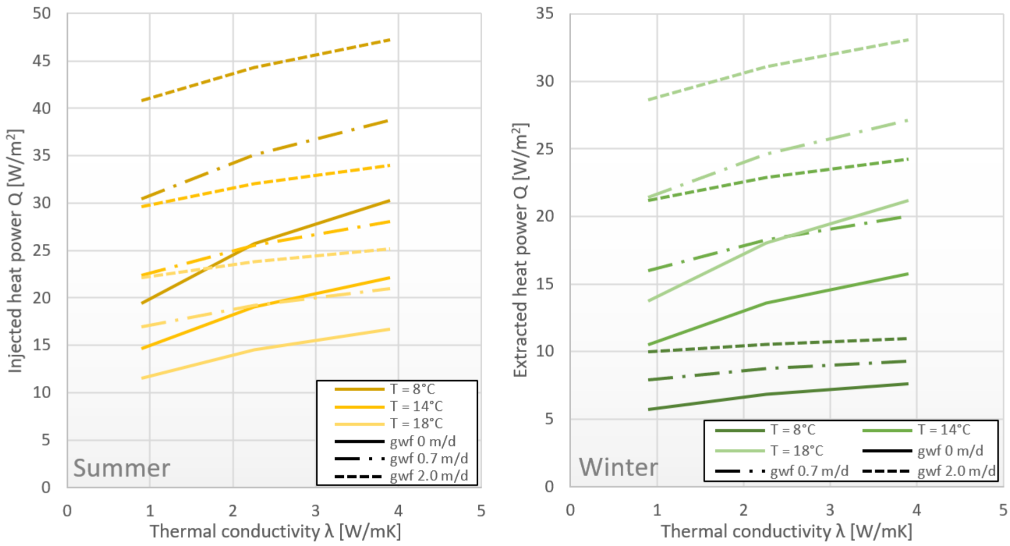

Figure 5.37 Effect of soil thermal conductivity on the energy performance, Case II (different colors = soil temperatures (T), different hatching = groundwater flow velocities (gwf)): on the left summer mode, on the right winter mode

5.4 Comparisons

In this chapter, the obtained results for Case I and Case II will be compared, in terms of outlet temperature and potential heat power. In the preliminary evaluations of this study a first distinction was made between tunnels (i.e. hotter excavations) and basements (i.e. colder excavations) and the comparison of the results aims to justify or contradict the initial choice.

Then, a comparison with the tunnel case study (Di Donna and Barla, 2015) will be made to evaluate differences in the feasibility of energy geostructures in different underground scenarios.

5.4.1 Outlet temperature

The same trends in terms of outlet temperature are appreciated in Case I and Case II analyses and they are summarised as it follows:

Summer:

- As soil temperature increases, outlet temperature increases, thus ΔT reduces;
- As thermal conductivity increases, outlet temperature decreases, thus ΔT rises;
- As groundwater flow velocity increases, outlet temperature decreases, thus ΔT rises;
- As groundwater flow velocity increases, the effect of the soil temperature on the outlet temperature rises, whilst the influence of the thermal conductivity reduces.

Winter:

- As soil temperature increases, outlet temperature increases, thus ΔT rises;
- As thermal conductivity increases, outlet temperature increases, thus ΔT rises;
- As groundwater flow velocity increases, outlet temperature increases, thus ΔT rises;
- As groundwater flow velocity increases, the effect of the soil temperature on the outlet temperature rises, whilst the influence of the thermal conductivity reduces.

The two sets of analysis can be compared within the same charts in Figure 5.38 and Figure 5.39 (summer and winter respectively), where the results for both cases are illustrated (listed in Table 5-6). Full stretch lines reproduce the results obtained with Heat Transfer BC (Case II), while the hatches represent the solutions with Constant Temperature BC (Case I).

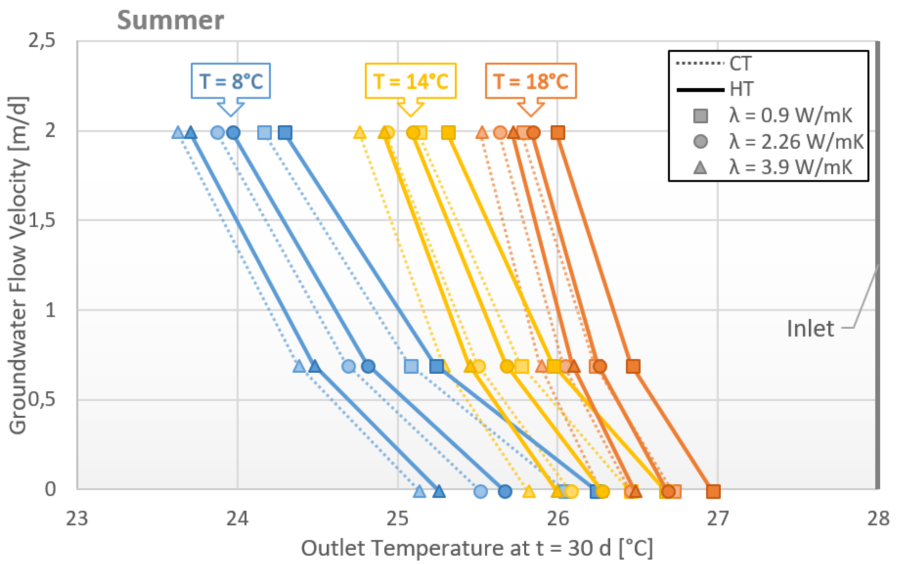

Figure 5.38 Outlet temperatures at t = 30 d for both the simulations in summer, as the parameters of the analysis vary (CT = Constant Temperature BC, HT = Heat Transfer BC)

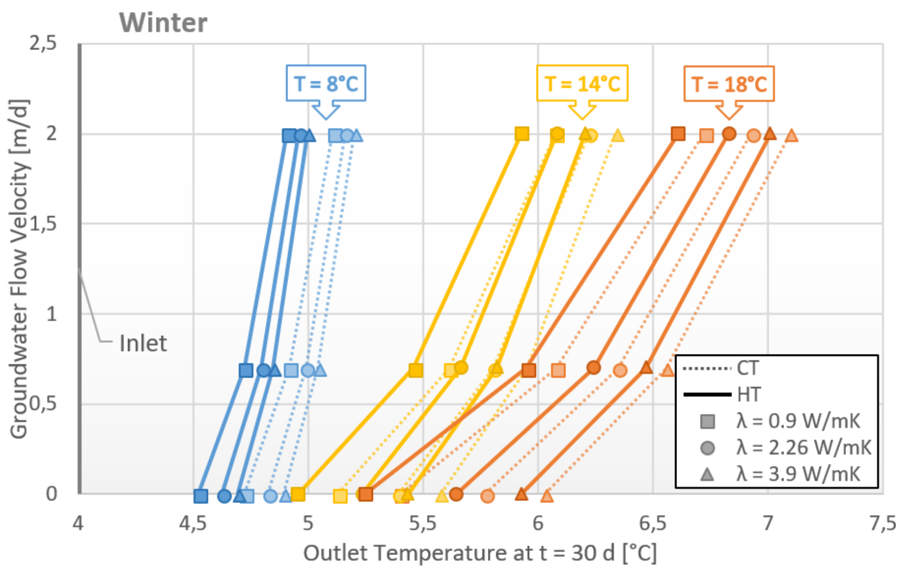

Figure 5.39 Outlet temperatures at t = 30 d for both the simulations in winter, as the parameters of the analysis vary (CT = Constant Temperature BC, HT = Heat Transfer BC)

The difference of outlet temperature between Case I and Case II is about 0.1-0.2 °C, with a maximum/minimum value of 0.243/0.074°C and 0.205/0.083°C for summer and winter respectively. It is possible to notice that the gap increases with the rise of the ground temperature in summer, while the opposite trend is shown in winter, as the highest values are registered for a soil temperature of 8°C.

	T = 8°C			T = 14°C			T = 18°C			
	λ = 0.9 W/mK	λ = 2.26 W/mK	λ = 3.9 W/mK	λ = 0.9 W/mK	λ = 2.26 W/mK	λ = 3.9 W/mK	λ = 0.9 W/mK	λ = 2.26 W/mK	λ = 3.9 W/mK	
S	-0,191	-0,153	-0,118	-0,222	-0,198	-0,177	-0,243	-0,228	-0,216	gwf = 0 m/d
W	0,202	0,199	0,198	0,171	0,154	0,140	0,150	0,123	0,100	
S	-0,161	-0,126	-0,096	-0,201	-0,180	-0,162	-0,228	-0,216	-0,206	gwf = 0.7 m/d
W	0,196	0,195	0,195	0,155	0,141	0,129	0,128	0,105	0,085	
S	-0,127	-0,099	-0,074	-0,179	-0,162	-0,148	-0,214	-0,204	-0,196	gwf = 2.0 m/d
W	0,199	0,202	0,205	0,146	0,138	0,132	0,111	0,095	0,083	

Table 5-6 Outcomes in terms of outlet temperature difference between Case I and Case II, °C (signs are in accordance)

In general, the excavation with a high airflow velocity, i.e. with a constant temperature BC, causes higher outlet temperatures in winter and lower ones in summer with respect to a heat transfer BC. It results into higher values of (T_{in} - T_{out}) for both the operational modes, thus excavations with a high air flow are expected to be a more effective condition in terms of exchanged heat power. As the heat transfer coefficient rises (thus constant temperature BC, being a good representation for high air flow velocities) heat is more readily conducted across the excavation/wall contact side and it results in lower temperatures at the interface, thus higher temperature differentials (i.e. higher exchanged heat) between the absorber pipes and the excavation.

On the other side, a low heat transfer coefficient (thus low air flow velocities) determines higher temperatures at the interface (because the heat exchange at the contact surface is slowed down) and thus lower temperature differences and heat power.

5.4.2 Heat power

According to the outlet temperatures, the same trends in terms of heat power are appreciated in Case I and Case II analyses and they are summarised as it follows:

Summer:

- Injected heat power decreases with the increasing of ground temperature, while it enhances with the increasing of thermal conductivity and groundwater flow velocity;
- As groundwater flow velocity rises up, the effect of ground temperature increases, while the influence of thermal conductivity reduces;

- As ground temperature grows, the effects of thermal conductivity and groundwater flow velocity decrease.

Winter:

- Extracted heat power increases with the rise of ground temperature, thermal conductivity and groundwater flow velocity;
- As groundwater flow velocity grows, the effect of ground temperature increases, while the influence of thermal conductivity decreases;
- As the ground temperature rises up, the effects of thermal conductivity and groundwater flow increase.

In the graphs in Figure 5.40 and Figure 5.41 (summer and winter respectively) the comparison between Case I and Case II data, in terms of heat power, can be appreciated, as full stretch lines reproduce the results obtained with Heat Transfer BC, while the hatches represent the solutions with Constant Temperature BC. As it was expected, heat power is higher for Case I both in heating and cooling mode.

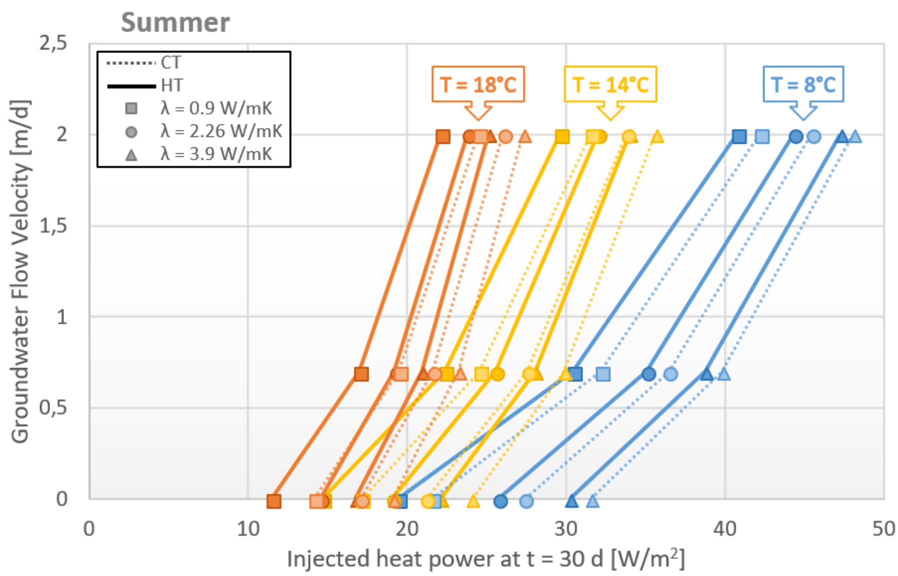

Figure 5.40 Injected heat power at t = 30 d for both the simulations in summer, as the parameters of the analysis vary (CT = Constant Temperature BC, HT = Heat Transfer BC)

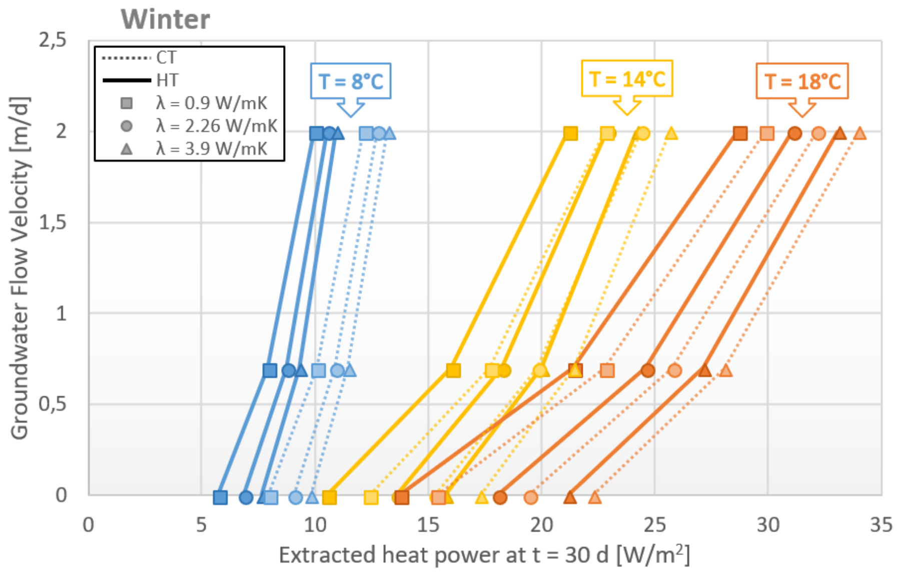

Figure 5.41 Injected heat power at t = 30 d for both the simulations in winter, as the parameters of the analysis vary (CT = Constant Temperature BC, HT = Heat Transfer BC)

The difference of exchanged heat power between Case I and Case II is about 1 – 2W/m^2, with a maximum/minimum value of 2.67/0.82°C and 2.25/0.91°C for summer and winter respectively. According to outlet temperature trends, it is possible to notice that the gap increases with the rise of the ground temperature in summer, while the opposite trend is shown in winter, as the highest values are registered for a soil temperature of 8°C.

In Table 5-7 the difference between Case I and Case II are shown, in terms of heat power, and the same results are illustrated in Figure 5.42.

	T = 8°C			T = 14°C			T = 18°C			
	λ = 0.9 W/mK	λ = 2.26 W/mK	λ = 3.9 W/mK	λ = 0.9 W/mK	λ = 2.26 W/mK	λ = 3.9 W/mK	λ = 0.9 W/mK	λ = 2.26 W/mK	λ = 3.9 W/mK	
S	2,10	1,68	1,30	2,44	2,17	1,95	**2,67**	2,50	2,37	gwf = 0 m/d
W	2,22	2,19	2,18	1,87	1,69	1,53	1,65	1,35	1,10	
S	1,77	1,38	1,05	2,21	1,98	1,78	2,50	2,37	2,26	gwf = 0.7 m/d
W	2,15	2,14	2,14	1,71	1,55	1,41	1,41	1,15	0,93	
S	1,40	1,09	0,82	1,97	1,78	1,62	2,35	2,24	2,15	gwf = 2.0 m/d
W	2,18	2,21	**2,25**	1,61	1,51	1,45	1,22	1,05	0,91	

Table 5-7 Outcomes in terms of heat power difference between Case I and Case II, W/m^2 (signs are in accordance)

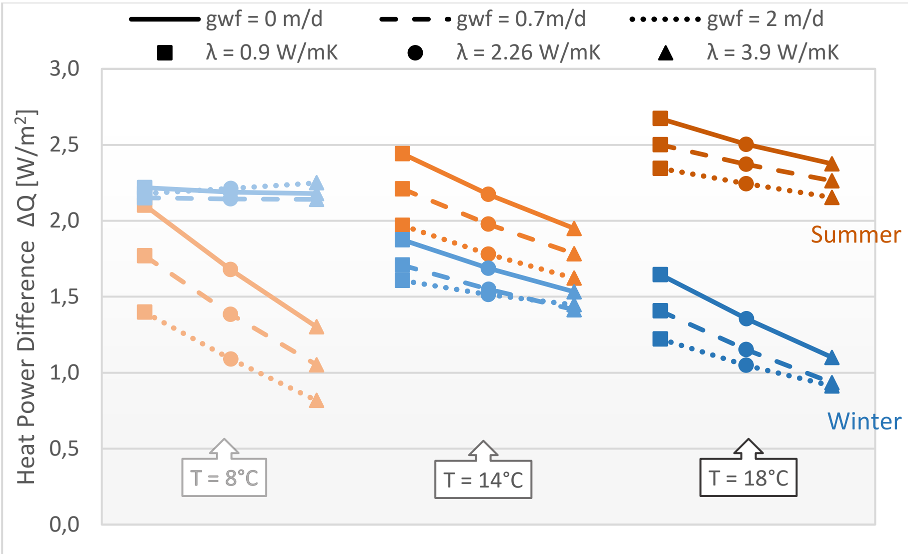

Figure 5.42 Difference in terms of heat power between Case I and Case II: different shades of colour (red=summer, blue=winter) represent different temperatures, different dotted lines represent different groundwater velocities and different shaped pointers are different values of thermal conductivity

Some similar trends, as well some singularities, can be noticed looking at the data. In accordance with the temperature variation (Figure 5.38), the maximum difference between the two different conditions occurs in summer, with hotter ground (T = 18°C), where it reaches a value of 2.67 W/m^2. As the soil temperature rises, the divergence increase in summer, while in winter the opposite trend is shown. In heating mode, the maximum values are obtained with a colder soil (a value of 2.22 W/m^2 for T = 8°C) and they decrease as the ground temperature increases.

The influence of groundwater flow velocity is more evident in summer, where it can be appreciated that as the velocity enhances, the difference reduces, even though its effect decreases with the increasing of soil temperature. A similar trend is obtained in winter only with a ground temperature of 18°C, while in the other conditions the tendency is more blurred. In particular, with a cold ground in winter the solutions of the two conditions can be confused and the variation of the different ground parameters does not have significant effects.

Both for summer and winter, as the thermal conductivity increases the difference decreases. A ground temperature of 8°C is again an exception because with ground water flow velocity equal to 0 and 0.7 m/d no influence of thermal conductivity can be appreciate and with gwf = 2 m/d the difference slightly increases.

5.4.3 Comparison with previous analysis on energy walls

The parametric analysis reported in Di Donna and Barla (2015) on energy tunnels produced some charts, shown in Chapter 2.5, useful to understand the influence of the ground characteristics on the efficiency of thermo active tunnels. Since the same parameters have been used in this study to characterise the soil, a comparison can be carried out. Moreover, Case I with a constant temperature BC has been defined as representative of a metro station or a tunnel, where thus an intense air flow velocity can be expected. However, in the numerical model defined in Di Donna and Barla (2015) a Cauchy boundary condition (e.g. a heat transfer BC) was used, proper feature of Case II. It can be useful to notice that dealing with energy tunnels, the authors had specific monitoring data for the internal temperature of the excavation, not available for this study.

Nevertheless, a correlation with both cases seems to be appropriate. However, the results for Case I and Case II are similar, thus only a comparison with a constant temperature BC will be carried out.

In Figure 5.43 the influence of the ground temperature for both tunnel (data from charts in Figure 2.12) and diaphragm wall (data from charts in Figure 5.18) is shown. As expected, the trends are similar, as the heat power rises with the increasing of ground temperature in winter and it reduces in summer. The maximum energy performance is reached in summer in both studies, even though in tunnel case the injected heat power gets to much higher values than in the wall case. Energy tunnels can reach an exchanged heat of about 110 W/m^2 and about 85 W/m^2, in summer and in winter respectively, against values for the same conditions of 50 W/m^2 and 35 W/m^2 for energy walls.

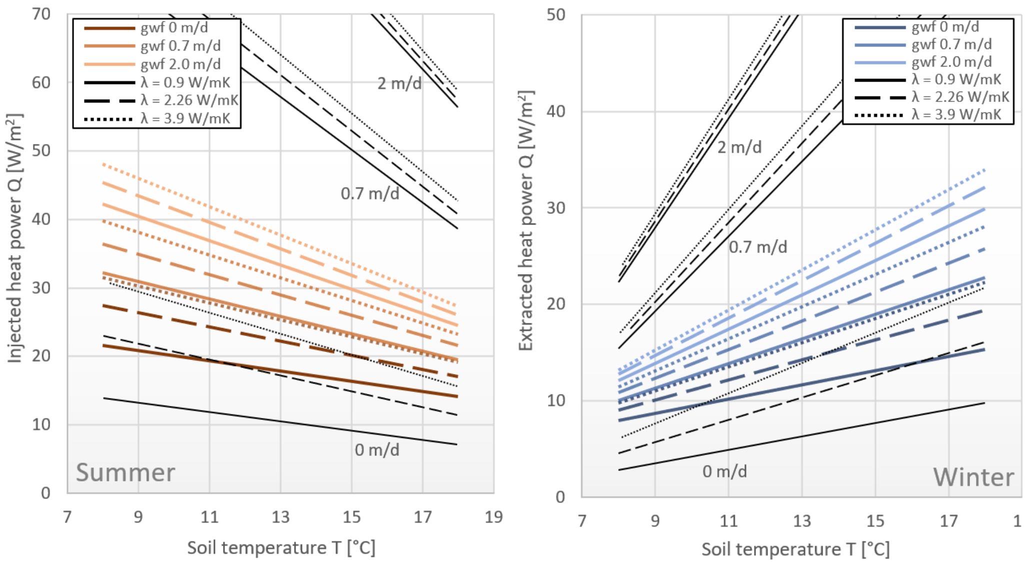

Figure 5.43 Effect of soil temperature on the energy performance of energy tunnels (in black, the numbers near the curves indicate groundwater flow velocities (gwf)) and energy walls (different colors = groundwater flow velocities (gwf)) where different hatching = bulk thermal conductivities (λ): on the left summer mode, on the right winter mode

When the water in the aquifer is in quiet the energy performance of both cases is comparable. In this condition, when the ground is colder, energy walls seem to be more efficient. This is can be associated to the different temperatures applied at the internal nodes of the excavation in the analyses since the heat transfer process with the tunnel air has an important role in the exchange.

In summer in Di Donna and Barla (2015) the temperature in the tunnel is higher with respect to this case study and thus it slows down the cooling of the fluid circulating in the pipes. It results in a lower value of T_{in}-T_{out} and thus a lower exchanged heat power. This is not the case in winter, where the internal environment in the tunnel is warmer and thus it should facilitate the heating of the fluid, increasing the difference between inlet and outlet temperature and thus the extracted heat. However, the graph shows the opposite effect.

Considering the complexity of the phenomenon, other possible explanations can lay in the different configurations of the geothermal equipment of the structural element, e.g. the thickness of the concrete layer (30 cm and 100 cm for tunnel and diaphragm wall respectively).

Differently, it comes out that as groundwater velocity increases, the exchanged heat for energy tunnels doubles the efficiency of energy walls. The role of the groundwater flow in the efficiency of the GSHP equipped tunnel proved to be more significant than in an energy wall. This can be attributed to the way the water flows in the two different geothermal models, as it is shown in Figure 5.44 and Figure 5.45. It is possible to notice in the pictures that in the case of the tunnel, completely below the water table, the geothermal loop in the lining is entirely surrounded by an intense groundwater flow, especially the area at the springline.

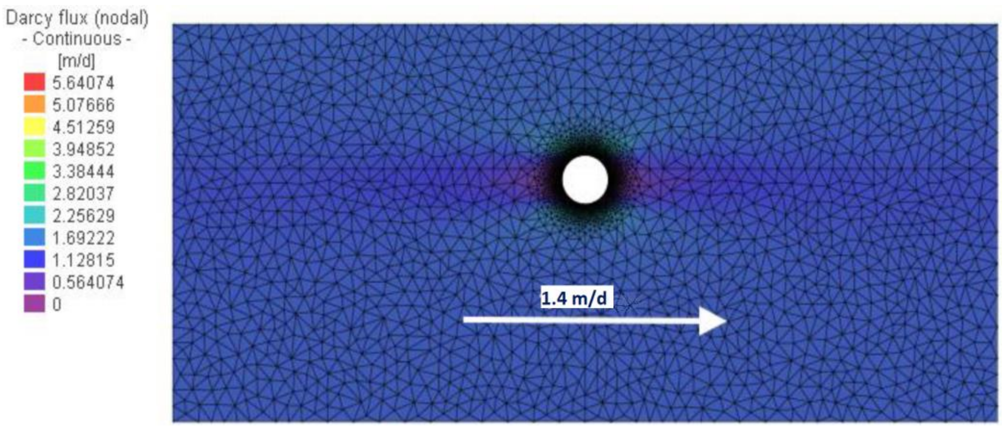

Figure 5.44 Groundwater flow rate in the tunnel case study (Zacco, 2017)

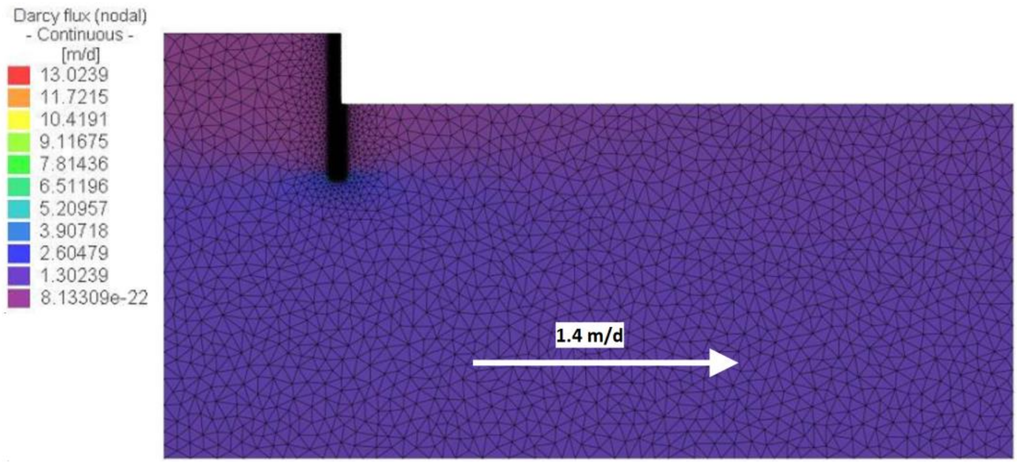

Figure 5.45 Groundwater flow rate in the diaphragm wall case study

Conversely, the water in presence of the retaining wall reaches its regime flow more deeply under the wall and the GSHP equipment is in contact with a near-zero groundwater flow. It results in a more relevant contribution of the groundwater flow velocity to the energy efficiency of the GSHP system for the tunnel case than for the energy wall.

It may be interesting then to investigate how the results would change with groundwater flowing in the direction parallel to the wall. The results so far may suggest that the effect of groundwater flow on the geothermal system would be more significant, even though adjacent wall panels might influence each other, reducing the same effect.

CONCLUSIONS

Finite-element numerical analyses were performed to investigate and quantify the effect of different underground scenarios on the heat exchange potential of energy walls.

After an introductive chapter, where geothermal energy and its traditional applications were presented and described, the attention was addressed to energy geostructures, that allow to combine structural function and energy supply. In particular, the work focused on energy walls, i.e. diaphragm walls equipped with a ground source heat pump system, that thanks to its geometry and its long extension can be efficient as heat exchanger. A literature review was presented and a lack in the study of the influence of the ground conditions on the efficiency of thermo active diaphragm walls was pointed out.

A study with the aim of quantifying the heat exchange potential of energy walls was thus defined and carried on. With the finite-element based software FEFLOW, where a thermo hydro mathematical formulation is implemented, a numerical model was determined and built, based on previous case studies dealing with energy walls. Then, the most affecting parameters of the ground were identified and a range of reasonable variation was attributed to them: ground temperature (8 – 18°C), soil thermal conductivity (0.9 – 3.9 W/mK) and groundwater flow velocity (0 – 2 m/d).

According to previous works on energy walls, it was taken into account that the efficiency of this thermo active element strongly depends on the intended use of the excavation, that is in contact with the wall on one side.

The temperature on the interface wall/excavation has an important role on the heat exchange, thus two different cases were analysed. A constant temperature boundary condition (referred so far as Case I) was applied on the external side of the wall to simulate rail tunnels or metro stations, where there is a potentially source of heat, while a heat transfer boundary condition (referred as Case II) was defined to be appropriate to represent basements or underground car parks.

For both Case I and Case II, the results show that the heat exchange increases with the increasing of soil thermal conductivity and groundwater flow velocity, in both winter and summer. Furthermore, when the system is used for cooling (summer mode) the higher the ground temperature the lower the heat exchange, while in heating mode (winter) the opposite is true.

In particular, in absence of groundwater flow, the soil thermal conductivity has a dominant role, since the heat exchange occurs essentially by conduction. When groundwater flow is present, the heat exchange results in a combination of conduction and convection, and the influence of thermal conductivity reduces while the most influencing factor becomes the intensity of groundwater flow velocity. However, the influence of the moving water in the aquifer is less significant in the efficiency of energy walls with respect to energy tunnels.

Based on the analyses and the results, for Case I and Case II some charts were developed and presented for winter and for summer. On the basis of the specific site conditions, the charts can be useful to preliminarily assess the heat that can be potentially extracted in winter and injected in summer, expressed in watts per square metre of wall panel.

The summer charts, for both Case I and Case II, outline that the most favourable condition for heat exchange is when the soil temperature is minimum and the groundwater flow velocity is maximum . Reasonable values of heat injection range between 15 and 50 W/m^2.

The winter charts, for both Case I and Case II, outline that the most favourable condition for heat exchange is when the soil temperature and groundwater flow velocity are maximum.

Reasonable values of heat extraction range between 10 and 35 W/m^2, being the heat exchange in winter lower due to the assumed lower difference between inlet and ground temperature with respect to the summer case.

These charts are developed with the numerical model presented so far, therefore they are valid only for groundwater flow perpendicular to the diaphragm wall and for the assumed geometry, inlet temperature and fluid velocity, which are reasonable and typical of energy walls applications. It should be interesting to validate the obtained results with experimental data, that seem difficult to be found though.

In particular, a groundwater flow along the parallel direction of the wall would probably result to have a more significant effect on the efficiency, even though adjacent wall panels might influence each other. This aspect should be considered in future developments. Moreover, it was made reference to a temperature range typical of European climate region. The results and the charts may not be applicable for other climatic regions.

The analyses show that the boundary condition applied at the excavation side of the wall has not an important role in the efficiency, since comparable results are obtained for Case I (constant temperature BC) and Case II (heat transfer BC). However, no difference in terms of computational time was recorded during the simulations, thus it may be appropriate to take into account the two different cases. Case I charts provide higher values of potential heat exchange that may be lightly optimistic for excavation where a nearly zero air flow velocity is expected (i.e. basements and underground car parks).

It should be considered in further investigations a variation of the internal temperature in the excavation, that in this study was neglected for simplicity of the analyses. It proved to significantly affect the efficiency of energy walls, since the heat exchange heat occurs both at the soil/wall interface and the wall excavation side.

APPENDIX

Case I

$A = 0{,}000327\ m^2$	$v = 0{,}4\ m/s$	$c_w = 4200\ J/kgK$	$\rho_w = 1000\ kg/m^3$	$m = 0{,}13072\ [kg/s]$	$S = 50\ m^2$	$L = 20\ m$

		Groundwater flow velocity = 0 m/d											
		$\lambda = 0.9\ W/mK$				$\lambda = 2.26\ W/mK$				$\lambda = 3.9\ W/mK$			
T = 8°C	Summer												
		T_{in} [°C]	28	ΔT [°C]	1,96	T_{in} [°C]	28	ΔT [°C]	2,49	T_{in} [°C]	28	ΔT [°C]	2,87
		T_{air} [°C]	30	Q [W]	1077,75	T_{air} [°C]	30	Q [W]	1369,79	T_{air} [°C]	30	Q [W]	1577,37
		T_{exc} [°C]	20	q [W/m²]	21,55	T_{exc} [°C]	20	q [W/m²]	27,40	T_{exc} [°C]	20	q [W/m²]	31,55
		T_{out} [°C]	26,04	q [W/m]	53,89	T_{out} [°C]	25,51	q [W/m]	68,49	T_{out} [°C]	25,13	q [W/m]	78,87
	Winter												
		T_{in} [°C]	4	ΔT [°C]	0,72	T_{in} [°C]	4	ΔT [°C]	0,82	T_{in} [°C]	4	ΔT [°C]	0,89
		T_{air} [°C]	2	Q [W]	396,99	T_{air} [°C]	2	Q [W]	452,54	T_{air} [°C]	2	Q [W]	489,98
		T_{exc} [°C]	10	q [W/m²]	7,94	T_{exc} [°C]	10	q [W/m²]	9,05	T_{exc} [°C]	10	q [W/m²]	9,80
		T_{out} [°C]	4,72	q [W/m]	19,85	T_{out} [°C]	4,82	q [W/m]	22,63	T_{out} [°C]	4,89	q [W/m]	24,50
T = 14°C	Summer												
		T_{in} [°C]	28	ΔT [°C]	1,56	T_{in} [°C]	28	ΔT [°C]	1,93	T_{in} [°C]	28	ΔT [°C]	2,19
		T_{air} [°C]	30	Q [W]	855,89	T_{air} [°C]	30	Q [W]	1059,82	T_{air} [°C]	30	Q [W]	1204,06
		T_{exc} [°C]	20	q [W/m²]	17,12	T_{exc} [°C]	20	q [W/m²]	21,20	T_{exc} [°C]	20	q [W/m²]	24,08
		T_{out} [°C]	26,44	q [W/m]	42,79	T_{out} [°C]	26,07	q [W/m]	52,99	T_{out} [°C]	25,81	q [W/m]	60,20
	Winter												
		T_{in} [°C]	4	ΔT [°C]	1,13	T_{in} [°C]	4	ΔT [°C]	1,39	T_{in} [°C]	4	ΔT [°C]	1,57
		T_{air} [°C]	2	Q [W]	619,48	T_{air} [°C]	2	Q [W]	763,32	T_{air} [°C]	2	Q [W]	864,13
		T_{exc} [°C]	10	q [W/m²]	12,39	T_{exc} [°C]	10	q [W/m²]	15,27	T_{exc} [°C]	10	q [W/m²]	17,28
		T_{out} [°C]	5,13	q [W/m]	30,97	T_{out} [°C]	5,39	q [W/m]	38,17	T_{out} [°C]	5,57	q [W/m]	43,21
T = 18°C	Summer												
		T_{in} [°C]	28	ΔT [°C]	1,29	T_{in} [°C]	28	ΔT [°C]	1,55	T_{in} [°C]	28	ΔT [°C]	1,74
		T_{air} [°C]	30	Q [W]	708,07	T_{air} [°C]	30	Q [W]	853,03	T_{air} [°C]	30	Q [W]	955,12
		T_{exc} [°C]	20	q [W/m²]	14,16	T_{exc} [°C]	20	q [W/m²]	17,06	T_{exc} [°C]	20	q [W/m²]	19,10
		T_{out} [°C]	26,71	q [W/m]	35,40	T_{out} [°C]	26,45	q [W/m]	42,65	T_{out} [°C]	26,26	q [W/m]	47,76
	Winter												
		T_{in} [°C]	4	ΔT [°C]	1,40	T_{in} [°C]	4	ΔT [°C]	1,77	T_{in} [°C]	4	ΔT [°C]	2,03
		T_{air} [°C]	2	Q [W]	767,80	T_{air} [°C]	2	Q [W]	970,48	T_{air} [°C]	2	Q [W]	1113,56
		T_{exc} [°C]	10	q [W/m²]	15,36	T_{exc} [°C]	10	q [W/m²]	19,41	T_{exc} [°C]	10	q [W/m²]	22,27
		T_{out} [°C]	5,40	q [W/m]	38,39	T_{out} [°C]	5,77	q [W/m]	48,52	T_{out} [°C]	6,03	q [W/m]	55,68

Table X.1 Extracted/injected heat at t = 30 d for each combination of the parametric analysis with gwf = 0 m/d, in winter and in summer (Case I)

Case I

A = 0,000327 m^2 v = 0,4 m/s c_w = 4200 J/kgK ρ_w = 1000 kg/m^3 m = 0,13072 [kg/s] S = 50 m^2 L = 20 m

		Groundwater flow velocity = 0,7 m/d											
		λ = 0.9 W/mK				λ = 2.26 W/mK				λ = 3.9 W/mK			
T = 8°C	Summer	T_{in} [°C]	28	ΔT [°C]	2,93	T_{in} [°C]	28	ΔT [°C]	3,32	T_{in} [°C]	28	ΔT [°C]	3,63
		T_{air} [°C]	30	Q [W]	1609,74	T_{air} [°C]	30	Q [W]	1823,40	T_{air} [°C]	30	Q [W]	1990,73
		T_{exc} [°C]	20	q [W/m^2]	32,19	T_{exc} [°C]	20	q [W/m^2]	36,47	T_{exc} [°C]	20	q [W/m^2]	39,81
		T_{out} [°C]	25,07	q [W/m]	80,49	T_{out} [°C]	24,68	q [W/m]	91,17	T_{out} [°C]	24,37	q [W/m]	99,54
	Winter	T_{in} [°C]	4	ΔT [°C]	0,92	T_{in} [°C]	4	ΔT [°C]	0,99	T_{in} [°C]	4	ΔT [°C]	1,04
		T_{air} [°C]	2	Q [W]	503,43	T_{air} [°C]	2	Q [W]	543,40	T_{air} [°C]	2	Q [W]	572,01
		T_{exc} [°C]	10	q [W/m^2]	10,07	T_{exc} [°C]	10	q [W/m^2]	10,87	T_{exc} [°C]	10	q [W/m^2]	11,44
		T_{out} [°C]	4,92	q [W/m]	25,17	T_{out} [°C]	4,99	q [W/m]	27,17	T_{out} [°C]	5,04	q [W/m]	28,60
T = 14°C	Summer	T_{in} [°C]	28	ΔT [°C]	2,24	T_{in} [°C]	28	ΔT [°C]	2,51	T_{in} [°C]	28	ΔT [°C]	2,72
		T_{air} [°C]	30	Q [W]	1228,24	T_{air} [°C]	30	Q [W]	1377,43	T_{air} [°C]	30	Q [W]	1493,19
		T_{exc} [°C]	20	q [W/m^2]	24,56	T_{exc} [°C]	20	q [W/m^2]	27,55	T_{exc} [°C]	20	q [W/m^2]	29,86
		T_{out} [°C]	25,76	q [W/m]	61,41	T_{out} [°C]	25,49	q [W/m]	68,87	T_{out} [°C]	25,28	q [W/m]	74,66
	Winter	T_{in} [°C]	4	ΔT [°C]	1,61	T_{in} [°C]	4	ΔT [°C]	1,80	T_{in} [°C]	4	ΔT [°C]	1,95
		T_{air} [°C]	2	Q [W]	885,52	T_{air} [°C]	2	Q [W]	990,38	T_{air} [°C]	2	Q [W]	1070,73
		T_{exc} [°C]	10	q [W/m^2]	17,71	T_{exc} [°C]	10	q [W/m^2]	19,81	T_{exc} [°C]	10	q [W/m^2]	21,41
		T_{out} [°C]	5,61	q [W/m]	44,28	T_{out} [°C]	5,80	q [W/m]	49,52	T_{out} [°C]	5,95	q [W/m]	53,54
T = 18°C	Summer	T_{in} [°C]	28	ΔT [°C]	1,77	T_{in} [°C]	28	ΔT [°C]	1,97	T_{in} [°C]	28	ΔT [°C]	2,11
		T_{air} [°C]	30	Q [W]	973,88	T_{air} [°C]	30	Q [W]	1079,80	T_{air} [°C]	30	Q [W]	1161,06
		T_{exc} [°C]	20	q [W/m^2]	19,48	T_{exc} [°C]	20	q [W/m^2]	21,60	T_{exc} [°C]	20	q [W/m^2]	23,22
		T_{out} [°C]	26,23	q [W/m]	48,69	T_{out} [°C]	26,03	q [W/m]	53,99	T_{out} [°C]	25,89	q [W/m]	58,05
	Winter	T_{in} [°C]	4	ΔT [°C]	2,08	T_{in} [°C]	4	ΔT [°C]	2,35	T_{in} [°C]	4	ΔT [°C]	2,56
		T_{air} [°C]	2	Q [W]	1140,19	T_{air} [°C]	2	Q [W]	1288,27	T_{air} [°C]	2	Q [W]	1403,12
		T_{exc} [°C]	10	q [W/m^2]	22,80	T_{exc} [°C]	10	q [W/m^2]	25,77	T_{exc} [°C]	10	q [W/m^2]	28,06
		T_{out} [°C]	6,08	q [W/m]	57,01	T_{out} [°C]	6,35	q [W/m]	64,41	T_{out} [°C]	6,56	q [W/m]	70,16

Table X.2 Extracted/injected heat at t = 30 d for each combination of the parametric analysis with gwf = 0.7 m/d, in winter and in summer (Case I)

Case I — A = 0,000327 m^2 v = 0,4 m/s c_w = 4200 J/kgK ρ_w = 1000 kg/m^3 m = 0,13072 [kg/s] S = 50 m^2 L = 20 m

		Groundwater flow velocity = 2 m/d											
		λ = 0.9 W/mK				λ = 2.26 W/mK				λ = 3.9 W/mK			
T = 8°C	Summer												
		T_{in} [°C]	28	ΔT [°C]	3,84	T_{in} [°C]	28	ΔT [°C]	4,14	T_{in} [°C]	28	ΔT [°C]	4,38
		T_{air} [°C]	30	Q [W]	2109,53	T_{air} [°C]	30	Q [W]	2271,37	T_{air} [°C]	30	Q [W]	2403,98
		T_{exc} [°C]	20	q [W/m^2]	42,19	T_{exc} [°C]	20	q [W/m^2]	45,43	T_{exc} [°C]	20	q [W/m^2]	48,08
		T_{out} [°C]	24,16	q [W/m]	105,48	T_{out} [°C]	23,86	q [W/m]	113,57	T_{out} [°C]	23,62	q [W/m]	120,20
	Winter												
		T_{in} [°C]	4	ΔT [°C]	1,11	T_{in} [°C]	4	ΔT [°C]	1,16	T_{in} [°C]	4	ΔT [°C]	1,20
		T_{air} [°C]	2	Q [W]	607,34	T_{air} [°C]	2	Q [W]	637,17	T_{air} [°C]	2	Q [W]	659,28
		T_{exc} [°C]	10	q [W/m^2]	12,15	T_{exc} [°C]	10	q [W/m^2]	12,74	T_{exc} [°C]	10	q [W/m^2]	13,19
		T_{out} [°C]	5,11	q [W/m]	30,37	T_{out} [°C]	5,16	q [W/m]	31,86	T_{out} [°C]	5,20	q [W/m]	32,96
T = 14°C	Summer												
		T_{in} [°C]	28	ΔT [°C]	2,87	T_{in} [°C]	28	ΔT [°C]	3,08	T_{in} [°C]	28	ΔT [°C]	3,24
		T_{air} [°C]	30	Q [W]	1578,34	T_{air} [°C]	30	Q [W]	1690,33	T_{air} [°C]	30	Q [W]	1781,00
		T_{exc} [°C]	20	q [W/m^2]	31,57	T_{exc} [°C]	20	q [W/m^2]	33,81	T_{exc} [°C]	20	q [W/m^2]	35,62
		T_{out} [°C]	25,13	q [W/m]	78,92	T_{out} [°C]	24,92	q [W/m]	84,52	T_{out} [°C]	24,76	q [W/m]	89,05
	Winter												
		T_{in} [°C]	4	ΔT [°C]	2,07	T_{in} [°C]	4	ΔT [°C]	2,22	T_{in} [°C]	4	ΔT [°C]	2,34
		T_{air} [°C]	2	Q [W]	1139,07	T_{air} [°C]	2	Q [W]	1218,93	T_{air} [°C]	2	Q [W]	1283,27
		T_{exc} [°C]	10	q [W/m^2]	22,78	T_{exc} [°C]	10	q [W/m^2]	24,38	T_{exc} [°C]	10	q [W/m^2]	25,67
		T_{out} [°C]	6,07	q [W/m]	56,95	T_{out} [°C]	6,22	q [W/m]	60,95	T_{out} [°C]	6,34	q [W/m]	64,16
T = 18°C	Summer												
		T_{in} [°C]	28	ΔT [°C]	2,23	T_{in} [°C]	28	ΔT [°C]	2,37	T_{in} [°C]	28	ΔT [°C]	2,49
		T_{air} [°C]	30	Q [W]	1224,15	T_{air} [°C]	30	Q [W]	1302,84	T_{air} [°C]	30	Q [W]	1365,27
		T_{exc} [°C]	20	q [W/m^2]	24,48	T_{exc} [°C]	20	q [W/m^2]	26,06	T_{exc} [°C]	20	q [W/m^2]	27,31
		T_{out} [°C]	25,77	q [W/m]	61,21	T_{out} [°C]	25,63	q [W/m]	65,14	T_{out} [°C]	25,51	q [W/m]	68,26
	Winter												
		T_{in} [°C]	4	ΔT [°C]	2,72	T_{in} [°C]	4	ΔT [°C]	2,93	T_{in} [°C]	4	ΔT [°C]	3,09
		T_{air} [°C]	2	Q [W]	1493,49	T_{air} [°C]	2	Q [W]	1606,68	T_{air} [°C]	2	Q [W]	1699,21
		T_{exc} [°C]	10	q [W/m^2]	29,87	T_{exc} [°C]	10	q [W/m^2]	32,13	T_{exc} [°C]	10	q [W/m^2]	33,98
		T_{out} [°C]	6,72	q [W/m]	74,67	T_{out} [°C]	6,93	q [W/m]	80,33	T_{out} [°C]	7,09	q [W/m]	84,96

Table X.3 Extracted/injected heat at t = 30 d for each combination of the parametric analysis with gwf = 2 m/d, in winter and in summer (Case I)

Case II — $A = 0{,}000327\ m^2$ — $v = 0{,}4\ m/s$ — $c_w = 4200\ J/kgK$ — $\rho_w = 1000\ kg/m^3$ — $m = 0{,}13072\ [kg/s]$ — $S = 50\ m^2$ — $L = 20\ m$

		Groundwater flow velocity = 0 m/d											
		λ = 0.9 W/mK				λ = 2.26 W/mK				λ = 3.9 W/mK			
T = 8°C	Summer	T_{in} [°C]	28	ΔT [°C]	1,77	T_{in} [°C]	28	ΔT [°C]	2,34	T_{in} [°C]	28	ΔT [°C]	2,75
		T_{air} [°C]	30	Q [W]	972,65	T_{air} [°C]	30	Q [W]	1285,90	T_{air} [°C]	30	Q [W]	1512,32
		T_{exc} [°C]	20	q [W/m^2]	19,45	T_{exc} [°C]	20	q [W/m^2]	25,72	T_{exc} [°C]	20	q [W/m^2]	30,25
		T_{out} [°C]	26,23	q [W/m]	48,63	T_{out} [°C]	25,66	q [W/m]	64,29	T_{out} [°C]	25,25	q [W/m]	75,62
	Winter	T_{in} [°C]	4	ΔT [°C]	0,52	T_{in} [°C]	4	ΔT [°C]	0,62	T_{in} [°C]	4	ΔT [°C]	0,69
		T_{air} [°C]	2	Q [W]	286,09	T_{air} [°C]	2	Q [W]	343,12	T_{air} [°C]	2	Q [W]	381,04
		T_{exc} [°C]	10	q [W/m^2]	5,72	T_{exc} [°C]	10	q [W/m^2]	6,86	T_{exc} [°C]	10	q [W/m^2]	7,62
		T_{out} [°C]	4,52	q [W/m]	14,30	T_{out} [°C]	4,62	q [W/m]	17,16	T_{out} [°C]	4,69	q [W/m]	19,05
T = 14°C	Summer	T_{in} [°C]	28	ΔT [°C]	1,34	T_{in} [°C]	28	ΔT [°C]	1,73	T_{in} [°C]	28	ΔT [°C]	2,02
		T_{air} [°C]	30	Q [W]	733,83	T_{air} [°C]	30	Q [W]	951,16	T_{air} [°C]	30	Q [W]	1106,61
		T_{exc} [°C]	20	q [W/m^2]	14,68	T_{exc} [°C]	20	q [W/m^2]	19,02	T_{exc} [°C]	20	q [W/m^2]	22,13
		T_{out} [°C]	26,66	q [W/m]	36,69	T_{out} [°C]	26,27	q [W/m]	47,56	T_{out} [°C]	25,98	q [W/m]	55,33
	Winter	T_{in} [°C]	4	ΔT [°C]	0,96	T_{in} [°C]	4	ΔT [°C]	1,24	T_{in} [°C]	4	ΔT [°C]	1,43
		T_{air} [°C]	2	Q [W]	525,76	T_{air} [°C]	2	Q [W]	678,94	T_{air} [°C]	2	Q [W]	787,52
		T_{exc} [°C]	10	q [W/m^2]	10,52	T_{exc} [°C]	10	q [W/m^2]	13,58	T_{exc} [°C]	10	q [W/m^2]	15,75
		T_{out} [°C]	4,96	q [W/m]	26,29	T_{out} [°C]	5,24	q [W/m]	33,95	T_{out} [°C]	5,43	q [W/m]	39,38
T = 18°C	Summer	T_{in} [°C]	28	ΔT [°C]	1,05	T_{in} [°C]	28	ΔT [°C]	1,33	T_{in} [°C]	28	ΔT [°C]	1,52
		T_{air} [°C]	30	Q [W]	574,45	T_{air} [°C]	30	Q [W]	727,85	T_{air} [°C]	30	Q [W]	836,38
		T_{exc} [°C]	20	q [W/m^2]	11,49	T_{exc} [°C]	20	q [W/m^2]	14,56	T_{exc} [°C]	20	q [W/m^2]	16,73
		T_{out} [°C]	26,95	q [W/m]	28,72	T_{out} [°C]	26,67	q [W/m]	36,39	T_{out} [°C]	26,48	q [W/m]	41,82
	Winter	T_{in} [°C]	4	ΔT [°C]	1,25	T_{in} [°C]	4	ΔT [°C]	1,64	T_{in} [°C]	4	ΔT [°C]	1,93
		T_{air} [°C]	2	Q [W]	685,55	T_{air} [°C]	2	Q [W]	902,75	T_{air} [°C]	2	Q [W]	1058,55
		T_{exc} [°C]	10	q [W/m^2]	13,71	T_{exc} [°C]	10	q [W/m^2]	18,05	T_{exc} [°C]	10	q [W/m^2]	21,17
		T_{out} [°C]	5,25	q [W/m]	34,28	T_{out} [°C]	5,64	q [W/m]	45,14	T_{out} [°C]	5,93	q [W/m]	52,93

Table X.4 Extracted/injected heat at t = 30 d for each combination of the parametric analysis with gwf = 0 m/d, in winter and in summer (Case II)

Case II

A = 0,000327 m^2 v = 0,4 m/s c_w = 4200 J/kgK ρ_w = 1000 kg/m^3 m = 0,13072 [kg/s] S = 50 m^2 L = 20 m

		Groundwater flow velocity = 0,7 m/d											
		λ = 0.9 W/mK				λ = 2.26 W/mK				λ = 3.9 W/mK			
T = 8°C	Summer												
		T_{in} [°C]	28	ΔT [°C]	2,77	T_{in} [°C]	28	ΔT [°C]	3,20	T_{in} [°C]	28	ΔT [°C]	3,53
		T_{air} [°C]	30	Q [W]	1521,31	T_{air} [°C]	30	Q [W]	1754,16	T_{air} [°C]	30	Q [W]	1938,15
		T_{exc} [°C]	20	q [W/m^2]	30,43	T_{exc} [°C]	20	q [W/m^2]	35,08	T_{exc} [°C]	20	q [W/m^2]	38,76
		T_{out} [°C]	25,23	q [W/m]	76,07	T_{out} [°C]	24,80	q [W/m]	87,71	T_{out} [°C]	24,47	q [W/m]	96,91
	Winter												
		T_{in} [°C]	4	ΔT [°C]	0,72	T_{in} [°C]	4	ΔT [°C]	0,79	T_{in} [°C]	4	ΔT [°C]	0,85
		T_{air} [°C]	2	Q [W]	395,87	T_{air} [°C]	2	Q [W]	436,23	T_{air} [°C]	2	Q [W]	464,97
		T_{exc} [°C]	10	q [W/m^2]	7,92	T_{exc} [°C]	10	q [W/m^2]	8,72	T_{exc} [°C]	10	q [W/m^2]	9,30
		T_{out} [°C]	4,72	q [W/m]	19,79	T_{out} [°C]	4,79	q [W/m]	21,81	T_{out} [°C]	4,85	q [W/m]	23,25
T = 14°C	Summer												
		T_{in} [°C]	28	ΔT [°C]	2,04	T_{in} [°C]	28	ΔT [°C]	2,33	T_{in} [°C]	28	ΔT [°C]	2,56
		T_{air} [°C]	30	Q [W]	1117,76	T_{air} [°C]	30	Q [W]	1278,58	T_{air} [°C]	30	Q [W]	1404,04
		T_{exc} [°C]	20	q [W/m^2]	22,36	T_{exc} [°C]	20	q [W/m^2]	25,57	T_{exc} [°C]	20	q [W/m^2]	28,08
		T_{out} [°C]	25,96	q [W/m]	55,89	T_{out} [°C]	25,67	q [W/m]	63,93	T_{out} [°C]	25,44	q [W/m]	70,20
	Winter												
		T_{in} [°C]	4	ΔT [°C]	1,46	T_{in} [°C]	4	ΔT [°C]	1,66	T_{in} [°C]	4	ΔT [°C]	1,82
		T_{air} [°C]	2	Q [W]	800,16	T_{air} [°C]	2	Q [W]	912,97	T_{air} [°C]	2	Q [W]	1000,02
		T_{exc} [°C]	10	q [W/m^2]	16,00	T_{exc} [°C]	10	q [W/m^2]	18,26	T_{exc} [°C]	10	q [W/m^2]	20,00
		T_{out} [°C]	5,46	q [W/m]	40,01	T_{out} [°C]	5,66	q [W/m]	45,65	T_{out} [°C]	5,82	q [W/m]	50,00
T = 18°C	Summer												
		T_{in} [°C]	28	ΔT [°C]	1,55	T_{in} [°C]	28	ΔT [°C]	1,75	T_{in} [°C]	28	ΔT [°C]	1,91
		T_{air} [°C]	30	Q [W]	848,87	T_{air} [°C]	30	Q [W]	961,24	T_{air} [°C]	30	Q [W]	1047,91
		T_{exc} [°C]	20	q [W/m^2]	16,98	T_{exc} [°C]	20	q [W/m^2]	19,22	T_{exc} [°C]	20	q [W/m^2]	20,96
		T_{out} [°C]	26,45	q [W/m]	42,44	T_{out} [°C]	26,25	q [W/m]	48,06	T_{out} [°C]	26,09	q [W/m]	52,40
	Winter												
		T_{in} [°C]	4	ΔT [°C]	1,95	T_{in} [°C]	4	ΔT [°C]	2,24	T_{in} [°C]	4	ΔT [°C]	2,47
		T_{air} [°C]	2	Q [W]	1069,88	T_{air} [°C]	2	Q [W]	1230,69	T_{air} [°C]	2	Q [W]	1356,45
		T_{exc} [°C]	10	q [W/m^2]	21,40	T_{exc} [°C]	10	q [W/m^2]	24,61	T_{exc} [°C]	10	q [W/m^2]	27,13
		T_{out} [°C]	5,95	q [W/m]	53,49	T_{out} [°C]	6,24	q [W/m]	61,53	T_{out} [°C]	6,47	q [W/m]	67,82

Table X.5 Extracted/injected heat at t = 30 d for each combination of the parametric analysis with gwf = 0.7 m/d, in winter and in summer (Case II)

Case II — $A = 0{,}000327\ m^2$ — $v = 0{,}4\ m/s$ — $c_w = 4200\ J/kgK$ — $\rho_w = 1000\ kg/m^3$ — $m = 0{,}13072\ [kg/s]$ — $S = 50\ m^2$ — $L = 20\ m$

		Groundwater flow velocity = 2 m/d												
		λ = 0.9 W/mK				λ = 2.26 W/mK				λ = 3.9 W/mK				
T = 8°C	Summer	T_{in} [°C]	28	ΔT [°C]	3,71	T_{in} [°C]	28	ΔT [°C]	4,04	T_{in} [°C]	28	ΔT [°C]	4,30	
		T_{air} [°C]	30	Q [W]	2039,61	T_{air} [°C]	30	Q [W]	2216,93	T_{air} [°C]	30	Q [W]	2363,16	
		T_{exc} [°C]	20	q [W/m^2]	40,79	T_{exc} [°C]	20	q [W/m^2]	44,34	T_{exc} [°C]	20	q [W/m^2]	47,26	
		T_{out} [°C]	24,29	q [W/m]	101,98	T_{out} [°C]	23,96	q [W/m]	110,85	T_{out} [°C]	23,70	q [W/m]	118,16	
	Winter	T_{in} [°C]	4	ΔT [°C]	0,91	T_{in} [°C]	4	ΔT [°C]	0,96	T_{in} [°C]	4	ΔT [°C]	1,00	
		T_{air} [°C]	2	Q [W]	498,33	T_{air} [°C]	2	Q [W]	526,50	T_{air} [°C]	2	Q [W]	546,82	
		T_{exc} [°C]	10	q [W/m^2]	9,97	T_{exc} [°C]	10	q [W/m^2]	10,53	T_{exc} [°C]	10	q [W/m^2]	10,94	
		T_{out} [°C]	4,91	q [W/m]	24,92	T_{out} [°C]	4,96	q [W/m]	26,33	T_{out} [°C]	5,00	q [W/m]	27,34	
T = 14°C	Summer	T_{in} [°C]	28	ΔT [°C]	2,70	T_{in} [°C]	28	ΔT [°C]	2,92	T_{in} [°C]	28	ΔT [°C]	3,10	
		T_{air} [°C]	30	Q [W]	1479,91	T_{air} [°C]	30	Q [W]	1601,34	T_{air} [°C]	30	Q [W]	1699,95	
		T_{exc} [°C]	20	q [W/m^2]	29,60	T_{exc} [°C]	20	q [W/m^2]	32,03	T_{exc} [°C]	20	q [W/m^2]	34,00	
		T_{out} [°C]	25,30	q [W/m]	74,00	T_{out} [°C]	25,08	q [W/m]	80,07	T_{out} [°C]	24,90	q [W/m]	85,00	
	Winter	T_{in} [°C]	4	ΔT [°C]	1,93	T_{in} [°C]	4	ΔT [°C]	2,08	T_{in} [°C]	4	ΔT [°C]	2,21	
		T_{air} [°C]	2	Q [W]	1058,75	T_{air} [°C]	2	Q [W]	1143,23	T_{air} [°C]	2	Q [W]	1210,96	
		T_{exc} [°C]	10	q [W/m^2]	21,18	T_{exc} [°C]	10	q [W/m^2]	22,86	T_{exc} [°C]	10	q [W/m^2]	24,22	
		T_{out} [°C]	5,93	q [W/m]	52,94	T_{out} [°C]	6,08	q [W/m]	57,17	T_{out} [°C]	6,21	q [W/m]	60,55	
T = 18°C	Summer	T_{in} [°C]	28	ΔT [°C]	2,02	T_{in} [°C]	28	ΔT [°C]	2,17	T_{in} [°C]	28	ΔT [°C]	2,29	
		T_{air} [°C]	30	Q [W]	1106,90	T_{air} [°C]	30	Q [W]	1190,62	T_{air} [°C]	30	Q [W]	1257,61	
		T_{exc} [°C]	20	q [W/m^2]	22,14	T_{exc} [°C]	20	q [W/m^2]	23,81	T_{exc} [°C]	20	q [W/m^2]	25,15	
		T_{out} [°C]	25,98	q [W/m]	55,35	T_{out} [°C]	25,83	q [W/m]	59,53	T_{out} [°C]	25,71	q [W/m]	62,88	
	Winter	T_{in} [°C]	4	ΔT [°C]	2,61	T_{in} [°C]	4	ΔT [°C]	2,83	T_{in} [°C]	4	ΔT [°C]	3,01	
		T_{air} [°C]	2	Q [W]	1432,38	T_{air} [°C]	2	Q [W]	1554,27	T_{air} [°C]	2	Q [W]	1653,59	
		T_{exc} [°C]	10	q [W/m^2]	28,65	T_{exc} [°C]	10	q [W/m^2]	31,09	T_{exc} [°C]	10	q [W/m^2]	33,07	
		T_{out} [°C]	6,61	q [W/m]	71,62	T_{out} [°C]	6,83	q [W/m]	77,71	T_{out} [°C]	7,01	q [W/m]	82,68	

Table X.6 Extracted/injected heat at t = 30 d for each combination of the parametric analysis with gwf = 2 m/d, in winter and in summer (Case II)

REFERENCES

Amis T., Robinson C. A. W., Wong S. (2010), “Integrating geothermal loops into the diaphragm walls of the Bvlgari Hotel Knightsbridge London” in Geotechnical Challenges in Urban Regeneration.

Amis T., Loveridge F. (2014), “Energy piles and other thermal foundations for GSHP—developments in UK practice and research”, REHVA J. 1.

Banks D. (2008), “An Introduction to Thermogeology: Gorund Source Heating and Cooling”, Blackwell Publishing, UK, 2008.

Barla M., Perino A. (2014), “Geothermal heat from the Turin metro south extension tunnels”. Proceedings of the World Tunnel Congress 2014: Tunnels for a Better Life, Iguaçu, Brazil.

Barla M., Di Donna A., Perino A. (2016), “Application of energy tunnels to an urban environment”, in Geothermics.

Barla M., Di Donna A., Santi A. (2017), “On the use of diaphragm walls as ground heat exchangers” (under revision).

Bourne-Webb P.J. (2013), “Observed response of energy geostructures”, in “Energy Geostructures: Innovation in Underground Engineering” (Laloui L., Di Donna A. (Eds.)), Wiley-ISTE, London.

Bourne-Webb P.J., Bodas Freitas T.M., da Costa Goncalves R.A. (2015), “Retaining walls as heat exchangers: a numerical study”, in Geotechnical Engineering for Infrastructure and Development, ICE Publishing, London, UK.

Bourne-Webb P.J., Bodas Freitas T.M., da Costa Goncalves R.A. (2016), “Thermal and mechanical aspects of the response of embedded retaining walls used as shallow geothermal heat exchangers” in Energy and Buildings 125.

Brandl H. (1998), "Energy piles and diaphragm walls for heat transfer form and into ground", in Proceedings of the 3rd International Symposium on Deep Foundations on Bored and Auger Piles, Ghent, Belgium.

Brandl H. (2006), "Energy foundations and other thermo active ground structures" in Géotechnique 56(2).

Brandl H., Adam D., Markievicz R., Unterberger W., Hofinger H. (2010), "Concrete absorber technology for earth coupled concrete structures using geothermal energy for the Vienna Underground line U2", in Ingenieur und Architekten Zeitschrift, 155.

Brandl H. (2016), "Geothermal Geotechnics for Urban Undergrounds" in Procedia Engineering 165.

BSI (2017), BS EN ISO 13789:2017: Thermal performance of buildings. Transmission and ventilation heat transfer coefficients. Calculation method. BSI, London, UK.

Callagaro M. (2017), "Geotechnical approach in the energy recovery designing of civil structures", Master dissertation, University of Padova, Italy.

Di Donna A., Barla M. (2015), "The role of ground conditions on energy tunnels' heat exchange", in Environmental Geotechnics 3(4).

Di Donna A. (2016), "Energy walls for an underground car park", in the 25th European Young Geotechnical Engineers Conference, Sibiu, Romania.

Di Donna A., Cecinato F., Barla M., Loveridge F. (2016), "Energy performance of diaphragm walls used as heat exchangers", Proceedings of the Institution of Civil Engineering, ICE Publishing, London, UK.

Diersch H. J. G. (2009), *DHI Wasy Software – FEFlow 6.1 – Finite Element Subsurface Flow & Transport Simulation System: Reference Manual,* DHI-Wasy GmbH, Berlin, Germany.

Directive 2009/28/EC of the European Parliament and of the Council of 23rd April 2009 on the promotion of the use of energy from renewable sources and amending and subsequently repealing Directives 2001/77/EC and 2003/30/EC.

Franzius J.N., Pralle N. (2011), "Turning segmental tunnels into sources of renewable energy". Proceedings of the ICE – Civil Engineering 164(1).

Gao J., Zhang X., Liu J., Li K., Yang J. (2008), "Numerical and experimental assessment of thermal performance of vertical energy piles: an application" in Appl Energy.

Gong J., Liu T., Wen B. (2015), "Analysis on Energy Geotechnical Engineering Technology in Diaphragm Wall", Atlantis Press, the Netherlands.

ICConsulten (2005), *Wirtschaftliche Optimierung von Tunnelthermie Absorberanlagen, Grundlagenuntersuchung und Planungsleitfaden*, ICConsulten, Vienna, Austria (in German).

Katzenbach R., Leppla S., Choudhury D. (2017), "Foundation Systems for High-Rise Structures", CRC Press, USA.

Knellwolf C., Peron H., Laloui L. (2011), "Geotechnical analysis of heat exchanger piles", in J Geotech Geoenviron Eng (ASCE), 137(10).

Kürten S. (2014), "Zur thermischen Nutzung des Untergrunds mit flächigenthermo-aktiven Bauteilen", PhD thesis, Aachen University, Aachen, Germany (in German).

Kürten S., Mottaghy D., Ziegler M. (2015), "Design of plane energy geostructures based on laboratory test and numerical modelling", in Energy and Buildings 107.

Loveridge F. A., Olgun C. G., Brettmann T., Powrie W. (2015), "Group thermal response testing for energy piles", in Geotechnical Engineering for Infrastructure and Development.

Markiewicz R. (2004), "Numerical and Experimental Investigations for Utilization of Geothermal Energy Using Earth-Coupled Structures and New Developments for Tunnels", PhD Thesis, Vienna University of Technology, Vienna, Austria.

Markiewicz R., Adam D. (2006), "Extraction of geothermal energy from tunnels", Millpress Science Publishers/IOS Press, the Netherlands.

Markiewicz R., Adam D. (2009), "Energy from earth-coupled structures, foundations, tunnels and sewers" in Géotechinique 59(3).

Mauri L. (2014), "Studio del comportamento di diaframmi energeticamente attivi mediante analisi numeriche termo-meccaniche", Tesi di Laurea, Politecnico di Milano, Italy (in Italian).

Mauri L., Sterpi D. (2015), " Analisi termo-meccaniche di diaframmi energeticamente attivi", in Incontro Annuale dei Ricercatori di Geotecnica 2015, Cagliari, Italy (in Italian).

Nicholson D. P., Cheng Q., de Silva M., Winter A., Winterling R. (2014), "The design of thermal tunnel energy segments for Crossril, UK". Proceedings of the Institution of Civil Engineers - Engineering Sustainability 167(3).

Rui Y. (2014), "Finite Element Modelling of Thermal Piles and Walls", PhD thesis, University of Cambridge, UK.

Stauffer F., Bayer P., Blum P., Giraldo N. M., Kinzelbach W. (2013), "Thermal use of shallow groundwater", CRC Press, USA.

Sterpi D., Angelotti A., Corti D., Ramus M. (2014), "Numerical analysis of heat transfer in thermo-active diaphragm walls" in "Numerical Methods in Geotechnical Engineering" (Hicks MA, Brinkgreve RBJ and Rohe A (eds)), CRC Press, USA.

Suckling T. P., Smith P. E. H. (2002), "Environmentally friendly geothermal piles at Keble College, Oxford, UK".

Sun M., Xia C., Zhang G. (2013), "Heat transfer model and design method for geothermal heat exchange tubes in diaphragm walls" in Energy and Buildings 61.

Xia C., Sun M., Zhang G., Xiao S., Zou Y. (2012), "Experimental study on geothermal heat exchangers buried in diaphragm walls" in Energy and Buildings 52.

Xia C., Zhu J. L., Cao S. D. (2014), Chinese Journal of Underground Space and Engineering, 10(1).

Zacco F. (2017), "Sfruttamento geotermico della galleria della Linea 2 della metropolitana di Torino", Tesi di Laurea, Politecnico di Torino, Italy (in Italian).

Zhang G., Xia C., Sun M., Zou Y., Xiao S. (2013), "A new model and analytical solution for heat conduction of tunnel lining ground heat exchangers", in Cold Regions Science and Technology 88.

ACKNOWLEDGMENTS

I would like to thank my **supervisors**, Prof. Marco Barla, Dr. Fleur Loveridge and Dr. Alice Di Donna, that gave me the chance to work at this project. It has been passionate and a life changing experience. For his precious help, Matteo Baralis deserves a special mention.

I would like to thank my **family**: my parents, always there to support me in my time of need and to encourage me every step of the way; my siblings, I hope I made you proud of me; my grandmother Grazia, whom support has been essential, as well as the love that bonds us; my grandparents Angelo and Sandra, just for being there, with our huge, noisy and crazy, but special, family, even those who are no longer here…

I would like to thank my **friends**.
My *fam* in Leeds, beautiful people that made me feel like home in a foreign country. Thanks for the laugh, the cider and the love. Especially Monica, Abhi and Priya will always have a special place in my heart.
My big family in Turin: those who have met and loved both the two versions of me, Laura, Marianna, Vittorio and Cristiano; my *famigghia*, too many to name them all, thanks for the *movida*, the great nights, the parties, the sharings; my flatmates, Santina, Katia and Elena, with whom I literally shared everything; my favourite *Maestro*, for the love and the time we spent together: despite all, I will miss you more than anyone.

Thanks to you all, those three years have been the best years of my life.

RINGRAZIAMENTI

Vorrei ringraziare i miei **relatori**, Prof. Marco Barla, Dr. Fleur Loveridge e Dr. Alice Di Donna, che mi hanno dato la possibilità di lavorare a questo progetto. È stato appassionante e un'esperienza che mi ha cambiato la vita. Una menzione speciale a Matteo Baralis, il cui aiuto è stato prezioso.

Vorrei ringraziare la mia **famiglia**: i miei genitori, sempre pronti a sostenermi nei momenti di bisogno e ad incoraggiarmi ad ogni passo del percorso; i miei fratelli, spero di avervi resi orgogliosi di me; nonna Grazia, il cui supporto è stato essenziale, così come l'affetto che ci lega; nonni Angelo e Sandra, semplicemente per esserci, insieme alla mia rumorosa e pazza, ma speciale, grande famiglia, anche quelli che non ci sono più…

Vorrei ringraziare i miei **amici**.
La mia *fam* a Leeds, persone fantastiche che mi hanno fatto sentire a casa in un altro paese. Grazie per le risate, il sidro e l'affetto. In particolare Monica, Abhi e Priya avranno sempre un posto speciale nel mio cuore.
La mia grande famiglia a Torino: quelli che hanno conosciuto e amato le due versioni di me, Laura, Marianna, Vittorio e Cristiano; la mia *famigghia*, troppo numerosi per nominarli tutti, grazie per la movida, le grandi serate, le feste e le condivisioni; le mie coinquiline, Santina, Katia ed Elena, con le quali ho condiviso letteralmente tutto; il mio *Maestro* preferito, per l'amore e il tempo passato insieme: nonostante tutto, mi mancherai più di chiunque altro.

Grazie a tutti voi, questi tre anni sono stati i migliori della mia vita.